THESIS

A COMPUTATIONAL STUDY OF AUTOIGNITION, SPARK IGNITION AND DUAL FUEL DROPLET IGNITION IN A RAPID COMPRESSION MACHINE

Submitted by

Siddhesh Bhoite

Department of Mechanical Engineering

In partial fulfillment of the requirements

For the Degree of Master of Science

Colorado State University

Fort Collins, Colorado

Summer 2017

Master's Committee:

Advisor: Anthony J. Marchese

Daniel B. Olsen
Hussam N. Mahmoud

ABSTRACT

A COMPUTATIONAL STUDY OF AUTOIGNITION, SPARK IGNITION AND DUAL FUEL DROPLET IGNITION IN A RAPID COMPRESSION MACHINE

A series of computational modeling studies were performed using the CONVERGE™ computational fluid dynamics (CFD) platform to gain in-depth understanding of the chemically reacting flow field, ignition and combustion phenomena in a various rapid compression machine (RCM) experiments conducted at CSU including homogeneous autoignition, laser ignition and droplet ignition experiments. A three-dimensional, transient computational modeling study was initially performed to examine premixed, homogeneous autoignition of isooctane/air and methane/air mixtures. A reduced chemical kinetic mechanism for isooctane comprising of 159 species and 805 reactions was developed using direct relation graph error propagation and sensitivity analysis (DRGEPSA) method. Computational results showed good agreement with experimental results capturing the negative temperature coefficient (NTC) behavior of isooctane. The premixed computations also revealed the importance of the piston crevice design for maintaining a homogenous flow field inside a RCM. The result showed that, as the volume of the piston crevices is increased, the roll up vortices are eliminated, which reduces the mixing of the lower temperature boundary layer gases with the higher temperature core gases, thereby maintaining the homogeneity of the flow field.

Next, three-dimensional computational modeling laser-ignited premixed fuel/air mixtures at elevated temperatures and pressures in the RCM was performed with detailed chemical kinetics (86 species, 393 reactions). For methane/air mixtures, the computational results were compared

against previously reported RCM experiments. Computations were also performed on laser-ignited n-heptane/isooctane/air mixtures under similar simulated conditions in the RCM. In the computations, a simulated spark modeled as a localized hotspot was introduced in the center of the combustion chamber resulting in an outwardly propagating flame, which, depending on the fuel reactivity, produced ignition in the end gas upstream of the flame. Methane/air computations were performed at equivalence ratio of $0.4 \leq \Phi \leq 1.0$ for direct comparisons with experimental measurements of instantaneous pressure, flame propagation rate, and lean limit. For compressed temperature of 782 K, a methane/air lean limit of $\Phi = 0.38$ was predicted computationally (combustion efficiency, $\chi = 0.8$), which was in good agreement with the experimental measurement of $\Phi = 0.43$. For n-heptane/isooctane/air computations, auto-ignition of the end gas was predicted depending on the compressed temperature and Octane Number, which suggests the use of the laser ignition/RCM system as a means to quantify fuel reactivity for spark ignited engines.

Lastly, RCM experiments in which single n-heptane droplets are suspended and ignited via compression-ignition in a quiescent, high-pressure, high-temperature, lean methane/air environments were simulated using the 86-species dual-fuel chemical kinetic mechanism developed previously. The simulations capture the ignition event in the vicinity of a spherical n-heptane droplet, which bifurcates into a propagating, premixed methane/air flame and stationary n-heptane/air diffusion flame. Comparisons against experimental measurements of droplet gasification rate, premixed flame propagation speed, and non-premixed flame position will be used to develop revised dual-fuel chemical kinetic mechanisms.

ACKNOWLEDGEMENTS

First and foremost, thank you to my advisor Dr. Anthony J. Marchese for introducing me to the world of combustion, guiding me through the M.S., and providing career advice. Thank you to Dr. Andrew Hockett for always helping me with my frantic problems by always replying to my mails. Thank you to Colin Gould for always helping me to provide the required experimental data for carrying my computational study. Thank you to Ciprian Dumitrache who provided a lot of insight in the field of optics and lasers along with great advices for computational simulations. Finally, thank you to my family for always supporting and trusting me with my desire of pursuing higher education.

TABLE OF CONTENTS

LIST OF TABLES

LIST OF FIGURES

CHAPTER 1: INTRODUCTION

1.1. Motivation

With the strict emission norms and the climate change effects on the environment, the world is moving towards new type of advanced engines like homogeneous charge compression ignition (HCCI) engines, reactivity controlled compression ignition (RCCI) engines and many other different engine systems. These new engine designs are under consideration to meet the strict norms of the Environmental Protection Agency (EPA) and also to increase the efficiency of engines and decrease the emission taking place by carrying out some controlled combustion strategies in the combustion chamber. Most of the advanced compression engines (ACI) utilize the intermediate temperature range of about 600 K to 800 K as the operating condition as compared to that of the conventional engines which utilizes high temperature and pressure operating conditions which basically results in a higher adiabatic flame temperature after combustion resulting in a greater NOx formation. Also, the present conventional engines utilize slightly richer mixture to achieve good combustion efficiency which further results in increasing the emissions from the combustion chamber.

Advanced compression engines like HCCI and RCCI, not only operate at lower operating temperature but also utilizes leaner mixture as the charge in the combustion chamber. Previous research has shown that as the mixture gets leaner, the adiabatic flame temperature goes down resulting in lower temperature after combustion, which further results in reduced formation of NO_x. Generally, all the advanced compression engines utilize the two stage combustion characteristics of fuel to carry out combustion process. Now to carry out the combustion process

in a most controlled way it is very important to develop an understanding regarding the low temperature heat release, high temperature heat release and the NTC region of the fuel.

To develop better understanding regarding the control parameters associated with the ACI engines, it is very important to study and develop chemical kinetics of the chemical reactions taking place at those intermediate temperature ranges. Many of the experimental devices like flow reactors, well stirred reactors, shock tubes and rapid compression machines (RCM) can be used to develop a better understanding regarding the chemical kinetics. The RCM is the most suitable device which can be used from the above devices because of its ability to develop the test conditions in the temperature ranges suitable for advanced compression engines without much of difficulty and thus proves as a valuable tool to carry out experimentations for studying the chemical kinetics associated with the advanced engines.

RCM experiments along with computational modelling serves as an ideal platform to develop a strong understanding regarding the different events taking place during the combustion processes. With the developments in the combustion chemistry solvers and increasing computational capabilities, it is now possible to carry out the computational simulations utilizing the same RCM experimental conditions to capture more details associated with the combustion event which experiments are not able to capture due to certain limitations. Computational modelling of RCM not only helps to gain better insight of the processes but also helps to validate the experimental results. It also proves to be a best platform to modify the chemical kinetic mechanism if any discrepancy is observed between the experimental and computational results.

With the above discussed details regarding the development of advanced engines utilizing controlled ignition and developing better understanding regarding chemical kinetics, presented herein is a computational study of RCM. The RCM in CSU has been modified to study diverse

combustion problems like homogeneous autoignition, laser induced spark ignition, and a dual fuel droplet ignition system.

1.2. Chemical Kinetics

Different fuels when introduced with the correct concentration of the oxidizer mixture undergo a chemical reaction to form products. The chemical reaction taking place in the system is complex leading to form a number of intermediate species before the final products are formed. The way the chemical reaction proceeds also depend on the conditions under which the combustion is taking place. So, in order to develop better understanding regarding the combustion processes, an increased research work has been carried to study the reaction rates and mechanisms which in turns require a comprehensive understanding of the chemical kinetics. With the availability of large amount of elementary kinetic data and increase in the computational power have enabled to carry out the combustion system study in a more precise and accurate way by considering the effects of chemistry and thus have enabled to understand the combustion systems and have helped to develop better combustion systems.

Generally, a chemical kinetic mechanism consists of a set of reactions and species along with the values of its reaction rates expressed in Arrhenius form. Such mechanisms are called as comprehensive mechanism or a detailed chemical kinetic mechanism. Such comprehensive mechanisms are usually developed and validated based on the experimental data which are carried over a wide range of operating conditions. After achieving a good validation against the experimental values, such comprehensive mechanisms can be used to carry out the computational simulations at the conditions which are not easy to achieve using the experimental setup due to some constraints. So, in general, the reaction mechanism scheme is used to carry out the validation

of the experimental data and to further to extent the kinetic study of the system for which the experimental data is not available.

Development and further refinement of the mechanism is a continuous process depending on the continuous collection and evaluation of experimental data. The chemical kinetic data which is obtained using the conditions which don't fall in the limits of model validation is very important for further refinement and validation of the chemical kinetic mechanism. If the experimental data matches with the modeling results, it helps to reveal the chemistry developed is understood properly and if there is a discrepancy between the experimental and modelling data, then there gives the opportunity to further refine the mechanism which widens its suitability over a large range of operating conditions.

For developing of the chemical kinetic mechanism, we basically need a kinetic data of chemical reactions taking place at a wide range of temperature and pressure conditions using different experimental approaches. Most of the facilities developing, testing, validating the chemical kinetic mechanism have developed a modelling unit alongside the experimental setup which can simulate the combustion system using the same operating conditions as used in the actual experiments to provide further insight into the development of kinetic mechanism. Since, the chemical kinetic development requires a large experimental data, it is very important that the experimental data should be of high fidelity. But generally, the experimental data is affected by various disturbances in the combustion systems like turbulences, fluid flow, rapid mixing etc. This fluid dynamic effect on the chemistry of the reacting mixtures makes the data interpretation more difficult from the practical combustion systems. In order to deal with the problem of fluid dynamics interaction with the chemical kinetics, experimental devices like static reactors, well stirred reactors, shock tubes, rapid compression machines are designed which produces homogenous

mixtures with reduced fluid dynamics effects thus allowing the study of chemistry in purely homogenous environment. Detailed description of various experimental devices is discussed in the following sections.

1.3. Static Reactor

Static reactors comprise of a spherical vessel that is usually filled with the gas or the reactive mixture. The operation of the static reactors is conceptually very simple in which the initial gas temperature is maintained at the desired temperature using a thermostated bath or by using an oven. The development and the progress of the reaction taking place in the static reactor is measured studying the pressure change taking place in the system or by studying the change in the concentration of some species over a period of time. Static reactors work on the assumption of negligible diffusive and convective effects which can only be seen if there is no gradient in temperature/concentration present in the system. To achieve the above assumption, the characteristic reaction time in the static reactor should be greater than the diffusion time which imposes certain limitations on the operating conditions of the static reactors and results in comparative large experimental time scales which limit its use to slow reaction schemes.

Static reactors are used to find the explosion limits of the various reactive mixtures which help us to separate the regions of slow and fast reaction. However, there are a lot of surface effects taking place on the chemical reactions in static reactors by exposing the mixtures to long reaction times which results in increasing the sensitivity of the reactor and thus makes the data obtained using the static reactor less reliable as compared to the other techniques described in the sections 1.4, 1.5, 1.6, 1.7 in this chapter.

1.4. Flow Reactor

A flow reactor is a simple continuous device which allows the mixture of reacting fuel/oxidizer to heat up to a desirable temperature and pressure and once the desire conditions are achieved the mixture is allowed to move down the tube. In the process of designing a chemical kinetic interpretation in a flow reactor, a plug flow condition is achieved where the temperature and the composition of the reactants are kept uniform over the cross section of the reactor such that the axial diffusion is negligible. To develop a plug flow condition, the mixture of reactants is highly diluted with the inert gas and total flow rate is increased which causes a stretching of reaction zone over a significant distance and the thermal gradient along with the axial concentration gradient become infinitesimally small.

Also since the reaction zone becomes large enough, it enables us to sample the gas temperature as well as the concentration of the products at different axial positions of flow reactor with different residual times. In the flow reactor, the sampling distance is compared with the experimental time by calculating the gas velocity allowing us to convert the quasi steady, one dimensional, spatial problem to a zero-dimensional temporal problem which provides an opportunity for direct and detailed measurement of the chemical kinetic scheme.

Data obtained using the flow reactor can be influence by the many experimental errors such as the sampling technique used may have problem linked with it, imperfect mixing of the reactive mixture, gradients in concentration and temperature in the axial direction is significantly high. To brief out regarding the flow reactor, it is basically a device which provides an ideal platform for the temperature and species measurement at ease but with a limitation of being applicable only for low reaction conditions in a highly diluted environment. A typical example of a flow reactor is a

variable pressure flow reactor at Princeton University operating at 0.2 to 20 bar and temperature until 1200 K [1][2].

1.5. Well Stirred Reactors

A Well Stirred Reactors are the devices which allows for the uniform mixing of the reactant species in a constant volume chamber. Entry and exit of the mixtures takes place through inlet and outlet provided to the chamber and generally operates at a constant pressure, steady state. The highly turbulent mixing taking place in the well stirred reactor causes a condition that can ideally be assumed to be homogenous with respect to the temperature and the species concentration distribution within the reactor which establishes a condition which is purely be governed and controlled kinetically.

The exhaust coming out from the outlet of the reactor is at the same condition as that found inside the reactor due to uniform mixing and the concentration of the exiting gas can be measured as the function of residence time which is defined as a ratio of mass of reactant present inside the reactor to the mass flow rate of the reactant species. The residence time can be varied by varying the mass flow rate of the reactants.

Well stirred reactors also have some problem when it comes to interpretation of data from the experiments. The challenge faced by the well stirred reactor is its inability to achieve rapid mixing. Well stirred reactor works on the assumption that the time scale of mixing is very small as compared to the reaction time of the fluid in the reactor. Considering this assumption, for certain experimental cases, the reliability of the data is not guaranteed as the conditions may not accord with the expected behavior. For a high temperature experiments, the reactions take place very fast which causes the reaction time to be of same scale as that of mixing time which influences the data

obtained from the well stirred reactor. So generally, it is taken care that for an experimental temperature condition of high temperatures of 1300 K to 1400 K, the data obtained from the well stirred reactors should be used with caution as the reaction time approaches to the mixing time resulting in the influence of mixing.

Well stirred reactors don't resolve the reaction zone spatially which allow it to operate with lower dilution and higher temperature as compared to the flow reactors thus allowing the chemical kinetic study at elevated temperature. Other disadvantage of well stirred reactor is its operation at steady state thus making it difficult for the study of time evolution of chemical reaction. An example study of well stirred reactor is a jet stirred reactor which was used for the n-heptane oxidation study in a temperature range of 550 K and 1150 K and up to pressure of 40 bar with highly dilute mixture to reduce the temperature gradient and heat release inside the reactor and maintain a steady state [3].

1.6. Shock Tube

Shock tubes are the devices which are used to carry out the auto ignition study of the reacting gases at higher temperatures and pressures which are generally not developed using the well stirred reactors or the flow reactors. Shock tube basically consists of two sections. The first section consists of a high driver inert gas which is maintained at high pressure and the other section consists of several meters long tube containing the potential reactants maintain at lower pressure compared to the high-pressure section. Both the high pressure and low pressure section is separated by a thin diaphragm. As the diaphragm is punctured, due to the pressure difference present in the system, a shock wave is produced which causes the mixture of reactants to get compressed causing the desired rise in the temperature and pressure of the reacting mixtures. Ignition delay in case of

the shock tube is defined as the time interval between the shock arrival which is determined by pressure trace and the onset of combustion inferred from the absorption spectra of an intermediate combustion species like OH or could also be inferred from the pressure trace. A high temperature of about 2800K and a pressure upto 550 bar can be achieved using the shock tube [4]. Example of a shock tube is one present in the Stanford University which can attain very high pressures of 1000 atm [5].

Disadvantages of using a Shock tube is that there is an effect of boundary layer acting on the chemical kinetics observed thus causing some errors in the data interpretation taken from the shock tube. Thus, to avoid the boundary layer effects, high temperature and pressure conditions are used so that the chemical kinetics become faster resulting in lesser chemical induction time which lowers the effect of boundary layer. As a result of these limitations, the shock tubes are generally used and suitable for high temperature and pressure conditions.

1.7. Rapid Compression Machine

Rapid Compression Machine (RCM) simulates an ideal compression stroke of an engine. The RCM does that by eliminating the geometric complexities generally observed in the engines thus eliminating the effects of mixing and turbulences on the chemical kinetics of the reacting mixture and allow for studying the accurate chemical kinetics of the reacting system. Rapid Compression Machine here in CSU is an opposed two piston machine which compresses the mixture to a pressure upto 25bar to 60bar and temperature of about 600 to 1200 K. Piston travels fast so that the reaction taking place during the compression stroke is suppressed till the top dead center (TDC) is reached and the heat loss taking place through the chamber wall can be negligible due to the rapid motion of the piston. The high velocity of the pistons is usually achieved using a

pneumatically control system. Variable compression ratio, initial temperature and composition and initial temperature are the parameters which can be controlled and tweaked to obtain the desired conditions after the compression stroke.

Generally, the data interpretation of the RCM is done by studying the pressure trace obtained for the reacting mixture. A sample pressure trace of using inert as nitrogen is as shown in figure 1.1. The sample pressure trace shows a rapid rise in the pressure during the initial compression stroke and once the peak pressure is obtained at TDC, the pressure trace starts falling due to the heat loss from the constant volume chamber.

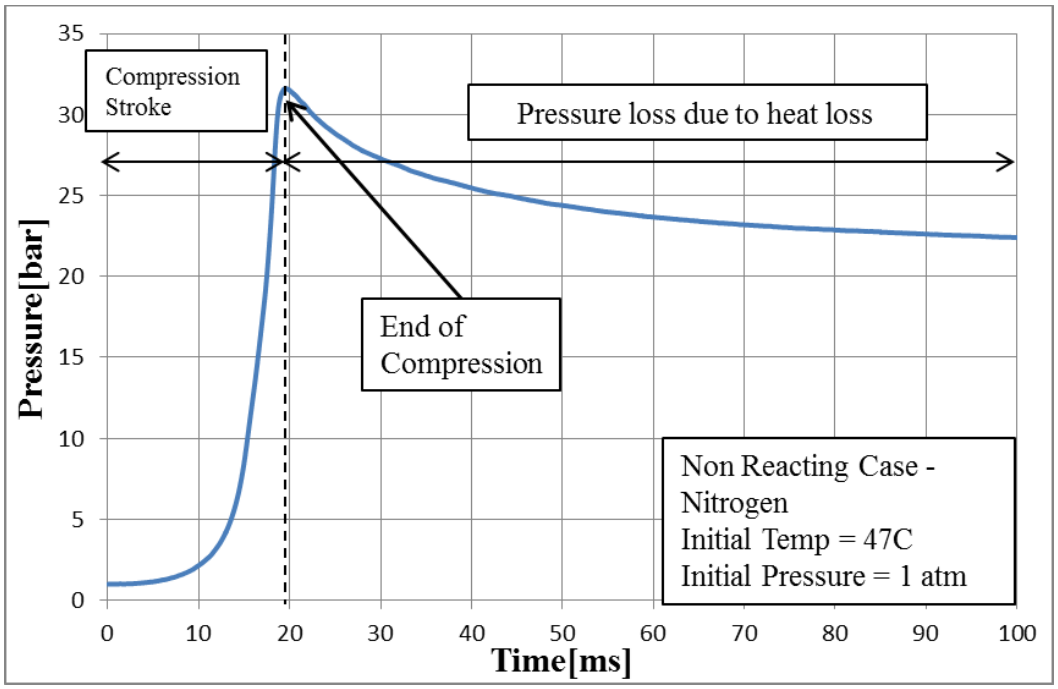

Figure 1.1 Typical Pressure trace obtained in a RCM for the compression stroke of inert gas N_2. Initial condition is $P_0 = 1$ atm, $T_0 = 47^oC$

Now, if the inert mixture is replaced by the reactive mixture than an auto ignition event takes place in the system if the temperature and pressure conditions after TDC are suitable for the auto ignition event which further causes the pressure rise to take place after the induction time as shown in figure 1.2. Ignition delay is defined as the difference in time between the TDC to the time of

auto ignition of the mixture characterize by steep rise in pressure which allows for the direct measurement of the ignition delay of the fuel as shown in figure 1.2.

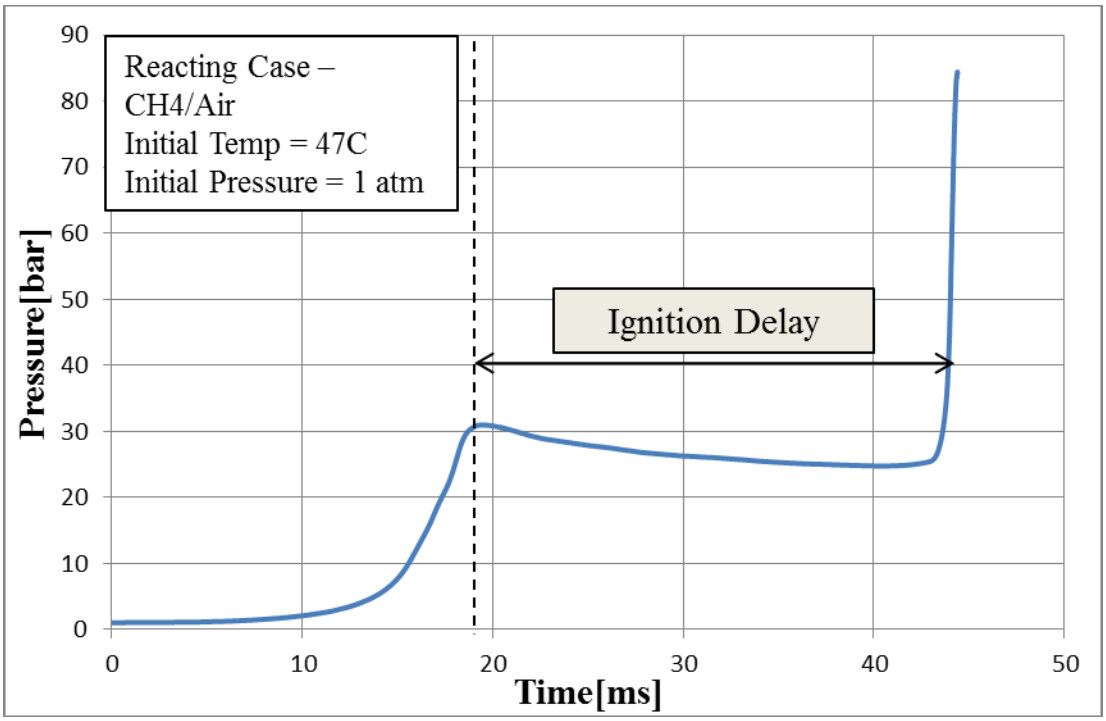

Figure 1.2 Typical pressure trace obtained in a RCM for a reacting case of CH_4/Air at stoichiometric condition with initial pressure P_0 = 1 atm, and initial temperature T_0 = 47°C

Following section describes the advantages and challenges associated with rapid compression machines in detail.

1.8. Advantages and Challenges with Rapid Compression Machine

A rapid compression machine allows us to do auto ignition study at various temperatures and pressures which are generally difficult to achieve using the devices presented above with direct measurement of the ignition delay. One more advantage of RCM is its capabilities to carry out the study of slow reactions with larger induction time which could be one magnitude greater than shock tube as there is no problem associated with the interference from reflected wave as seen in shock tube which limits the shock tube only for high temperature reactions with induction time of

less than 5 ms. Thus, RCM are used to study the combustion of slow reactions mechanism at high elevated pressures with a temperature ranging from typically 600 K to 1200 K.

Phenomenon of auto ignition in the intermediate temperature region of 600 K to 1200 K is studied by most of the researchers worldwide as it could be of practical importance for some large-scale applications like achieving a desired way of combustion in Homogeneous Charge Ignition (HCCI) engines, studying the knocking phenomenon in case of the HCCI engines, Spark ignition (SI) engines [6]. With the aim of controlling the auto ignition events taking place in the conventional and modern engines, there is a need to develop better understanding regarding the two-staged ignition phenomenon and the negative temperature coefficient (NTC) which happens at an intermediate temperature range [7]. With reference to the HCCI engines, the control of the ignition delay using additives is of great importance and relevance as we need a greater control over the speed and the heat release over a wide range of engine load [8]. Unwanted knocking results in damaging the engines components which needs to be controlled. When the fuel is in the inlet manifold of the engine chamber, it may get heated up to high temperature and pressure and if the ignition delay time of the mixture is less than the residence time than the fuel mixture may auto ignites in the inlet manifold instead of burning it in the combustion chamber. So, the phenomenon of auto ignition is a serious issue which leads to question the reliability of the advanced engines like HCCI and Lean Prevapourized Premixed (LPP) gas turbines. So, it is very important to understand, control and predict the ignition delays and the auto ignition event at those intermediate temperatures and pressures which could be studied using RCM.

RCM also has challenges associated with it. Even if RCMs are used to replicate the compression stroke of engine with negligible turbulence effect, different RCMS present at different locations are different and the data obtained from them can be different based even if the

conditions used are the same. This differences in the data obtained from different facilities can be attributed to the heat loss effects and the different aerodynamics effects present in various RCMs. Various studies [9] [10] [11] [12] have been conducted which shows the formation of the roll up vortices during the compression stroke of the RCM which causes the mixing of cold gas boundary layer with the hot gases present in the chamber resulting in temperature inhomogeneity affecting the data interpreted from the RCM. Study of the roll up vortices is carried out and described in the Chapter 2.

The other challenge which RCM faces is its limitations of direct temperature measurements due to rapid compression and ignition process. The temperature profile of RCM is developed indirectly using the pressure trace obtained from the experiments. Also, while deducing the temperature from the RCM, it is assumed that the effect of heat loss to the walls during and after the compression stroke is only limited to the thin boundary layer near the chamber and piston walls. And this hypothesis is called 'adiabatic core hypothesis'. With this hypothesis, even when the compression process is not purely adiabatic, the center core of the chamber is assumed to be adiabatically compressed. And for this adiabatic case, the temperature and pressure at top dead center is given as follows,

$$\int_{T_o}^{T_{ac}} \frac{1}{\gamma - 1} \frac{dT}{T} = In(CR) \tag{1.1}$$

$$\int_{T_o}^{T_{ac}} \frac{1}{\gamma - 1} \frac{dT}{T} = In(\frac{P_{ac}}{P_o}) \tag{1.2}$$

where T_{ac} and P_{ac} are the temperature and pressure at TDC for truly adiabatic compression, CR is the compression ratio with T_o and P_o are the initial temperature and pressure. γ is the ratio of specific heat at constant pressure to the specific heat at constant volume. But when the compression takes place, it is not purely adiabatic compression and thus the temperature and pressure obtained at TDC in actual experiments are little less as compared to the one obtained using the above equations (T_{ac} and P_{ac}).

To obtain the correct temperature at the TDC, the pressure trace obtained from the RCM experiment is used and the pressure value at TDC (P_c) is plugged in the above equation to yield the correct temperature at TDC. The equation 2 transforms as follows,

$$\int_{T_o}^{T_c} \frac{1}{\gamma - 1} \frac{dT}{T} = In(\frac{P_c}{P_o}) \tag{1.3}$$

The above equation can be solved for the unknown parameter T_c as we know all the other parameters in the above equation. The assumption of the adiabatic core assumption only holds true if the heat loss only takes place through the thin boundary layer and there is no heat loss from the center of the chamber. But with the presence of the roll up vortices in the chamber, the homogeneity of temperature is disturbed violating the adiabatic core assumption. So, a proper design of RCM is necessary such that the heat loss can be minimized and the adiabatic core hypothesis holds true to obtain a valuable and accurate data from RCM.

CHAPTER 2: COMPUTATIONAL METHOD FOR RAPID COMPRESSION MACHINE

2.1. CONVERGE and Numerical Scheme

Computational modeling of Rapid Compression Machine was performed using the commercial CONVERGE™ version 2.2.0 code. The CONVERGE™ code eliminates the mesh generation from the simulation process by automatically generating a perfect structured grid during the execution of the simulation controlled by simple user defined grid control methods such as Adaptive Mesh Refinement (AMR), Grid Scaling, Fixed Embedding which is discussed later in the thesis. Finite Volume Method was used to solve the transport equations where the surface fluxes of mas, momentum and energy transport were found using second order central differencing. Transient solver was used which uses Pressure Implicit with Splitting of Operators (PISO) method of Issa et al. (1986) to solve the transport equations and to couple the pressure and the velocity. This technique is predictor corrector type that solves for the velocity field implicitly and then updates the velocity field iteratively based on the solution obtained for pressure field.

Conservation of mass, momentum and energy are the governing equations in CONVERGE which additionally includes transport of species and turbulence equations. The partial differential equations (PDE) for mass, momentum, and energy are solved simultaneously to ensure the correct pressure gradient. Energy equation is coupled with the mass and momentum equations and solved iteratively to include the convection term in the energy equation along with the diffusion term. The compressible form of the mass and momentum PDE's are respectively given as follows,

$$\frac{\partial \rho}{\partial t} + \frac{\partial \rho u_i}{\partial x_i} = \mathrm{S}, \tag{2.1}$$

and,

$$\frac{\partial \rho u_i}{\partial t} + \frac{\partial \rho u_i u_j}{\partial x_j} = -\frac{\partial P}{\partial x_i} + \frac{\partial \sigma_{ij}}{\partial x_j} + S_i, \tag{2.2}$$

where σ_{ij} is a viscous stress tensor, given as,

$$\sigma_{ij} = \mu\left(\frac{\partial u_i}{\partial x_j} + \frac{\partial u_j}{\partial x_i}\right) + \left(\mu' - \frac{2}{3}\mu\right)\frac{\partial u_k}{\partial x_k}\delta_{ij}. \tag{2.3}$$

In the above equations, ρ is the density, u_i is the velocity component, S is the source term, P is the pressure, μ is the dynamic viscosity, μ' is the dilation viscosity (assigned to be zero), and δ_{ij} is the Kronecker delta. When the turbulence model is employed the viscosity is replaced by the sum of molecular and turbulent viscosity as shown below,

$$\mu_{tot} = \mu + \mu_t = \mu + C_\mu \rho \frac{k^2}{\varepsilon}, \tag{2.4}$$

where k is the turbulent kinetic energy, C_μ is a model constant, and ε is the turbulent dissipation rate. Equations (2.1) and (2.2) include a source term S which arises in the momentum equation due to acceleration due the gravity or mass sources and in the mass equation the source term may arise from evaporation.

The energy equation is given as shown below,

$$\frac{\partial \rho e}{\partial t} + \frac{\partial u_j \rho e}{\partial x_j} = -P\frac{\partial u_j}{\partial x_j} + \sigma_{ij}\frac{\partial u_i}{\partial x_j} + \frac{\partial}{\partial x_j}\left(K\frac{\partial T}{\partial x_j}\right) + \frac{\partial}{\partial x_j}\left(\rho D \sum_m h_m \frac{\partial Y_m}{\partial x_j}\right) + S, \tag{2.5}$$

where K is the thermal conductivity, T is the temperature, e is the specific internal energy, D is the mass diffusivity, Y_m is the mass fraction of all species m, and S is an energy source term, h_m is the

specific enthalpy of all species m. When a turbulence model is active, the thermal conductivity is replaced by turbulent conductivity according to,

$$K_t = K + c_p \frac{\mu_t}{Pr_t}, \tag{2.6}$$

where c_p is the specific heat capacity at constant pressure, Pr_t is a user specified turbulent Prandtl number, μ_t is the turbulent viscosity. In energy equation, S is the energy source term specified by the user, $-P\frac{\partial u_j}{\partial x_j}$ is the pressure work term added from compression and expansion of the gases. $\sigma_{ij}\frac{\partial u_i}{\partial x_j}$ is the viscous dissipation term accounting for kinetic energy dissipation into heat, and $\frac{\partial}{\partial x_j}\left(\rho D \sum_m h_m \frac{\partial Y_m}{\partial x_j}\right)$ is species diffusion term which accounts for transport of energy due to the diffusion of species.

The species transport equation is solved separately to calculate the mass fraction of all the species present in the domain and is defined as,

$$\frac{\partial \rho_m}{\partial t} + \frac{\partial \rho_m u_j}{\partial x_j} = \frac{\partial}{\partial x_j}\left(\rho D \frac{\partial Y_m}{\partial x_j}\right) + S_m, \tag{2.7}$$

where,

$$\rho_m = \rho Y_m \tag{2.8}$$

and u_j is the velocity, ρ_m is the species density of species m, D is the mass diffusion coefficient, Y_m is the mass fraction of species m, ρ is the density and S_m is the species source term due to the chemical reaction taking place in the domain. Based on Schmidt number, *Sc*, the molecular mass diffusivity is calculated according to,

$$D = \frac{\nu}{Sc}, \tag{2.8}$$

where ν is the kinematic viscosity. The molecular mass diffusivity is replaced by the turbulent mass diffusivity when turbulence model is used which is defined as follows,

$$D_t = \frac{\nu_t}{Sc_t}, \tag{2.9}$$

where Sc_t is a user supplied turbulent Schmidt number and ν_t is the turbulent kinematic viscosity. To evaluate the species properties, it is very important to initialize the species even when the species are not solved.

The diffusive terms involved in the energy and momentum equations require thermal conductivity and diffusivity of the mixture. A mixture averaged values was calculated for the conductivity and the diffusivity of the species present in the domain as a function of temperature. Dynamic viscosity, μ, and thermal conductivity, k is defined in the input file *gas.dat* as functions of temperature from 0 K to 5000 K.

Finally, we need a method to couple density, pressure and temperature which is done by using equation of state. Redlich Kwong equation of state was used in the current study which utilizes critical pressure and critical temperature of air for solving the governing equations as explained in the CONVERGE™ theory manual [13].

CONVERGE provides two different time step control method namely the fixed time step and variable time step. In this study, variable time step was employed in which if the governing equation is not converging during the specified number of iteration, the time step is reduced. The parameters which control the time steps are *itmax* (maximum number of iteration), *itmax_pres_ideal (*ideal number of iterations for pressure) and *max_piso (maximum number of*

PISO iterations). We have also considered three different Courant-Friedrichs-Lewy (CFL) numbers to control the time step, which include the CFL number based on convection, the CFL number based on diffusion, and the CFL number based on Mach number which are respectively defined as follows,

$$CFL_u = u\frac{\Delta t}{\Delta x}, \tag{2.10}$$

$$CFL_\nu = \nu\frac{\Delta t}{\Delta x^2}, \tag{2.11}$$

$$CFL_{mach} = a\frac{\Delta t}{\Delta x}, \tag{2.12}$$

where u is the velocity, ν is the kinematic viscosity, a is the speed of sound, Δx is the cell width, and Δt is the time step size. The CFL numbers specified by the user are the maximum CFL numbers allowed during the simulation and the time step during the execution of the code is controlled in such a way that the CFL numbers will not exceed the user specified values. In addition, the time step was restricted based on the chemistry. When the combustion model was active, the maximum time step allowed was,

$$dt_{chem} = dt_{prev} * \min\left[\frac{T}{\Delta T}\right] * mult\_dt\_chem, \tag{2.13}$$

where *mult_dt_chem* is a user specified input, T is the initial cell temperature, ΔT is the change in the temperature due to combustion event. Thus, if *mult_dt_chem* =0.15, then the time step is restricted such that maximum cell temperature change is 15% of the cell temperature.

While solving the equation implicitly, solution convergence is check iteratively by comparing the iteration errors in the solution with the user specified convergence criterion. A solution is said

to have converged when the iteration error is less than or equal to user specified tolerances. The iteration error is defined as follows,

$$error = \frac{\Delta\varphi}{norm}, \tag{2.14}$$

where φ is a solution field variable, $\Delta\varphi$ is the change in the solution field variables between successive iterations, and *norm* is a normalization for φ. PISO algorithm first couples the pressure and velocity fields and solves the density, species and energy equations and based on the results obtained in that particular iteration it updates the velocity and pressure field for the next iteration such that the solution convergence is achieved for each time step. Detailed description of the PISO algorithm is given in the CONVERGE theory manual [13]. After convergence is achieved during the PISO algorithm it is necessary to check the conservation of transport equations which is carried out using Jacobi algorithm since it conserves perfectly. After the transport equations are conserved, turbulence model gets active to solve the turbulence equations which are discussed in the section 2.3.

2.2. Geometry

All the simulations carried out in this work utilized a geometry which was made using the RCM drawing obtained from the manufacturers. The geometry was made using SolidWorks 2012 and exported to the CONVERGE preprocessor in Stereo Lithography (STL) format which represents geometry as closed triangulated surfaces as shown in figure 2.1. Representation the geometry as closed triangulated surfaces helps in easy and time efficient creation of the surfaces in CONVERGE preprocessor. To find the correct piston profile, simulations where conducted using a complete geometry as shown in the figure 2.2 and for the simulation which were carried

out to study the auto ignition, spark ignition and dual fuel ignition combustion, a $1/8^{th}$ section model of the RCM geometry was used as shown in the figure 2.3.

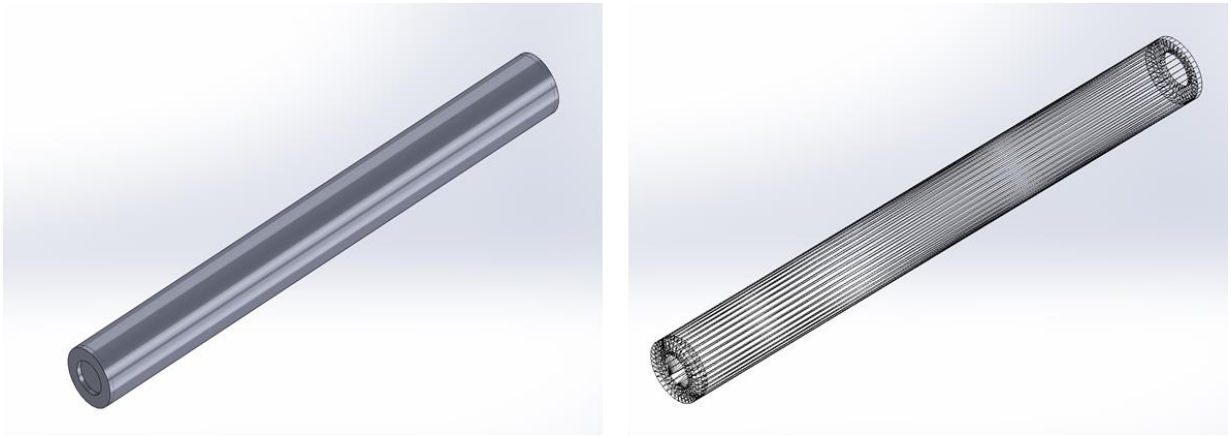

(a) (b)

Figure 2.1(a) Complete RCM geometry in SolidWorks. (b) RCM geometry represented as triangulated surfaces.

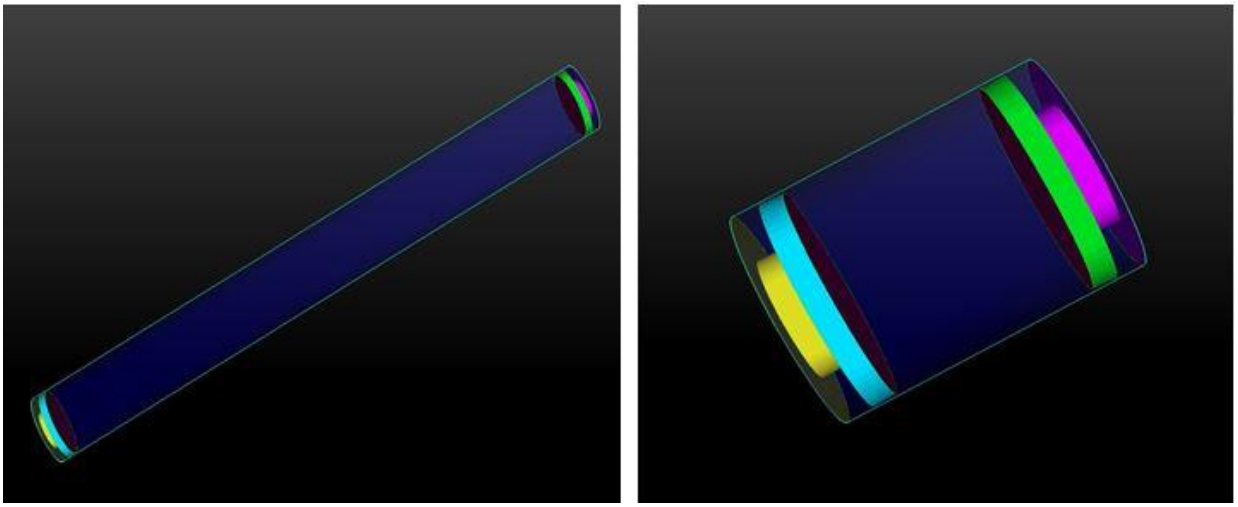

(a) (b)

Figure 2.2 Complete RCM geometry(a) before compression (b) after compression stroke.

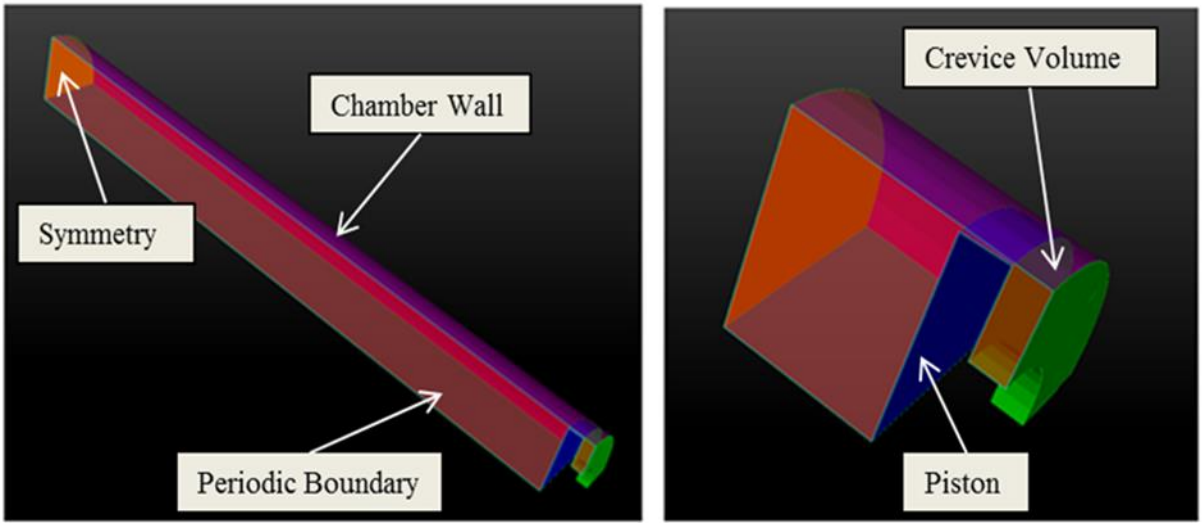

(a) (b)

Figure 2.3 1/8th RCM geometry (a) before compression stroke (b) after the compression stroke.

1/8th RCM geometry helped to reduce the computational time for carrying out the simulation and allowed for finer detailed meshing around area of interest without compromising on the simulation time scale. Periodic boundary conditions are used for the boundaries forming the sector with angle of 90 degree and a symmetry boundary condition is used to apply the slip velocity and neumann conditions at the boundary closing the two periodic boundaries which establishes symmetry.

2.3. Turbulence model

Turbulence helps in increasing the mixing rate of species, energy, and momentum. In most of the applications such as internal combustion engines, Rapid Compression Machine, turbines, turbulent –enhanced mixing takes place due to the presence of eddies which are having different length scales. In order to account for the enhanced turbulent mixing it is very important to resolve the small eddies during the simulation. But with the current computational power and model available it is very difficult to resolve all small eddies to accurately represent the enhanced

turbulent mixing and thus to account for additional mixing we make use of the turbulence model. Turbulence is very critical for studying the physics of Rapid Compression Machine specially studying the roll up vortices resulting from the motion of the piston. For all the work in this study Renormalized k- ε Reynolds Averaged Navier-Stroke (RANS) model is used. In this model the flow variables are split into two components namely the ensemble mean term and fluctuating term. For example, the instantaneous velocity component is split into ensemble mean term ($\bar{u}_i$) and fluctuating term (u'_i). The fluctuating term represents the effect of the turbulence on the flow variables.

$$u_i = \bar{u}_i + u'_i \tag{2.15}$$

In order to account for the turbulence effects in the transport equations, the flow variables obtained after RANS decomposition are substituted in the Navier-Strokes equation. When ensemble averaging of momentum equations is done, it results in introduction of additional terms in those equations called Reynolds stresses. This Reynold stresses represents the effect of turbulence and is introduce to close or conserve the momentum equation. Reynold stresses are represented as a tensor defined below,

$$\tau_{ij} = -\overline{\rho u'_i u'_j}, \tag{2.16}$$

In RNG model, we generally use effective turbulent viscosity to model the Reynolds stresses. The modeled Reynold stress is as shown below,

$$\tau_{ij} = 2\mu_t S_{ij} - \frac{2}{3}\delta_{ij}\left(\rho k + \mu_t \frac{\partial \tilde{u}_i}{\partial x_i}\right), \tag{2.17}$$

where S_{ij} is the mean strain rate tensor given by

$$S_{ij} = \frac{1}{2}\left(\frac{\partial \tilde{u}_i}{\partial x_j} + \frac{\partial \tilde{u}_j}{\partial x_i}\right), \tag{2.18}$$

Turbulent viscosity, μ_t is used to model the momentum transfer caused by the eddies present in the system and is defined as,

$$\mu_t = C_\mu \rho \frac{k^2}{\varepsilon} \tag{2.17}$$

where C_μ is the model constant and can be tuned based on the desired flow for particular simulation. The turbulent kinetic energy (k) is the mean kinetic energy present per unit mass present in eddies and is defined as follows,

$$k = \frac{1}{2}\widetilde{u'_i u'_j}. \tag{2.19}$$

Momentum equation is closed using the Reynold stress term which balances the instability in the momentum equation due to turbulence. Similarly, to balance the instabilities present in the mass and the energy equation, turbulent diffusion (D_t) and turbulent conductivity (K_t) terms are introduced.

Turbulent conductivity is the ability of eddies to conducts heat and is defined as,

$$K_t = \left(\frac{1}{\mathrm{Pr}_t}\right)\mu_t c_p, \tag{2.20}$$

Turbulent diffusion is the transfer of mass in the system due to the randomness in the system imposed by the presence of turbulence and is defined as,

$$D_t = \left(\frac{1}{\mathrm{Sc}_t}\right)\mu_t \tag{2.21}$$

The turbulent Schmidt number (Sc_t) and turbulent Prandtl number (Pr_t) are defined by the user. Sc_t = 0.78 and Pr_t = 0.9 were the typical value used for most of the work presented here. Turbulent viscosity given by Equation (2.18) is dependent on the turbulent kinetic energy and dissipation rate of kinetic energy. In RNG k- ε method, there are two additional transport equations which are solved to define the turbulent kinetic energy dissipation, ε and turbulent kinetic energy, k for each cell in the simulation. The transport equation for ε is given as,

$$\frac{\partial \rho\varepsilon}{\partial t} + \frac{\partial(\rho u_i \varepsilon)}{\partial x_i} = \frac{\partial}{\partial x_j}\left(\frac{\mu}{\mathrm{Pr}_\varepsilon}\frac{\partial \varepsilon}{\partial x_j}\right) + c_{\varepsilon 3}\rho\varepsilon\frac{\partial u_i}{\partial x_i} + \left(c_{\varepsilon 1}\frac{\partial u_i}{\partial x_j}\tau_{ij} - c_{\varepsilon 2}\rho\varepsilon + c_s S_s\right)\frac{\varepsilon}{k} - \rho R, \tag{2.22}$$

where S_s is a source term used for the spray model to represent interrelation between gas phase and liquid phase. For the work presented here, spray model was not used and hence the source term S_s is zero for all the simulation. For the k- ε RNG model, the R term is defined as

$$R = \frac{C_\mu \eta^3(1-\eta/\eta_0)}{(1+\beta\eta^3)}\frac{\varepsilon^2}{k}. \tag{2.23}$$

In equation (2.23) the η term is defined as,

$$\eta = \frac{k}{\varepsilon}|S_{ij}| = \frac{k}{\varepsilon}\sqrt{2S_{ij}S_{ij}}. \tag{2.24}$$

In equation (2.22), $c_{\varepsilon 1,}$ $c_{\varepsilon 2}$ and $c_{\varepsilon 3}$ are model constants and Pr_ε is the ratio of viscous diffusion to the diffusion of ε.

Therefore, the RANS model presented here represents the effect of increase diffusion rates from turbulences in the system by increasing the thermal and viscous conductivity and not by resolving the structure of eddies. RNS k-ε model solves the transport equation by averaging the flow field variables using ensemble mean method. Thus, the flow field obtained using this model does not represent the instantaneous flow fields which are generally observed in the experiments. For most of the simulations for various applications, the average behavior of turbulence is sufficient to get useful data with comparatively less computational resources and time. Large Eddy Simulation (LES) model resolves eddies without averaging the value of flow field variables and thus accurately captures the turbulence. But LES model is computationally very costly model and generally is not used for simulation where turbulence model is coupled with other models like combustion, spray, energy source model.

2.4. Piston Profile Development

In order to carry out the simulation of the Rapid Compression Machine, having a correct accurate piston profile was very important. To develop the profile, CHEMKIN® kinetic simulation software and pressure traces obtained from the experiment were used. Pressure traces from experimental data were reduced by averaging the data set and was exported to the CHEMKIN pre-processor. The idea behind using the pressure trace was to obtain the volume trace and from the volume trace the piston motion could be obtained.

Experiments were performed on RCM for reacting mixture and non-reacting mixture and the pressure traces were obtained for both the cases using pressure transducer. The pressure traces were almost in accord with each other with slight variation between them as shown in figure 2.4. Hence, to account for those deviations, a mean average pressure trace was develop from the

reacting and non-reacting pressure traces as shown in figure (2.4) which was then given to the CHEMKIN as the input.

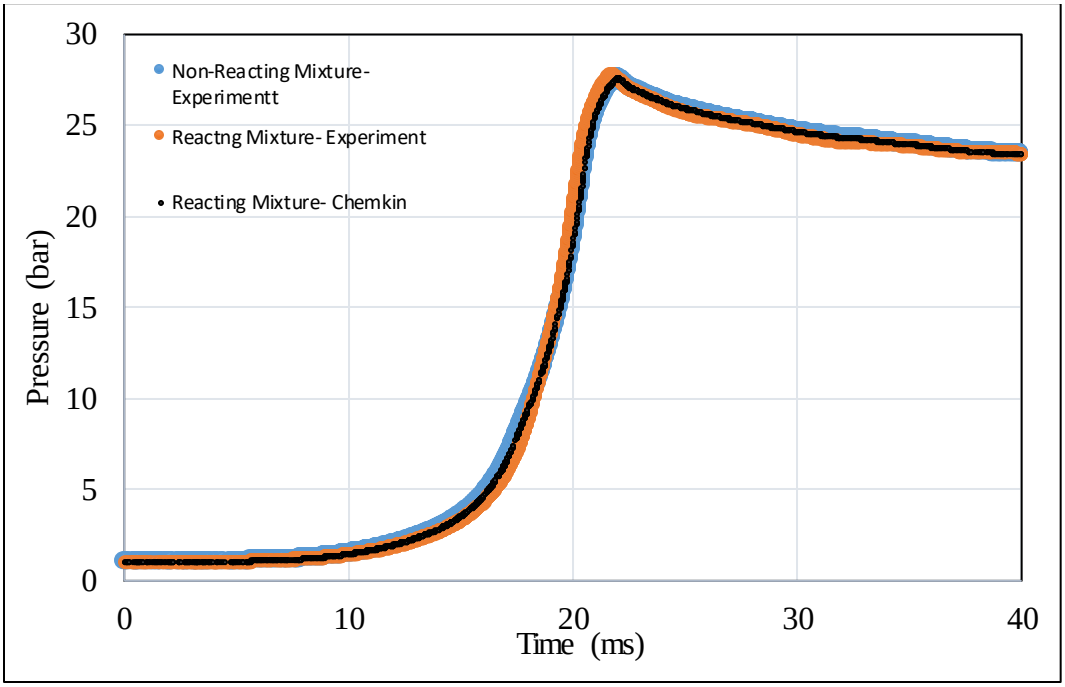

Figure 2.4 Comparison of pressure traces of experimental data and the CHEMKIN input pressure trace.

Zero- Dimensional simulation was carried out with the given pressure trace and the initial conditions where set same as the experimental initial conditions and the volume trace was obtained as shown n figure (2.5). The volume trace obtained was little messy with fluctuations in the values and thus could not be used directly as the input file for the CONVERGE preprocessor. Also, when we look at the volume trace we see that the volume decreases once the piston reaches TDC which is not generally observed in any RCM. CHEMKIN simulation model did not involve the heat loss to the wall which is generally observed for the experiments and hence to replicate the heat loss effect, CHEMKIN model increases the volume after top dead center (TDC) to account for the fall in pressure. CONVERGE simulations accounts for the heat loss to the walls and thus we need not to worry about increasing volume after TDC in case of three dimensional simulations. Since

CONVERGE takes care of the heat loss after TDC, the volume trace from bottom dead center (BDC) till TDC was used to obtain the piston profile. Smoothening was done on volume trace to remove any kind of fluctuations and the piston trace was developed as shown in the figure (2.6).

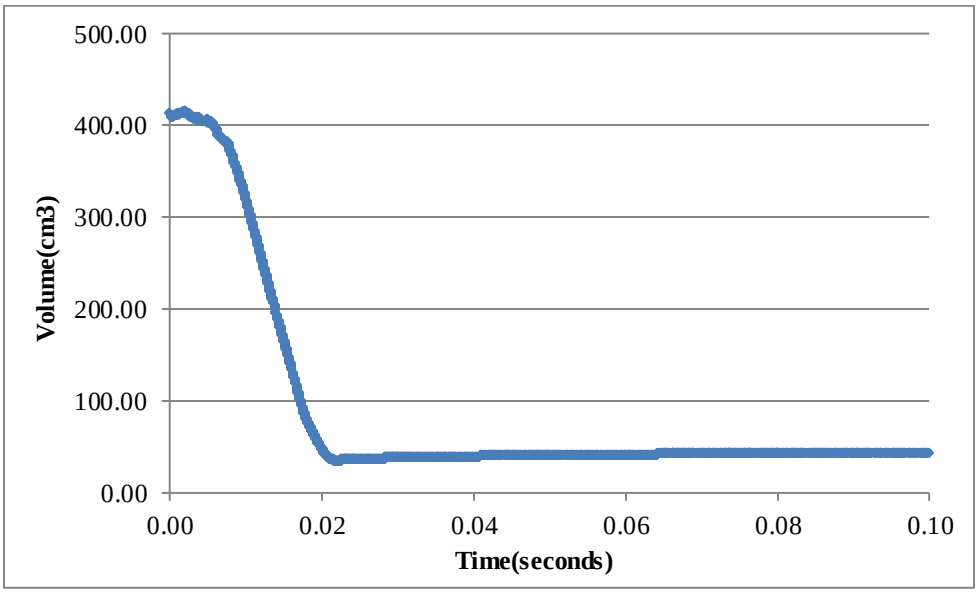

Figure 2.5 Volume Trace of RCM obtained after CHEMKIN simulation

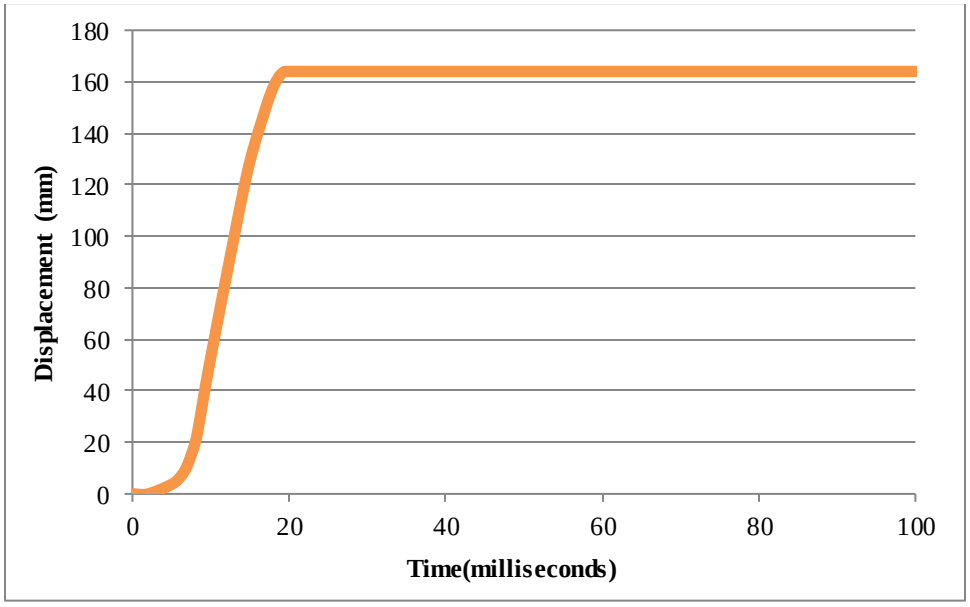

Figure 2.6 Piston Profile for a single piston of RCM

At TDC, the piston stops and stays at that position for the entire simulation thus allowing to maintain a constant volume after TDC as seen in the experiments. A comparison was made with the experimental pressure trace and simulation pressure trace for a stoichiometric mixture of methane/air with 100% argon as inert with initial conditions of 47 degree Celsius and initial pressure of 1 bar and a close agreement was achieved as shown in the figure 2.7.

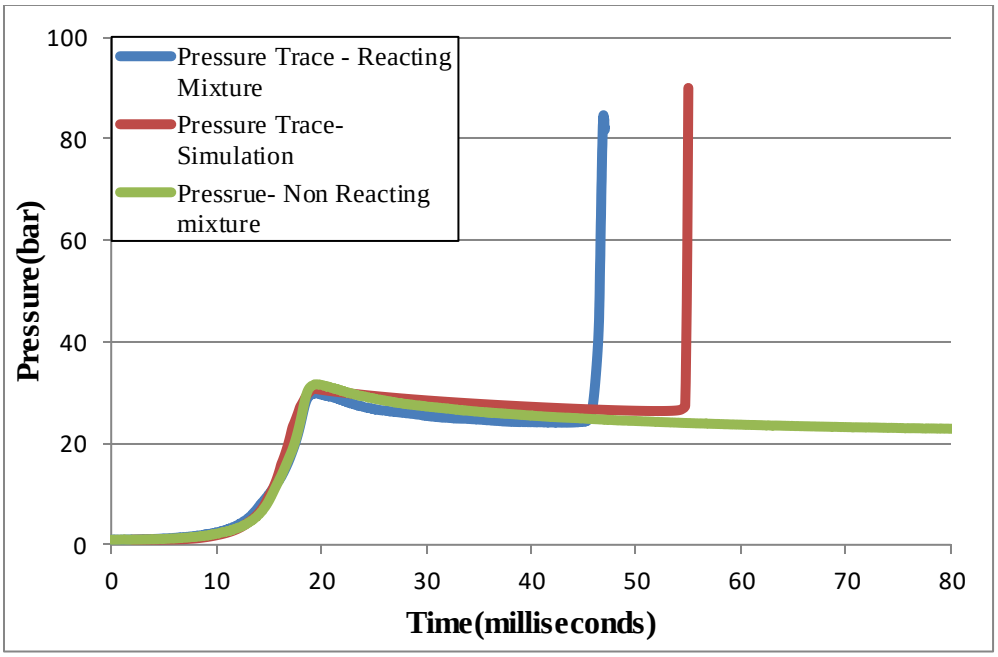

Figure 2.7 Comparison of pressure traces between simulation and experiment

During the experiments, there is lot of variation in the motion of the pistons which results in a little change in the pressure profile for every experimental run and thus the piston profile develop for simulation can deviate a little from the experimental pressure traces but the deviation is within the experimental uncertainty and does not have significant impact on the results interpretation. While developing the piston profile, crevice volume was considered. Crevice volume does not account to be significant at BDC accounting for 1.86% of the total volume but when the piston reaches TDC the crevice volume accounts for 21.51% of total volume.

2.5. Boundary Conditions

Simulation which involved sector geometry, periodic boundary conditions were used at the boundaries where there could be transfer of mass, energy, momentum from one part of the boundary to the other. For the piston, crevice and the piston head boundaries, wall boundary condition was used with wall motion specified as translating and a user input file was given for the motion profile of piston which was developed as discussed in the section 2.4. The outer cylinder wall of RCM was specified as stationary wall. For all the boundaries specified as wall, a law of wall condition was used for the velocity and temperature. In case of a turbulent flow or flow with greater Reynold number, it is very important to resolve the flow up to viscous sub layer to carry out the simulation accurately which is generally not resolved in most of the cases. Law of wall condition is used as a remedy in such conditions which provides a logarithmic curve fit of turbulent boundary layer to determine the tangential components of the stress tensor at the wall.

For κ-ε turbulence model, a standard law of wall with turbulence model based on the work of Launder and Spalding [14] for velocity boundary condition and temperature law of wall model based on the work of Amsden [15] for temperature boundary conditions were used. Both models use a Von Karman constant of 0.419 and a detailed description of these wall functions can be found in CONVERGE^{TM} theory manual [13]. The sector geometry is $1/8^{th}$ of the total geometry and to close the boundary at the TDC by not changing the physics taking place in RCM, a symmetry boundary condition was used which sets the scalar fluxes and velocity at that boundary to zero. In RCM, the physical geometry of interest and the expected pattern of combustion/flow solution have a mirror symmetry which allowed us to use the symmetry boundary condition. The periodic boundary conditions and symmetry boundary conditions helped in carrying the simulation with faster and reduced the computational cost.

2.6. Grid Manipulation

For all the simulations presented in this study, meshing methods like base grid, adaptive mesh refinement (AMR) and fixed embedding were used. Before defining the parameters to coarsen or finer the mesh, a base grid size is required. By specifying the base grid, the entire geometry is meshed with a group of cells whose cell size is determined by user specified grid size. A base size of 4 mm was chosen for most of the simulations presented in this study.

RCM used in this study has creviced pistons to reduce the effects of roll up vortices. To study the effects of roll up vortices which takes place near the piston walls, it is very important to make the mesh finer near the piston faces. Also, law of wall boundary condition is used for temperature condition at piston and cylinder walls which require resolving the mesh to accurately predict the heat loss to the surrounding. Fine mesh was developed near the piston face, crevice and cylinder wall using a technique of fixed embedding as shown in figure 2.8. Crevice is a very critical area where the roll up vortices starts coming into the chamber domain and a very fine mesh was developed near the crevice. Fixed embedding requires specifying a user embedded scale which determines the levels of embedding to be given in the particular region of interest. An embedding scale of crevice was set to 5, scale for piston and the cylinder wall was set to 2 whose influence can be clearly seen in the figure 2.8.

Spark simulation in this study utilized a time varying fixed embedding technique. A spherical fixed embedding was done at the center of the RCM as shown in the figure 2.9. The embedding

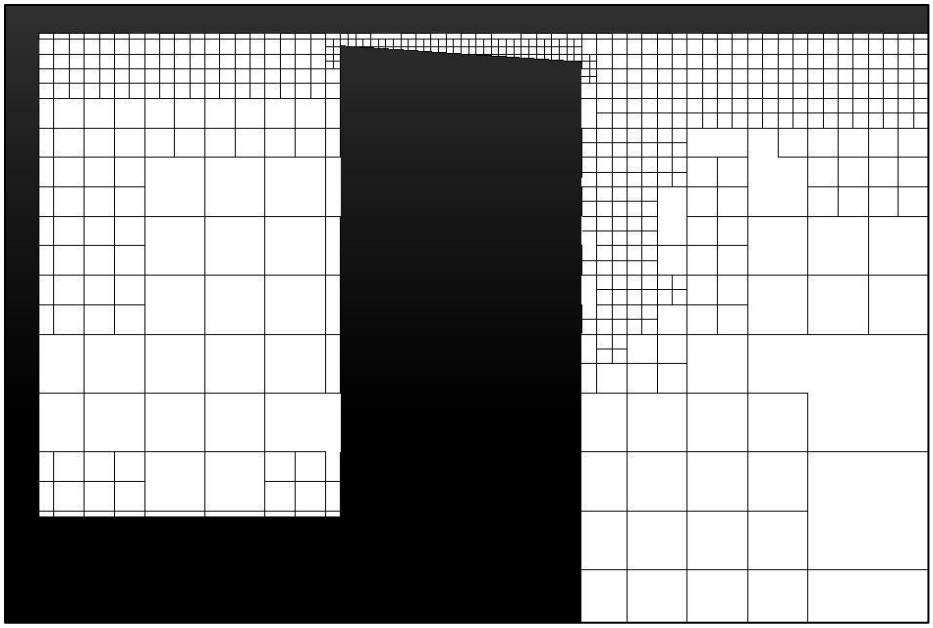

Figure 2.8 Bound fixed embedding at the piston face, crevice and the cylinder wall

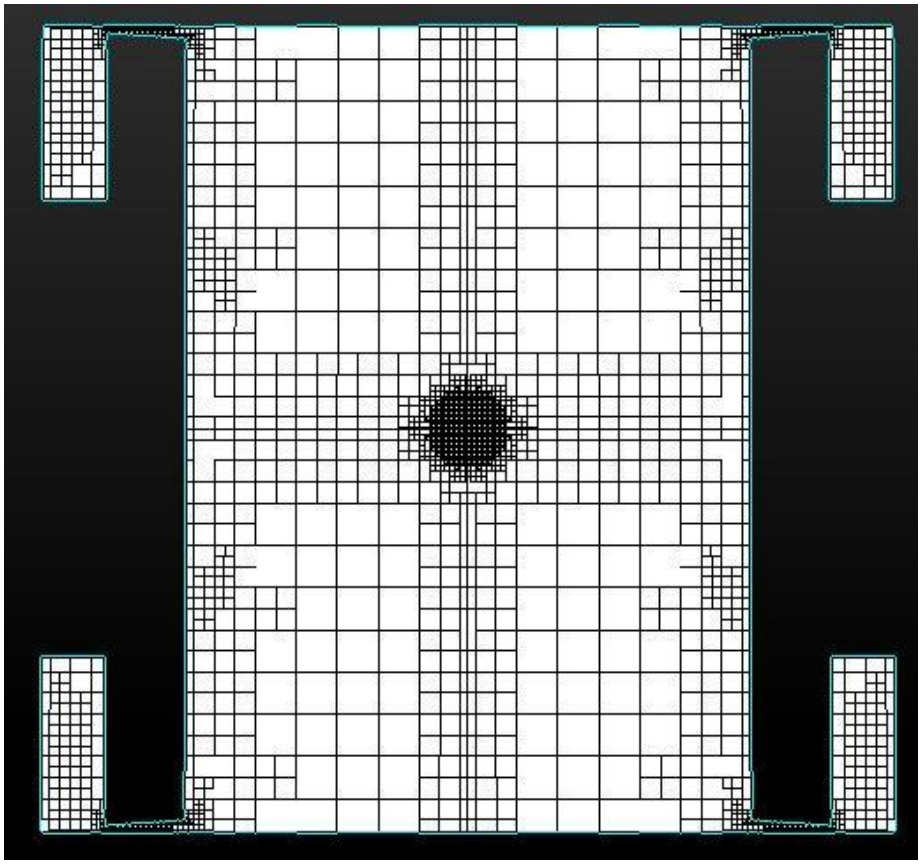

Figure 2.9 Spherical embedding at the center of RCM for spark simulation

was set ON at time just before the spark took place and was switch OFF when the kernel was completely developed. Once the embedding was turned OFF, the care of keeping the mesh fine was taken by adaptive mesh refinement. Adaptive mesh refinement helps in creating a finer mesh by using the field variables such as velocity, temperature, and species. A user defined scaling factor is given in the method for the above flow variables which decides the level of refinement to be done in the area of interest. Adaptive mesh refinement creates a finer mesh when there is a gradient in the flow variables which helps in maintaining the solution accuracy as shown in figure 2.10.

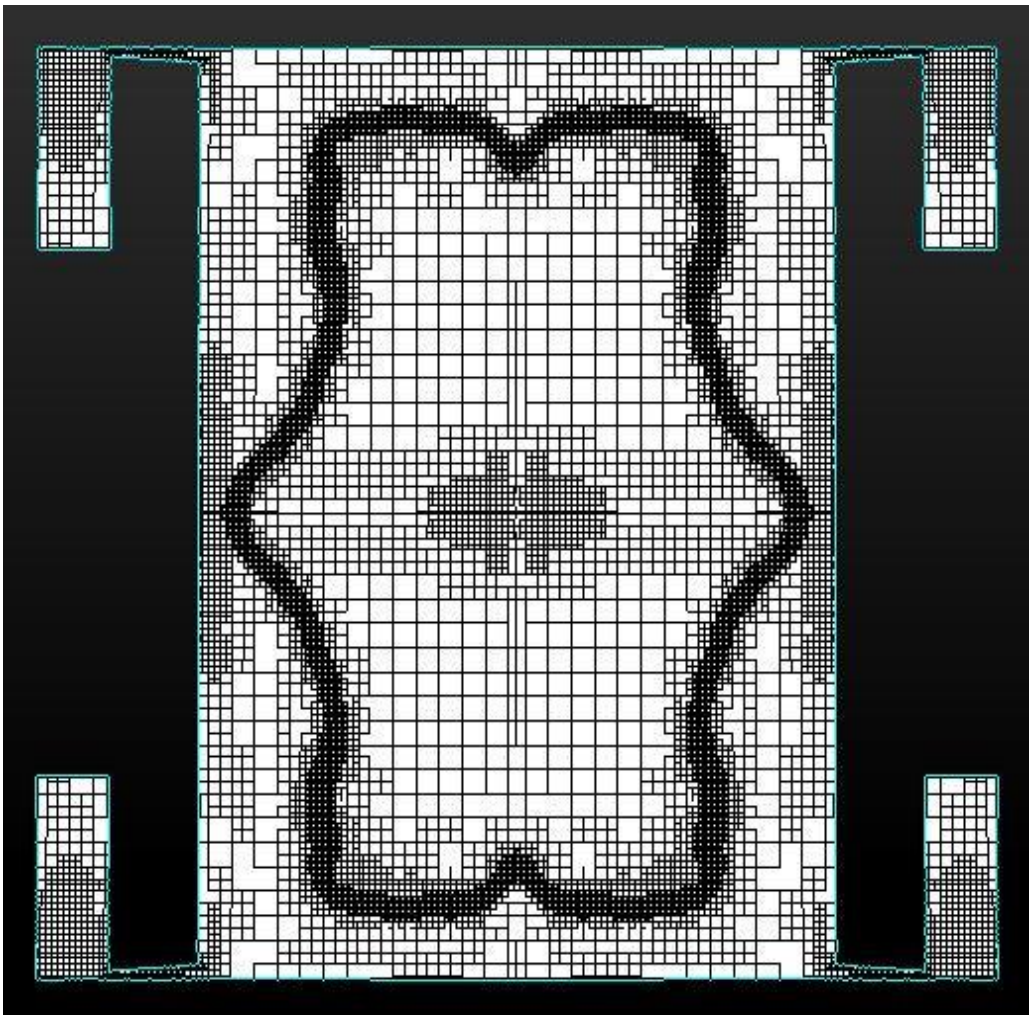

Figure 2.10 Adaptive mesh refinement on the propagating flame

2.7. Chemistry model

For all the simulation presented in this work, SAGE combustion model is being used as the model to solve the chemistry between different species. This model basically allows us to use the chemical kinetic mechanism as input file which is in CHEMKIN format. A CHEMKIN kinetic mechanism file consist set of reactions followed by the rate constants. To accurately replicate the combustion events taking place in the domain, SAGE model also accounts for the third body reactions by specifying the third body efficiency for different species. The SAGE combustion model solves the above elementary reactions to yield the overall chemical reaction rate in the domain while the PISO and turbulence solver solves the transport equations. A threshold of minimum temperature (T_{cut}) and minimum hydrocarbon mole fraction (HC_{min}) is used, below which the chemical kinetics are not solved which helps to save some computational time as during the very low temperature of around 273 K – 600 K, the reaction rates are very low and can be neglected. For all the simulation in this work, the T_{cut} used was 550 K and the HC_{min} was 1e-08. Automatic Mesh Refinement (AMR) which is described in the section 2.8 was used along with the SAGE model to accurately capture the ignition events such as auto ignition in case of premixed mixtures, spark propagation events and also to capture the premixed and diffusion flame propagation event in case of the dual fuel droplet ignition.

Multizone modeling developed by Babajimopoulos et al. [16] is included in the SAGE model to speed up the solving of the chemical kinetic mechanism. In this mechanism, at each discrete time step, cells are grouped together depending on their thermodynamic state and forms a region called zones. Criteria and the method of zoning is described in the CONVERGE theory manual [13]. Once the zones are formed, the SAGE model solves for elementary reactions for those particular zones instead of solving for each cell which helps in reducing the computational time

without compromising on the preciseness and accuracy of the solver. Along with the multizone modeling, CONVERGE has more option which helps in saving the computational time. CONVERGE does not solves for the temperature in a particular cell unless there the change in the temperature in the same cell due to combustion from previous time step exceeds a user specified value which for the current work was set to 2 K.

Reduced chemical kinetic mechanisms where used to solve the reaction rates for each cells for all the simulation work presented. Generally, solving a detailed chemical kinetic mechanism is computationally expensive and generally takes more than 24 hours to finish the multi-dimensional simulation and makes the reduction of chemical mechanism very significant. CONVERGE™ uses a preconditioned iterative solver for chemical mechanisms over 100 species. It also provides a separate model to carry out the mechanism reduction to save computational time. Reduction of the mechanism was carried out using direct relation graph error propagation and sensitivity analysis (DRGEPSA) method which utilizes a set a target species or important species and also a range of temperature, pressure, and equivalence ratio to initialize the reduction process which involves removing of the unimportant species which doesn't affect the ignition delay values more than the user specified tolerances. A detailed explanation of the DRGEPSA algorithm is explained in Chapter 4.

Apart from using the SAGE combustion model, an extended Zel'dovich NOx model developed by Heywood et al. [17] was also used in the simulations to predict the NO formation. The NOx mechanism consists of three equations which uses the chemical rate constants and quasi steady assumption to solve for the NOx formation. The concentration of the NO can easily be converted to NO_2 concentration by multiplying a factor of 1.533.

2.8. Computational Hardware

A local Linux cluster was used for all the simulation carried out in this work. This was a system of high performance processors with each node having 16 cores and 32 MB of RAM. Running of CONVERGE was carried out using HPMPI to handle the parallel processing. Most of the simulation used two nodes and for the dual fuel droplet ignition system three nodes were used.

CHAPTER 3: STUDYING THE ROLL UP VORTICES IN RAPID COMPRESSION MACHINE

3.1. Introduction

A Rapid Compression Machine used here in CSU is a dual opposed piston system that can operate at compressed pressure of about 20 bar to 60 bar, with compressed temperature of 600 K to 1200 K and a compression ratios from ~ 10 -14. Typically, it takes 16 -25 milliseconds for the pistons to reach the top dead center. Basic operation of the RCM is to take in the charge of fuel and air and compress it rapidly via pistons [23]. There are few other methods also used to raise the initial temperature and pressure [24]. In RCM, initial pressure, temperature and mixture composition have an effect on the compressed condition. The heat loss from the RCM walls makes the walls to act as heat sink and become a reason of temperature stratification within the system. All this effects can be neutralized by assuming so called 'adiabatic core region' which allows the gas present in the main core to compressed isentropically[18][19][20]. Adiabatic core region assumption helps in creating a homogenous temperature distribution in the chamber which in turns helps in accurate interpretation of data from Rapid Compression thus helping to design the accurate chemical kinetic mechanism without any disturbance in the flow field.

Reducing the in-cylinder fluid dynamics effects and minimizing the heat loss to the chamber wall helps in accurate interpretation of data. Previous RCM studies depended on flat face piston which generates roll up vortices due to the piston motion which causes the cool boundary layer gases to enter the reacting core disturbing the uniformity of thermodynamic parameters violating the adiabatic core hypothesis. These difficulties are exasperated due to differences in the RCMs which were examined by Goldsborough [21].

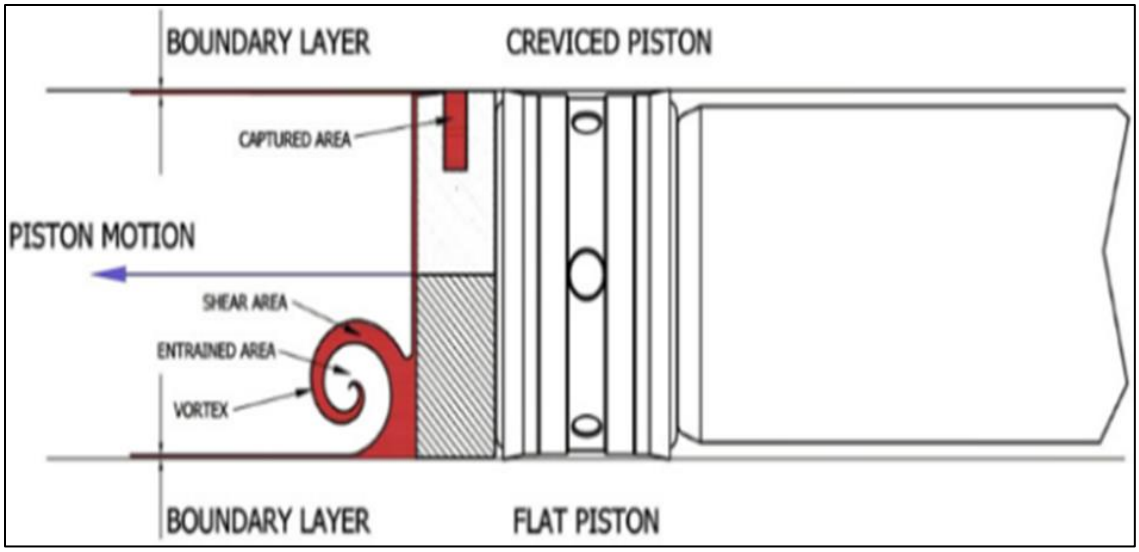

Figure 3.1 Illustration from [23] showing how a flat piston (bottom half) creates roll-up vortices during compression whereas a creviced piston (top half) serves to prevent the cool boundary layer gasses from influencing the core region

In this study, RCM having creviced piston is employed. Piston with crevice helps in reducing the roll up vortices by making the cool boundary layer gases to enter the crevice avoiding the mixing with hot gases present in the adiabatic core region as shown in figure 3.1 and thus allowing a homogeneous temperature profile within the chamber validating the adiabatic core assumption. Mittal and Sung [22] used acetone planar laser-induced fluorescence(PLIF) to find the temperature profile of both creviced and flat face pistons and validated the adiabatic core assumption.

In this study, multi-dimensional computational fluid dynamic (CFD) model of RCM is used to characterize the roll up vortices. RCM with different crevice size pistons were computationally studied to understand the physics forming and reducing the roll up vortices.

3.2. Computational Details

Computational model used here follows the same models discussed in Chapter 2. Turbulence model was used to capture the roll up effects (if any) and combustion model was turned off to save

the computational time and space. Law of wall was used as heat transfer model for the walls which refines the boundary layer for precise prediction of heat transfer. Adaptive mesh refinement and fixed embedding techniques were used to generate fine mesh near the walls of the chamber which helped in accurate interpretation of the roll up vortices present in the chamber during compression stroke of the pistons. The domain was initialized with methane/air mixture having equivalence ratio of 1.0 with 100% argon as inert with initial temperature of gases and walls as 323K.

3.3. Results

The effects of roll up vortices on temperature distribution and the flow field in the domain during the induction time when there is heat loss taking place to the surrounding were studied using the piston with different crevice lengths of 3 mm, 4 mm and 5 mm. To quantify the vortices that are produced and to find out the energy content in those eddies, plots of turbulence length scale for different crevice lengths were studied which is as shown in figure 3.2. Turbulence length scale is a physical quantity which describes the size of eddies in turbulent flows and acts as an indication of the energy content present in those eddies.

As seen in the above figure, in case of a 3mm crevice piston, the low temperature gas first moves into the crevice volume and since the volume available for the gases inside the crevice is less, there is a back flow taking place resulting in larger eddies with higher energies thus resulting a greater mixing of cold gases with the hot gas which disturbs the uniformity of the temperature violating the adiabatic core assumption. But as we increase the crevice volume by increasing the length, the roll up vortex intensity starts going down as the cold gas now is getting enough space in the crevice to stay there and only small fraction of cold gases mixes with the hot gases in the chamber domain. So, in case of 4 mm crevice piston, there is still a little roll up vortex disturbing

the thermodynamic parameters but with the 5 mm crevice piston, cold gases stay in the crevice volume thus making the roll up effect negligible as shown in figure 3.2 (c).

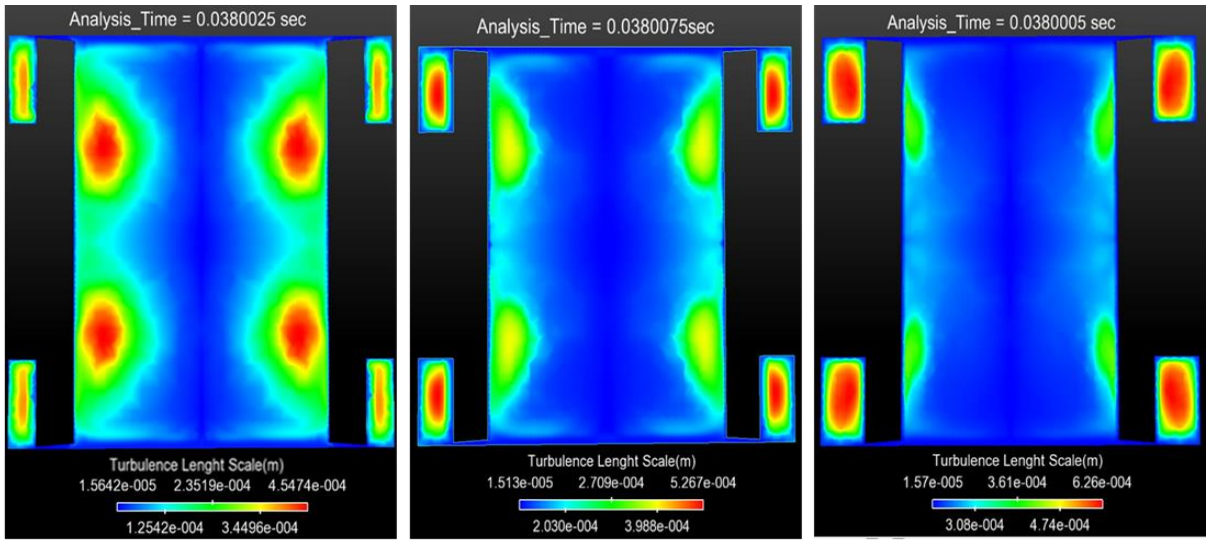

(a) (b) (c)

Figure 3.2 Contour of turbulence length scale (a) 3mm crevice piston (b) 4 mm crevice piston (c) 5 mm crevice piston

The effect on the temperature distribution is as shown in figure 3.3. It clearly shows a homogenous temperature distribution in case of the 5 mm crevice piston which validates the assumption of adiabatic core. The fall of temperature around the wall of pistons shown in figure 3.3 (c) is mostly by the heat loss to the walls and a negligibly amount by small eddies which are still able to enter the chamber domain and thus making interpretation of data taken from Rapid compression machine very reliable.

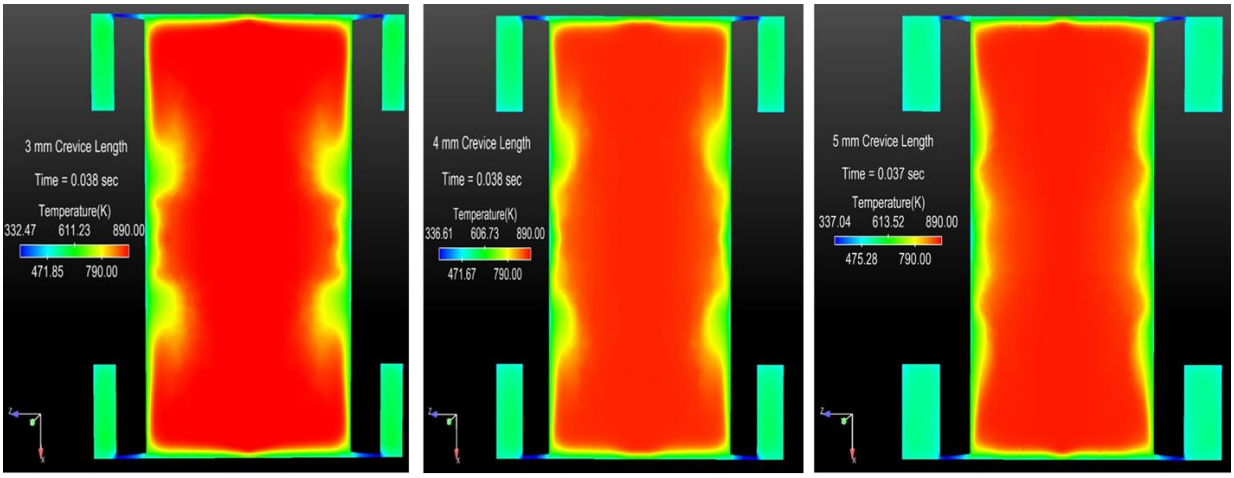

(a) (b) (c)

Figure 3.3 Contour of Temperature (a) 3mm crevice piston (b) 4 mm crevice piston (c) 5 mm crevice piston

3.4. Conclusion

For accurate interpretation of data taken from the Rapid Compression Machine, it is very important to design the pistons of RCM very carefully. Introduction of crevice design in piston has helped a lot in reducing the roll up vortices which requires a proper design. If the crevice volume is increase it causes a greater cooling effects as most of the fuel enters the crevice volume and if the crevice volume is small than it results in causing the roll up vortices causing it to disturb the adiabatic core assumption.

Roll up vortices also have an adverse impact during the flame propagation. As the roll up causes the mixing of the cold and hot gases, it results in the localized temperature drop near the piston boundaries. This falling temperature and the vortices present causes the flame to move slowly as the temperature is low affecting the flame speed. Sometime the temperature may fall below the flammability limit of the fuel/air mixture which causes the flame to quench near the piston wall affecting the results desired. So, to get rid of the unwanted effects and interpret the data accurately from RCM, a careful designing of the RCM piston is required.

CHAPTER 4: REDUCED CHEMICAL KINETIC MECHANISM FOR SIMULATION OF ISO OCTANE/AIR AUTO IGNITION SYSTEM

4.1. Introduction

Simulating a comprehensive combustion kinetic model involves a large number of species and reactions. Carrying a simulation which involves combustion chemistry coupled with the other phenomenon such as mass transfer, heat transfer and gas motion, the computational model becomes more computational expensive and increases the computational time. Generally, the computational time is directly proportional to N^2 where N is the number of the species involved in the combustion kinetic model [13].

Computational models involving fluid dynamics and combustion effects can be made computationally efficient by reducing the number of the species and reactions involved in the kinetic mechanism by maintaining the computational accuracy. Converge™ software carries out reduction of mechanism in a zero-dimensional environment where the validation of the reduced mechanism is achieved by comparing the output of the reduced mechanism at various different steps of reduction with the comprehensive mechanism. By carrying tests at different thresholds, a quantitative agreement is achieved between the reduced and comprehensive model and the precision with which the agreement is established drives the extent up to which the reduction can be carried out with optimal number of species.

Converge™ software uses a method called direct relation graph error propagation algorithm and sensitivity analysis (DRGEPSA) for carrying out the reduction of the mechanism in which the species which do not contribute significantly in the reaction model or the species which are

considered unimportant are removed from the mechanism. With the removal of the species, the reactions that are associated with those species are eliminated.

4.2. Direct Relation Graph Error Propagation and Sensitivity Analysis (DRGEPSA)

To understand the DRGEPSA method, we first need to understand the basic model of direct relation graph (DRG), DRG with error propagation (DRGEP) and finally the sensitivity analysis on the DRGEP. In DRG method developed by Lu and Law (2005), each species involved in the mechanism represents a vertex and linkages connect the species to each other as shown in figure 4.1. The link between the species A and species B remains if the removal of the species B induces a significant error in the production rate of species A. The effect on the production rate is measured by introducing a normalized co-efficient r_{AB} which is shown on the top of the linkage in figure 4.1.

DRG method read the file containing the chemical kinetic mechanism and arranges the species present in the file as a vertex and links each of the species using linkages. Once the link is established, the DRG method takes a user defined tolerance or a threshold which is used to reduce the mechanism. Figure 4.1 represents a simple DRG model with the number over the linkages represents the normalized co-efficient for each of the linkage. A user specified tolerance selected for a demo reduction is 0.15.

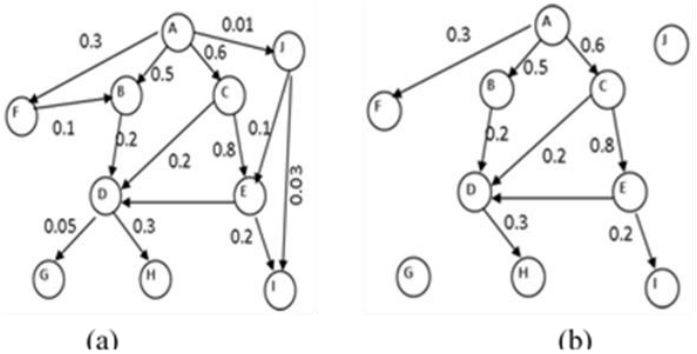

Figure 4.1(a) Base mechanism before DRG, (b) Reduced mechanism obtained after DRG method with threshold of 0.15 [13]

Species G and J are having a lower coefficient value compared to the user defined threshold and hence were removed from the base mechanism as shown in figure 4.1.b during DRG reduction. In this method, the species are removed based on the influence of that particular species with the immediate species with which it is linked. But while removing the species and the reactions associated with it, a relationship between the species which have an indirect influence on the production rate of other species should be considered important to reduce the error while reducing the mechanism. This relation is considered in Direct Relation Graph Error Propagation method using a path dependent co-efficient $R_{AB,i}$, where R_{AB} is defined as the product of normalized contributions of species A and B along the path i where the path dependent co–efficient is maximum and the reduction is carried out using the same principals of DRG method by comparing the path dependent co efficient with the threshold value specified by the user.

DRGEP method coupled with the sensitivity analysis (DRGEPSA) helps in yielding an accurate reduced mechanism. Figure 4.2 shows the work flow taking place in the DRGEPSA method. DRGEPSA method requires user specified values for pressure, temperature and equivalence ratio which are used as the conditions for the first step of the analysis which is to run the auto ignition simulations for different cases. A set of data points are selected for each case along the integration curve at 10 K temperature difference time intervals for which DRGEPSA coefficients are calculated and several cut off tolerances are established. Skeletal mechanism is developed for each cut off value and auto ignition simulations are carried out on each of the skeletal mechanism. Ignition delay values obtained for various skeletal mechanisms are compared with the detailed comprehensive kinetic mechanism and a final mechanism is chosen from a set of various skeletal mechanisms in such a way that the final skeletal mechanism has less number of species and the ignition delay time error values are well within the user specified limits.

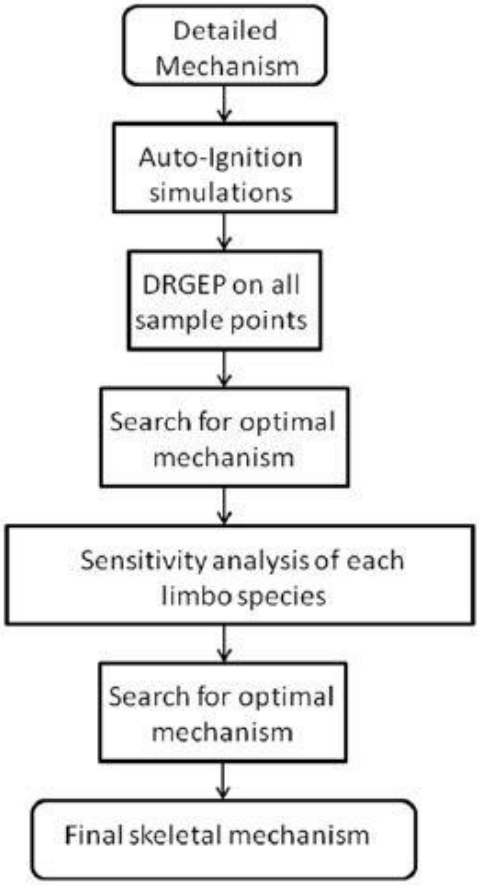

Figure 4.2 Work flow of DRGEPSA analysis [13]

Sensitivity analysis is carried out on the final optimum reduced kinetic mechanism obtained using DRGEP method to further reduce the number of species and reactions where the species are first arranged in the ascending order based on their values of DRGEP coefficients. A fixed number of species from the top of the list is selected for the sensitivity analysis and are designated as limbo species. These limbo species are now removed one by one from the final skeletal mechanism to study the error it induces on the ignition delay time values which is an indication of the sensitivity of that particular species in predicting the ignition delay. Later, the species are again arranged in ascending order based on the value of the ignition delay error value and each species is removed from the top one by one until the error induced by removing the species is less than the user

specified tolerance. Using this reduction model, a reduced chemical kinetic mechanism was developed for iso-octane which is discussed in detail in section 4.3.

4.3. Computational Details

The base comprehensive chemical kinetic mechanism used for the reduction was Henry Curran's Iso- octane version III [25] mechanism which consisted of 893 species and 3600 reactions. This chemical kinetic mechanism was tested and validated by comparison with number of experiments performed using the shock tube and rapid compression machine. This mechanism behaves well at both high and low temperature for various range of pressure generally observed in the internal combustion machine. Table 4.1 shows the details specified for carrying out the reduction using DRGEPSA.

Table 4.1 User specified parameters given to DRGEPSA model.

Base detailed mechanism	LLNL iso-Octane Version 3
Target species	IC8H18, O2, AR, OH, IC4H8, C3H6, CH3, CH4, CO, H2O2, H, IC4H7O, H2
Fuel composition (mole fraction)	$X_{IC8H18} = 0.0165$
Temperature (K)	$600 < T < 1200$
Pressure (bar)	20,24, 26, 28,30
Equivalence ratio, φ	1.0, 0.5,0.7
Ignition delay tolerance (%)	0.3
Sensitivity analysis fraction	0.15

Rapid compression machine replicates a single compression stroke of internal combustion engine with pressure varying from 20 bars to 30 bars depending upon the mixtures used and a temperature ranging from 600 K to 1200 K. Therefore, the conditions represented in the table 4.1 were chosen so as the reduced mechanism developed will have a good behavior with RCM's thermodynamic conditions. Once the conditions were given to the mechanism reduction solver, the reduction was carried out using DRGEPSA mechanism.

4.4. Results

A reduced mechanism was successfully developed consisting of 159 species and 805 reactions. A zero-dimensional ignition delay calculation was carried out for reduced mechanism and was compared with the comprehensive mechanism for the pressure of 20 bars, 24 bars, 30 bars and temperature varying from 600 K to 1000 K at different equivalence ratio using CHEMKIN^{TM} software as shown in figure 4.1, figure 4.2 and figure 4.3.

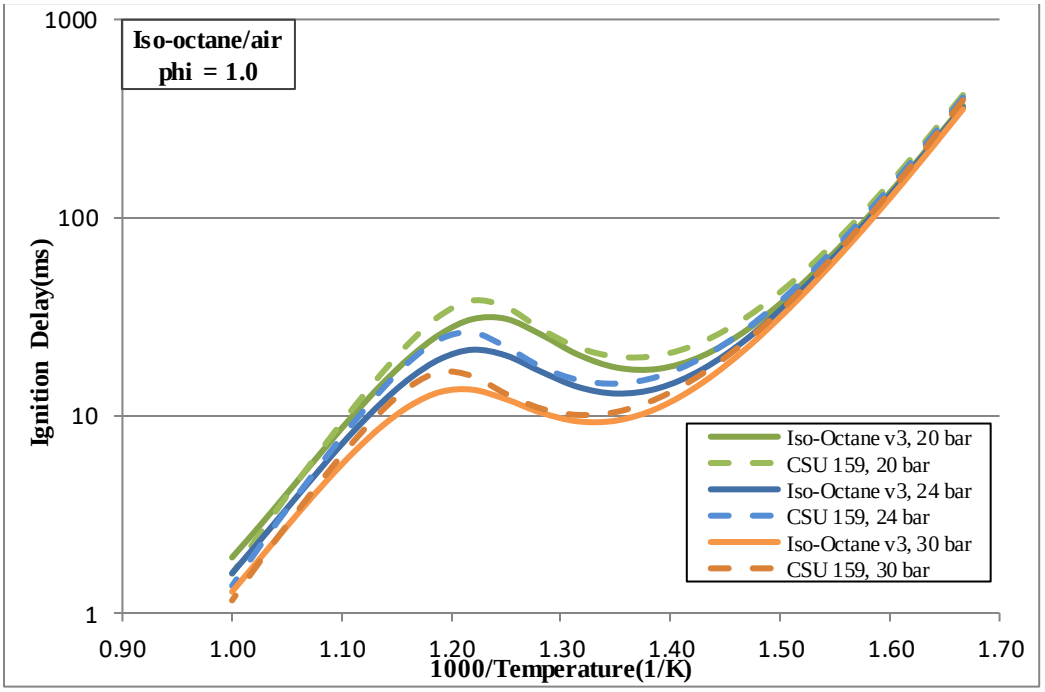

Figure 4.3 Ignition delay comparison between 159 species reduced mechanism and comprehensives 893 species mechanism at equivalence ratio of 1.0

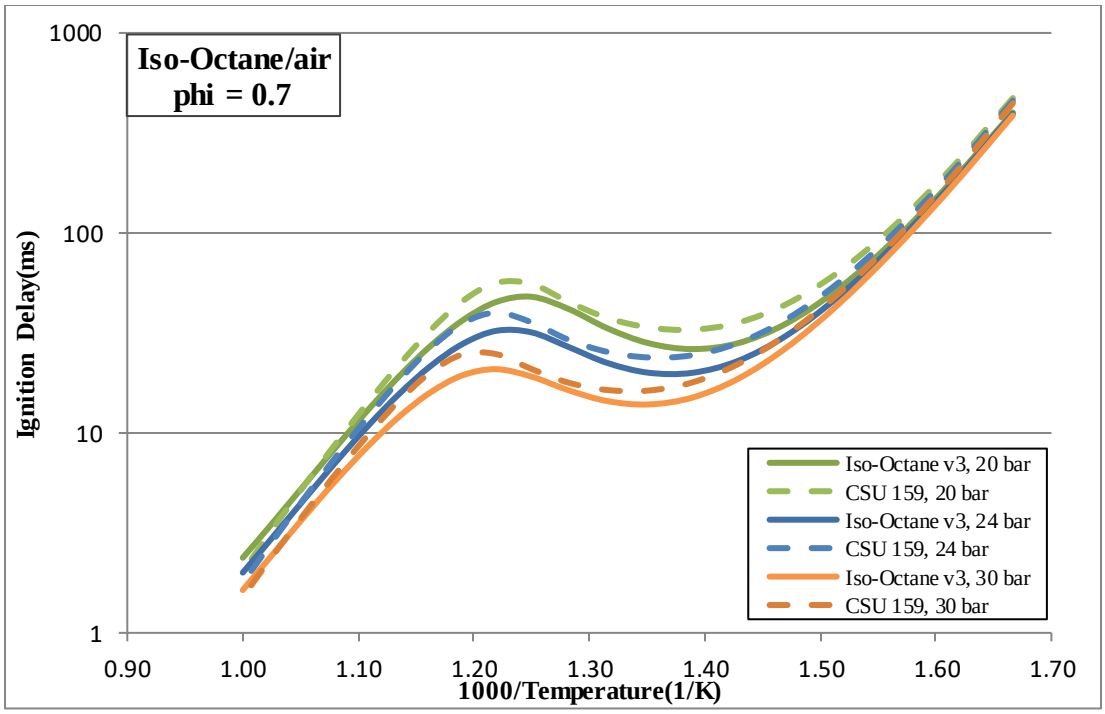

Figure 4.4 Ignition delay comparison between 159 species reduced mechanism and comprehensives 893 species mechanism at equivalence ratio of 0.7

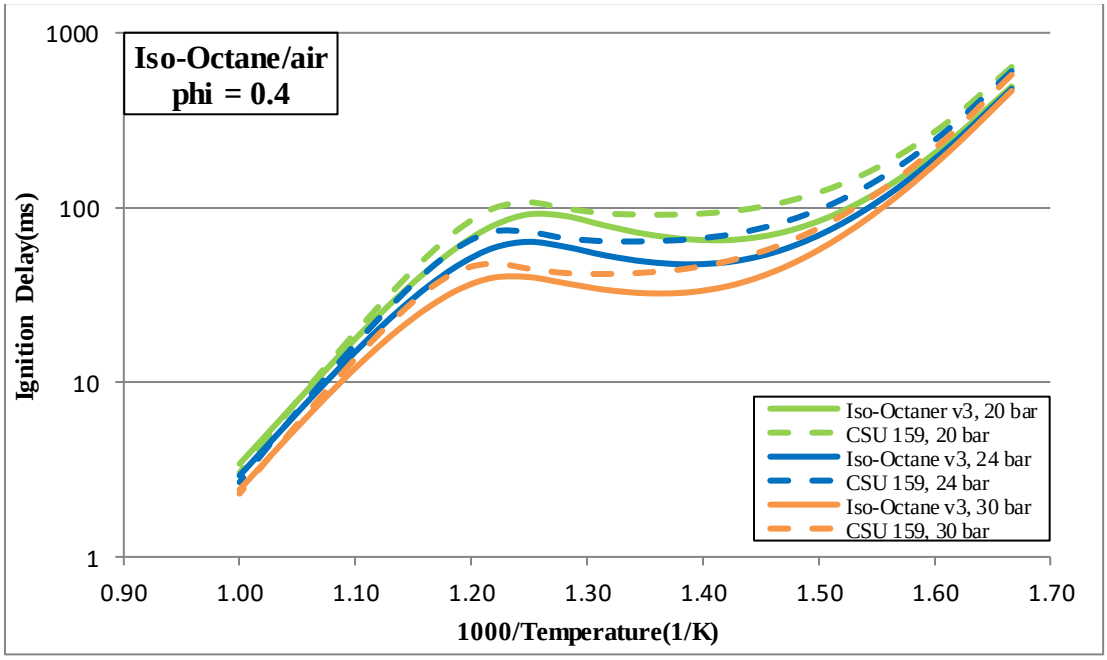

Figure 4.5 Ignition delay comparison between 159 species reduced mechanism and comprehensives 893 species mechanism at equivalence ratio of 0.4

Studying the above plots, 159 species reduced mechanism has a very agreement with the comprehensive Iso-octane version 3 mechanism for all the conditions of pressure, temperature and equivalence ratio. Along with the high temperature chemistry, the chemical kinetic mechanism also included the low temperature chemistry which allowed us to capture the low temperature heat release by capturing the negative temperature coefficient region. Also, studying the above plots, we found that a very good agreement between the reduced mechanism and the detailed mechanism was obtained for the cases of higher equivalence ratio. But at lower equivalence ratio, for low temperature of 600 K to 750 K and high temperature of 1000 K to 1200 K a good agreement was achieved. There was a small ignition delay difference for the temperature interval of 750 K to 1000 K where the NTC region of iso octane lies, and could still be considered as a good agreement considering the amount of the reduction that has been carried.

This developed 159 species reduced mechanism was used to carry out the multi- dimensional simulations of RCM to validate the chemistry of premixed homogenous autoignition of iso octane/air taking place in the RCM which is discussed in Chapter 5.

CHAPTER 5: VALIDATION OF CHEMSITRY IN RAPID COMPRESSION MACHINE

5.1. Introduction

After studying the physics taking place in the RCM in chapter 3, it was very important to study and validate the chemistry taking place in RCM. RCMs are design to study the auto ignition phenomenon of hydrocarbons at different conditions of temperature, pressure, equivalence ratio and the ignition delay values obtained from the RCM are used in validating the chemical kinetics typically used for zero dimensional and multi-dimensional CFD simulations. Presented herein is the auto ignition study of iso- octane/ air and methane/air mixtures at various different pressure and temperature conditions. The chemical kinetic mechanism used for the above study was 159 species reduced mechanism developed as discussed in chapter 4 and CSU 86 mechanism which was validated with laminar flame study and zero-dimensional analysis and was tested in a dual fuel engine experiments. Therefore, zero dimensional and multi-dimensional auto ignition study using above chemical kinetic mechanism served as a validating tool for the chemistry taking place in RCM.

5.2. Auto Ignition Study of Iso – Octane/Air mixtures

The chemistry of Iso octane or 2,2,4- trimethyl pentane is studied by many scientists due to the fact of its knock reducing tendency when blended with the gasoline surrogate and this developed a method of octane number scaling which helps in quantifying the knocking tendency of fuel. This draw our attention in studying the chemistry of iso – octane by performing auto ignition experiments using RCM and the validation of experimental data was carried out by performing zero dimensional and multi-dimensional CFD analysis.

5.2.1. Experimental setup

A stoichiometric mixture of iso- octane/air was used for conducting the experiments at different temperature and pressure conditions. The initial pressure and temperature used in the experiments was 1 bar and 300 K and was used as the baseline for all the cases. The pressure obtained after the compression stroke was around 26 bars to 29 bars and the temperature at the TDC was varied by adding inert argon gas at different concentrations. Typical temperature range obtained at TDC by adding argon is from 600 K to 900 K. For each compressed temperature data, the experiments were repeated three to five times and the average value of ignition delays are obtained for different conditions which are typically plotted using logarithmic scale for y axis and the temperature was on the x-axis represented as 1000/Temperature as shown in figure 5.1.

An initial chemistry check was done on the experimental values obtained from the RCM by comparing the ignition delay values with those published in literature. Experimental results were compared with the work of Goldsborough's study of Iso – Octane ignition delays obtained using shock tubes and RCMs across a wide range of pressures and temperatures. Goldsborough collected the data from various RCMs and shock tubes which does not have a standardized design and hence the data collected by him was spread over different pressures and temperatures and thus, Goldsborough normalized the ignition delay data to two pressure values of 10 atm and 45 atm and compared the data over the varied range by creating two trend lines which bounds the results from different facilities [26]. CSU RCM produces a pressure of 26 bar to 28 bar which means that the ignition delay values obtained using this RCM should exactly lies between the 10 bar and 45 bar which is what we observed as shown in figure 5.1. This provided the initial verification of the RCM.

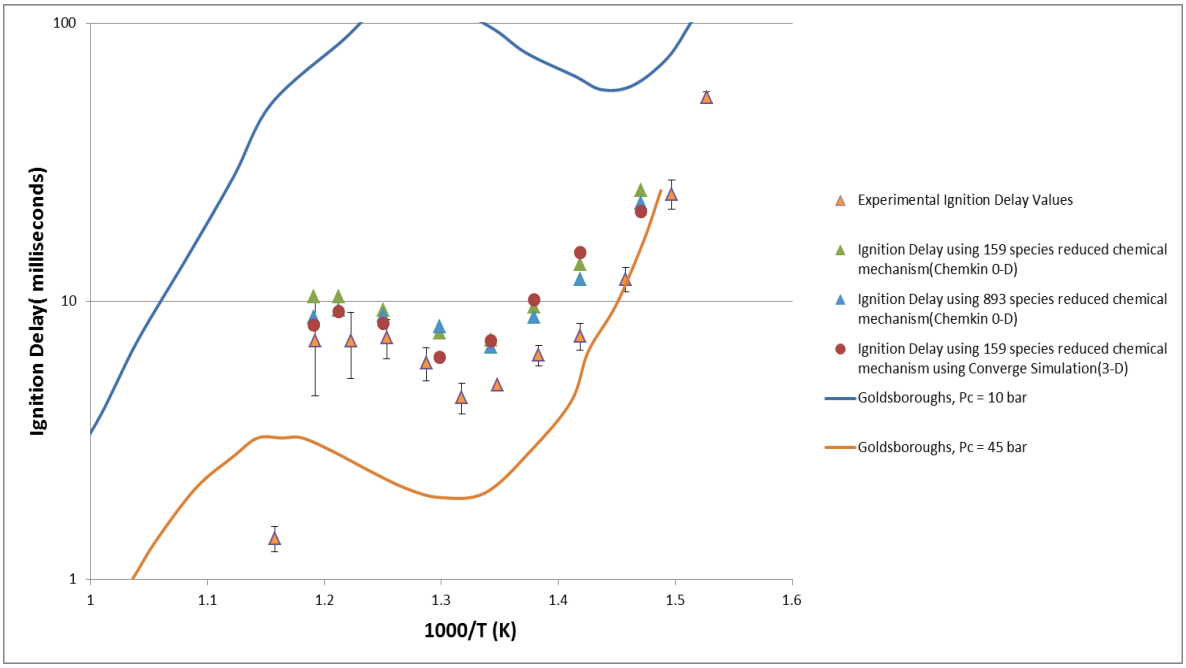

Figure 5.1 Isooctane Ignition Delay Curves

5.2.2. Zero dimensional CHEMKIN simulation model

CHEMKINTM software was used to carry out the zero-dimensional ignition delay study. The zero-dimensional analysis was carried out using a constant volume reactor model where the initial conditions where set as the conditions obtained after the compression stroke of the piston (i.e. conditions at TDC). Previous work shows us that the data obtained using the constant volume simulations are reasonable with little fluctuation in the ignition delay compared to the solution obtained using varying volume simulation [27]. Also, a constant volume simulation is advantageous as it saves the computational time and allows the investigations of various different experimental conditions such as compressed temperatures and pressures, fuel compositions. The initial conditions given to the zero dimensional CHEMKIN model was taken from the TDC conditions obtained using CONVERGE multi-dimensional simulation model which is discussed in the section 5.2.3. A 159-species chemical kinetic mechanism and Iso - octane version III mechanism consisting of 893 species was used for the zero-dimensional study of autoignition.

Comparing the zero-dimensional ignition delay values with the experimental values, it shows that the zero dimensional values have a good agreement with the experimental values which lies a little above the experimental values as shown in figure 5.1. The possible reason for the zero dimensional models reading a little above the experimental value could be the chemical kinetic mechanism is not accurate enough to capture the chemistry of the iso-octane taking place or could be some errors associated with the experiments such as loss of mass during the compression stroke.

5.2.3. CONVERGE multi-dimensional model

The zero dimensional models didn't include the heat loss taking place at the cylinder walls which generally takes place in the experiments. Hence to replicate accurate experimental conditions, a multi-dimensional modeling of RCM was done using CONVERGE. RCM's 1/8th geometry was used for the simulations and the conditions used for the simulation was same as the experimental conditions. The other advantage of using the multi-dimensional analysis is its ability to visualize the chemistry taking place in the RCM which is not possible in case of experiments due to some constraints and limitations. A heat model was also used to account for the heat losses to the walls. A fine meshing was developed near the walls of piston and cylinder in order to accurately replicate the heat loss using law of wall boundary conditions as discussed in chapter 2 which also describes the other boundary conditions given for this simulation. Comparing the multi-dimensional ignition delay with zero dimensional and experimental data, a good agreement was seen between the multi-dimensional ignition delay and zero-dimensional ignition delay. Experimental ignition delay values fall little below the simulation values at lower temperature with average ignition delay difference of 4 milliseconds. But in the higher temperature region at and after crossing the NTC region, an excellent agreement was obtained as shown in figure 5.1.

It can also be seen from the pressure trace of the simulation shown in figure 5.2 and from the experiment that once the piston reaches the TDC, there is an induction time where the pressure goes down by a small amount due to the heat loss to the wall followed by two stage ignition event. The first stage ignition is a low temperature heat release event which causes a small rise in the pressure and temperature. This event last short due to the fact that as the temperature of the mixture increases, the mixture enters the NTC region of Iso- Octane explosion limit. This is the region where the reactivity of the fuel decreases with rise in temperature. Due to this phenomenon, the heat release decreases as gas travels through the NTC region which results in plateauing of the pressure trace. But as the gas comes out of the NTC region, the pressure shoots up which marks the second stage ignition of Iso- Octane. In this stage, high temperature heat release takes place which auto-ignites the entire gas resulting to a high pressure rise as shown in figure 5.2. After maximum pressure is reached, the pressure trace starts falling steeply due to the heat loss to the walls.

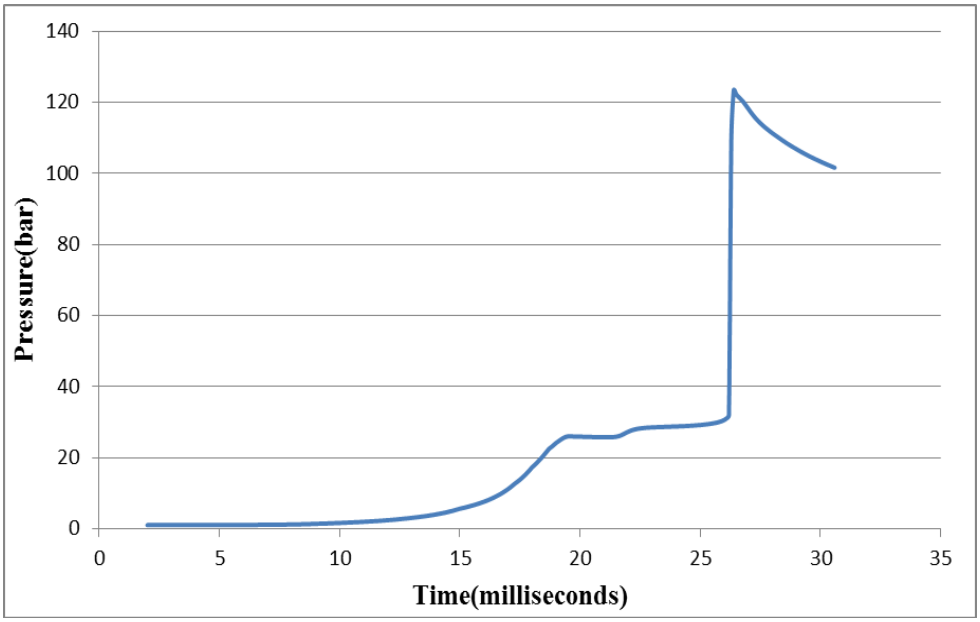

Figure 5.2 Pressure Trace from simulation of stoichiometric iso-octane mixture at a compressed temperature of 782 K

Heat Release Contours were developed and it clearly shows the low temperature heat release and high temperature heat release phenomenon as shown in figure 5.3. The analysis time shown in the figure 5.3 corresponds to the time of simulation. Heat Release Rate is expressed in W/mm^3. During the high temperature heat release, the gas present near the wall does not get ignited instantly because of the low temperature region created by the roll up vortices coming from the crevice of the piston.

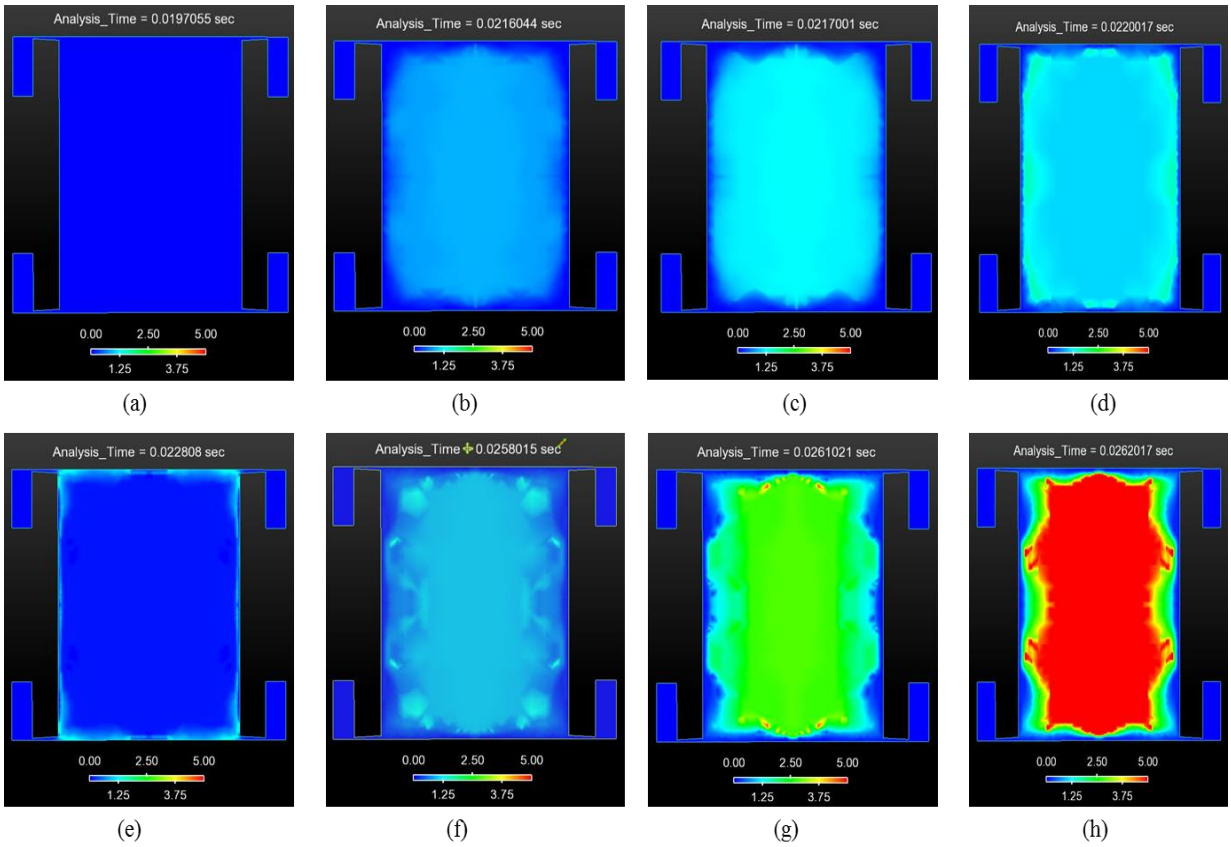

Figure 5.3 Heat Release Contours of auto ignition of stoichiometric mixture of iso-octane in RCM with compressed temperature of 782 K

5.3. Auto Ignition Study of Methane/Air mixtures

For having a second validation over the chemistry, experimental and computational study where carried out using methane/air mixtures.

5.3.1. Experimental Setup

A stoichiometric mixture of methane/air was used for conducting the experiments at different temperature and pressure conditions. The initial pressure used in the experiment was 1 bar and instead of using nitrogen as the inert, 100% argon was used to achieve a high enough temperature for methane to auto ignite. The pressure obtained after the compression stroke was about 31 bars and the temperature at the TDC was varied by varying the initial temperature of the mixture. For each compressed temperature data, the experiments are repeated three to five times and the average values of ignition delay are obtained for different conditions which are typically plotted using logarithmic scale for y axis and the temperature was on the x axis represented as 1000/Temperature as shown in figure 5.4.

5.3.2. Zero Dimensional CHEMKIN computational model and CONVERGE Multi-Dimensional Model

CHEMKINTM^{TM} software was used to carry out the zero-dimensional ignition delay study in the same way as we used for iso-octane. The zero-dimensional analysis was carried out using a constant volume reactor model where the initial conditions where set as the conditions obtained after the compression stroke of the piston. A zero-dimensional analysis was carried to find a suitable mechanism for three-dimensional computational study of methane/air mixture which could predict close to the experimental values with less number of species and reactions involved to carry out the simulation with less computational cost and time. We started with a 19 species and 84 reactions mechanism called MD 19[28] and did a zero-dimensional simulation with initial pressure of 31 bars and temperature varying from 600 K to 1000 K. The ignition delay differences predicted using MD-19 mechanism was much higher as compared to the experimental value as

shown in the figure 5.4 and hence was not selected for this study. GRI-Mech 3.0[29] mechanism designed by University of California, Berkeley having 53 species and 125 reactions was picked and zero-dimensional analysis was performed. Results were still not improved compared to the experimental values. NUIG_NGM mechanism [30] developed by combustion chemistry center, NUI Galway with 229 species and 1359 reactions reduced the ignition delay but still the difference between the ignition delay values was large enough to use for the multi-dimensional simulation.

LLNL v3.1[31] developed by Lawrence Livermore National Laboratory with 561 species and 2539 reactions and NUIG lll [32] developed by NUI Galway with 292 species and 1593 reactions had a close match with the ignition delay obtained in the experiments with the values obtained using simulations being little higher than compared with the experiments as shown in figure 5.4. The above two mechanisms have a good agreement with the experimental values and proves its potential to be used in the multi–dimensional study. But using the above mechanisms will make the computations expensive and time consuming since the mechanisms have a large set of species and reactions. Now it was very important to have a reduced mechanism with less number of species and reactions behaving in accord with the above two reaction mechanism. CSU 141[33] and CSU 86[34] mechanism developed by Colorado State University utilized NUIG 3 and LLNL v3.1 mechanism as their base mechanism for reduction. The two mechanisms were reduced using DRGEPSA analysis as discussed in Chapter 4. After reduction, both the mechanisms were combined and reduced mechanisms were obtained. CSU 86 mechanism has 86 species and 394 reactions and CSU 141mechanism has 141 species and 709 reactions which behaves in accordance with their base mechanism as shown in figure 5.4.

Since CSU 86 and CSU 141 mechanism has almost same ignition delay values, CSU 86 mechanism was chosen to carry out the multi-dimensional analysis to save the computational time.

Multi- dimensional analysis was carried with the same initial conditions used for zero dimensional conditions. Comparing the multi-dimensional ignition delay with the experimental values, we find that the simulation values are in good agreement reading a little higher than the experimental values which is also seen in case of the zero-dimensional ignition delay calculations. The reason that the simulation values are reading a little higher compared to the experimental values is that the mechanisms developed may not be very accurate to predict the actual realistic behavior or there could be some parameters involved in the experiments which is making the experimental values of ignition delay lower than the simulation values.

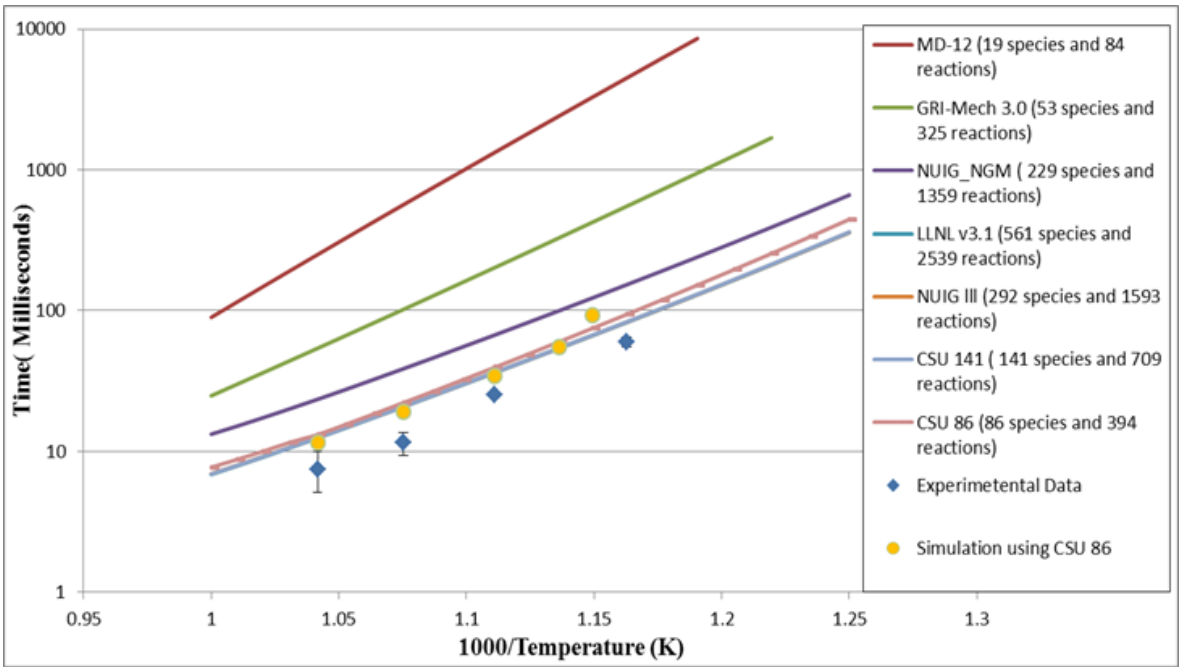

Figure 5.4 Experimental and Computational ignition delay of stoichiometric methane/air mixture.

5.4. Conclusion

Computational study of homogenous auto ignition of iso-octane and methane with 159 species reduced chemical kinetic mechanism for iso-octane and CSU 86 mechanism for methane respectively shows a good agreement with the experimental results. This provides a good

validation study of the chemistry and physics (discussed in chapter 3) in a RCM. With the physics and chemistry working well, it allowed to modify the RCM to study the homogenous spark ignition and dual fuel droplet ignition system as discussed in chapter 6 and chapter 7.

CHAPTER 6: COMPUTATIONAL STUDY OF LASER IGNITION OF PREMIXED FUEL AIR MIXTURES IN A RAPID COMPRESSION MACHINE

6.1. Introduction

Recent advances in computational power and availability of high performance clusters have enabled computational fluid dynamic (CFD) modeling that can be performed in conjunction with experiments to provide further insight into physical parameters that are not readily measured. In the field of combustion, for example, experimental speciation, flow and temperature measurements are highly constrained due to cost and complexity. By calibrating the results with experimental measurements, CFD modeling of complex, chemically reacting systems (e.g. engines) has been shown to be an effective tool to predict the change in combustion behavior with change in the input parameters such as equivalence ratio, pressure and temperature [35,36]. Presented herein are the results of three dimensional, time-dependent CFD modeling using CONVERGE^{TM} of laser ignited fuel/air mixtures in Rapid Compression Machine (RCM).

Experiments were conducted previously by our research group to address the gap in literature of high temperature/pressure laser ignition of methane/air mixtures. An RCM was used to conduct laser ignition experiments in which lean limit, minimum ignition energy was measured and flame propagation was observed using Schlieren imaging [37, 38]. In support of the previous work, the computational study presented herein was performed and good agreement was established with the experimental results. The computational study allowed visualization of the flame propagation beyond the field of view of the experiments and showed that flame quenching occurred near the walls of chambers and pistons, which resulted in the incomplete combustion observed in the experiments. The lean limit study was also conducted using the computational fluid dynamics

(CFD) approach and a good agreement was obtained between the computational and the experimental results.

Advanced compression ignition (ACI) concepts are currently under development as a means to reduce emissions and improve efficiency for the next generation of internal combustion engines. The optimum fuels for these ACI engines might be fuels of moderate reactivity and traditional metrics such as octane number (ON) and cetane number (CN) are not directly applicable to characterize the auto ignition under homogenous premixed or partially premixed conditions [39]. To demonstrate the feasibility of the RCM/laser ignition system to quantify fuel reactivity (and knock propensity), computations were performed on laser ignited n-heptane/iso-octane/air mixtures in RCM. The results presented herein predict auto ignition to occur in the end gas as the reactivity of mixture and therefore demonstrate the potential for the RCM/laser ignition system as a means to quantify fuel reactivity and knock propensity.

6.2. Computational Model

Transient, three-dimensional computational modeling of the RCM/laser system was performed using CONVERGE™ version 2.2.0. Finite volume method was used to solve the mass, momentum and energy transport equations. The energy equation is coupled with the mass and momentum equations and solved iteratively to include the convection term in the energy equation. A variable time step method was employed, which reduces the time step if governing equations are not converging during the specified number of iterations to ensure computational accuracy and convergence. A 3-D model of the RCM geometry was created using SolidWorks and exported to the CONVERGE preprocessor where boundary conditions and necessary solvers were specified which is as described in chapter 2.

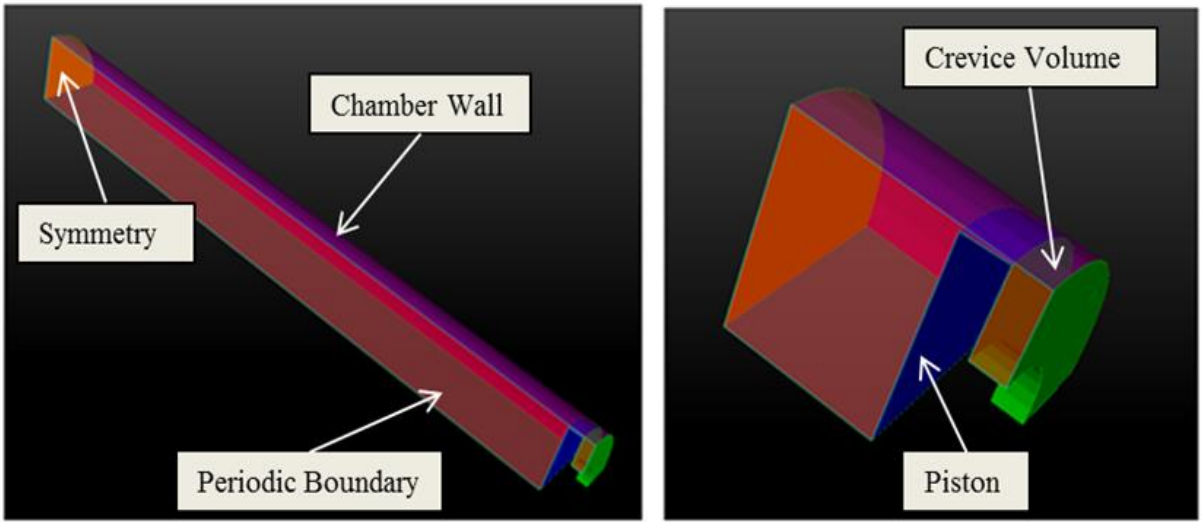

Figure 6.1 1/8th sector RCM geometry (a) before compression and (b) after the compression stroke

The SAGE combustion model and RANS turbulence model were used to study the combustion chemistry and the fluid dynamics effects present in the system. A reduced natural gas/n-heptane chemical kinetic mechanism (86 species, 393 reactions) was used as the chemistry set for the computation [34]. The AMR technique was used to refine the mesh at the area of high temperature and velocity gradient to improve the accuracy of simulation. The fixed embedding meshing technique was used along the wall of RCM chamber to resolve the boundary layer for accurate prediction of the heat loss to the wall. The laser spark was modelled as a localized hotspot of temperature for all the computations with no plasma kinetics reactions included. For all the simulations, a 1/8th sector of the RCM geometry was used to save computational time as shown in Figure 6.1. In the computations, a spark modeled as hotspot of temperature is triggered at 14 ms after top dead center (TDC).

6.3. Results

6.3.1. Ignition of methane/air mixtures

Computational modeling of laser induced ignition of methane/air mixtures inside RCM was performed at equivalence ratios of $0.4 \leq \Phi \leq 1.0$. As described in Dumitrache, et al. [3, 4], mixtures of different equivalence ratio were introduced into the RCM chamber and, after compressing at a volume ratio of 11.6, were subjected to a laser induced spark at the chamber centerline at 14 ms after compression. With varying equivalence ratio, the specific heat of mixture varies, which affects the temperature after compression. Hence, for a valid comparison between different cases of experiments and computations, the temperature at TDC (T_{comp}) is kept constant at 782 K by varying the initial temperature of the mixture accordingly. It is also important to note that all experimental and computational conditions were chosen such that autoignition would not occur without introduction of the laser spark. For the computations, the spark was simulated as a localized hotspot of elevated temperature.

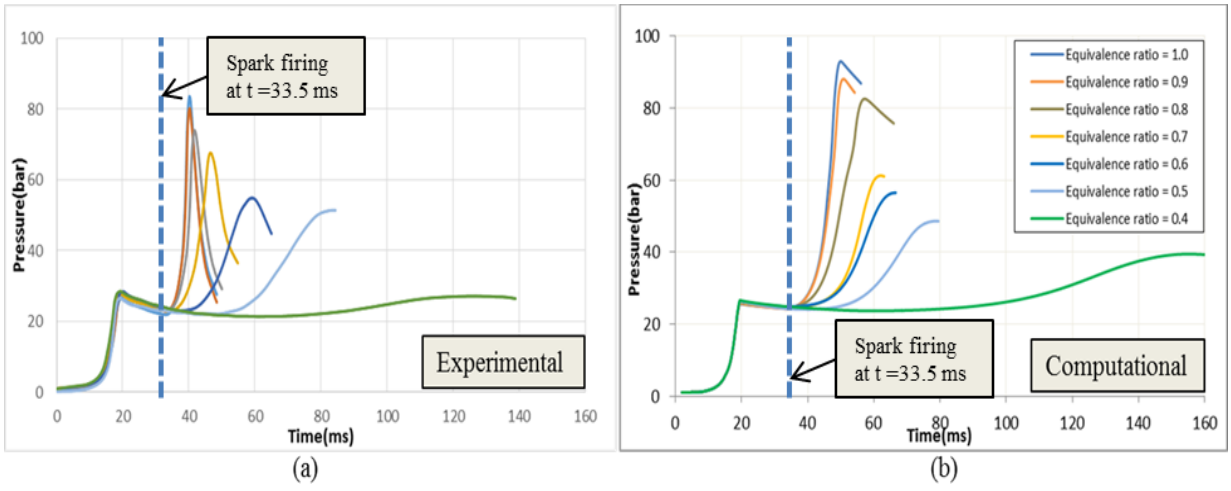

Figure 6.2 (a) Experimental pressure measurements and (b) simulated pressure history for ignition of methane/air mixtures at various equivalence ratios with initial pressure P_o = 1 bar, Tcomp = 782 K

Figure 6.2 shows the experimental and computational pressure data for methane/air mixtures at compressed temperature of 782 K and various equivalence ratios. As shown, the pressure initially increases during the compression stroke (with a peak at 19.5 ms), which is followed by a decrease in pressure caused a gas temperature decrease due to heat transfer to the combustion chamber walls. The spark is initiated at 33.5 ms (14 ms after TDC), which produces an outwardly propagating flame that results in elevated temperature downstream of flame and pressure rise in the chamber. The peak pressure decreases as the mixture gets leaner due to decreased flame temperature and decreased flame propagation rate (which results in decrease in combustion efficiency due to increased heat loss). The pressure rise rate also decreases dramatically with decreasing equivalence ratio flame due to decreased flame propagation rate. For the near stoichiometric cases, the increased flame propagation rate and increased flame temperature nearly produces a homogenous ignition event in RCM chamber.

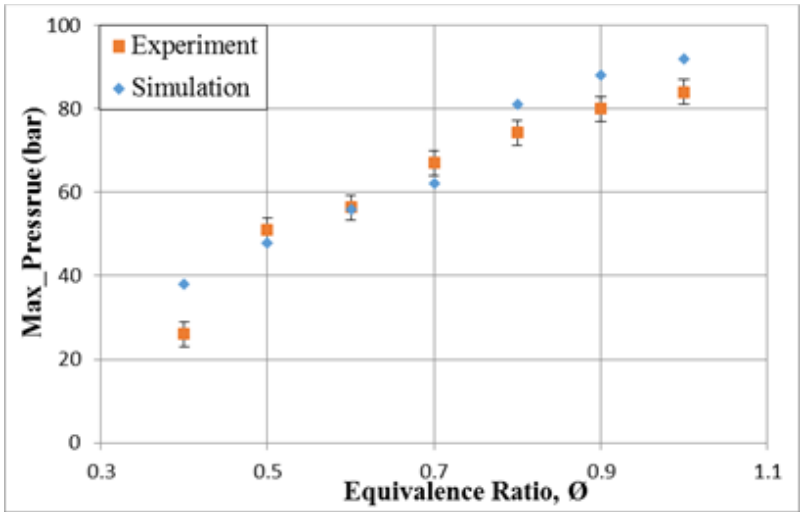

Figure 6.3 Comparison between experimental and computational peak pressure (bar)

As shown in Fig. 6.3, for the near stoichiometric mixtures, the computed peak pressure is higher than that observed experimentally, which is a likely a consequence of the pressure transducer not being temperature compensated (or water cooled). At lower Φ, excessive heat loss

results in decreased temperature of the system and drastically reduces the reaction rate decreasing the pressure rise. At lower equivalence ratio like $\Phi = 0.4$, heat loss plays a very crucial role in the combustion process affecting the flame propagation and flame quenching at the walls and the simulated peak pressure and simulated peak pressure temporal location deviate slightly from experiments.

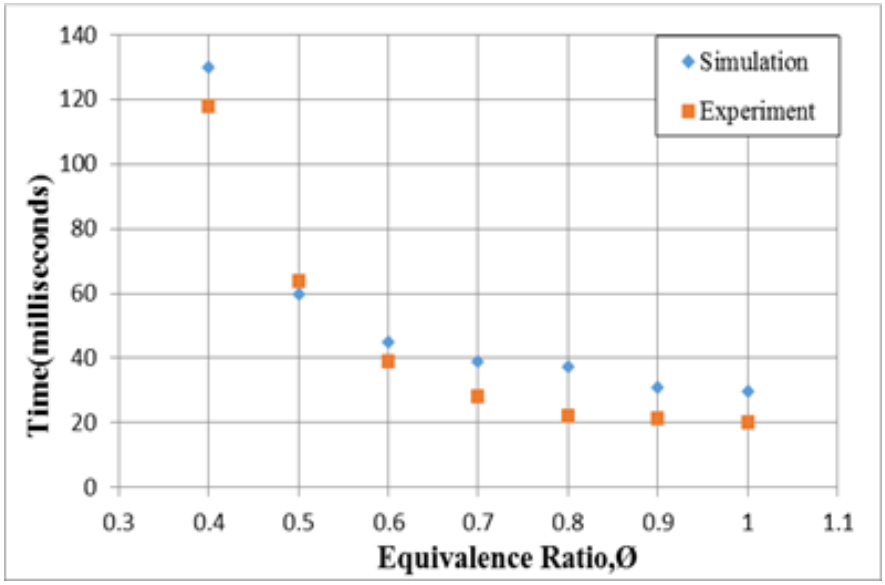

Figure 6.4 Comparison between experimental and computational time to reach the peak pressure (ms)

A difference in the computed peak pressure timing from TDC is also reported for near stoichiometric mixtures as shown in figure 6.4, which could be attributed to the lack of any plasma physics in the spark ignition mechanism. The laser spark process is known to introduce an additional pool of radicals, which enhances the reaction rate and flame speed during early flame kernel growth. In this study, a plasma mechanism was not included.

6.3.2. Flame Propagation

Computed heat release contours were used to study the flame position and propagation pattern for comparisons with high speed Schlieren images obtained from Dumitrache et al [37,38].

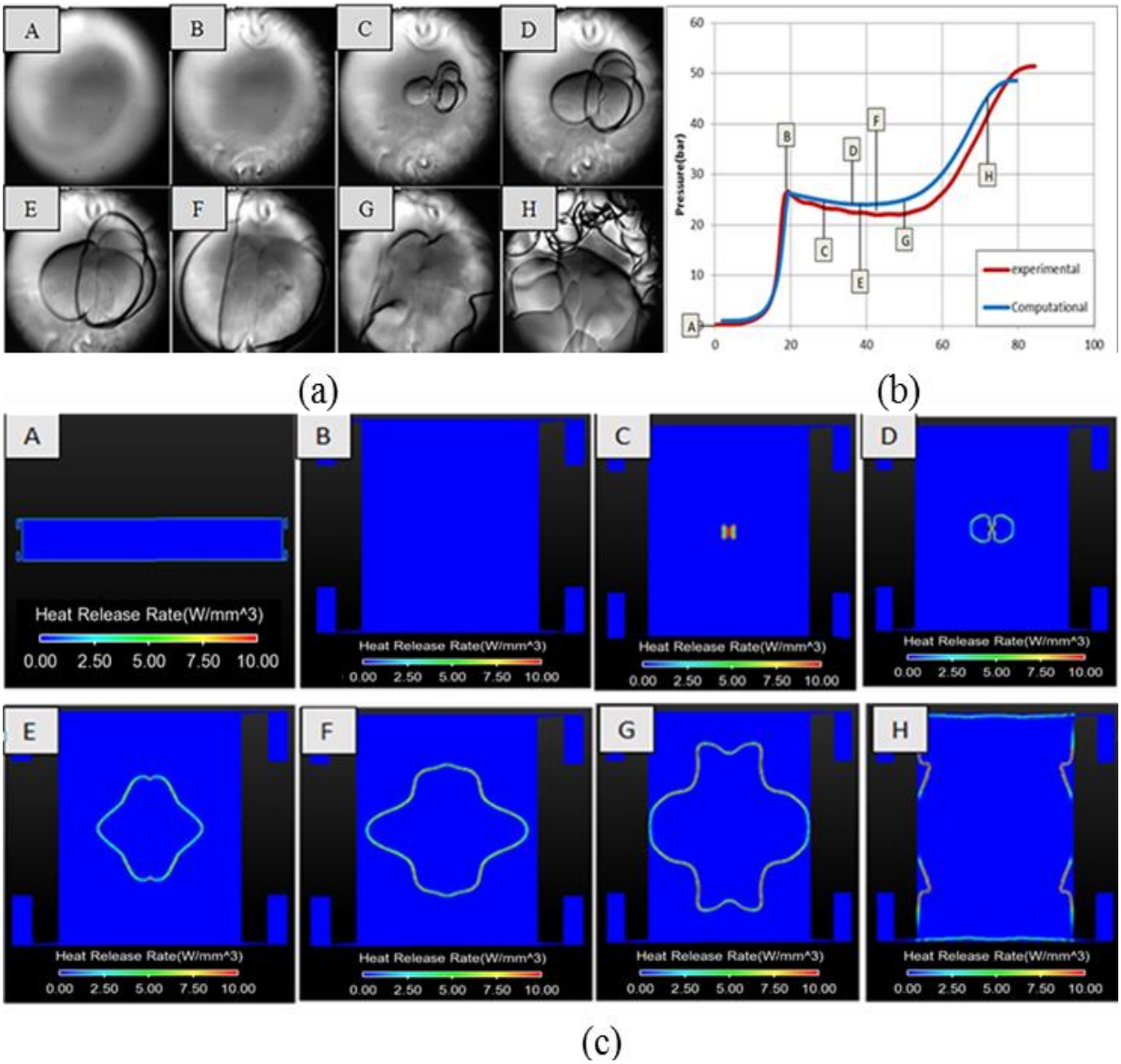

Figure 6.5 (a) Schlieren images at different test times (3,4), (b) experimental and computational pressure data corresponding to the image sequences and (c) computational heat release contours at different test times for a laser ignited mixture of CH4/Air (Φ = 0.5) inside the chamber of RCM

The view port window of the Schlieren imaging system is 20 mm in diameter and the piston diameter is 38 mm with TDC clearance of 25 mm, which limits the view area to only 30% of the

total chamber volume. The computations enable us to capture the latter stages of the flame propagation, which the Schlieren imaging did not capture due the view port limitations. Figure 6.5(b) shows the pressure traces taken from experiment and computation, which are marked with a letter indicating the time when the images were taken during the experiments [37] [38] and computation.

Figure 6.5 is a comparison between experimental Schlieren images from Dumitrache, et al. [37] [38] and computed heat release contours for CH4/Air at $\Phi = 0.5$ and compressed conditions of 782 K and 28.6 bar. At TDC (image B), Schlieren images shows two opposite vortices forming due to the sudden stop of the pistons. There is no disturbance at the center of the chamber, which validates the adiabatic core assumption. In image C, a spark is initiated and a flame kernel appears, which transitions to an outwardly propagating premixed laminar flame (images D to F) that reaches the piston wall at 55 ms (image G). The computed heat release contours (and velocity field, species contours, not shown) further reveal the physical phenomena outside the view of the imaging system. The computations reveal the effect of roll up vortices on the flame propagation. The vortices cause mixing of the low temperature unburned gases in the RCM boundary layer with higher temperature unburned gases in the adiabatic core, which reduces the localized flame speed in the vicinity vortex regions and causes a localized temperature variation shown in figure 6.6(c - d) that results in a non-spherical flame shape (images F to H, figure. 6.5).

During experiments, water vapor formed by combustion gets condensed on the windows of the chamber limiting the imaging before the peak pressure is reached. The computed heat release contours show the flame propagation pattern at the time of peak pressure as shown in figure 6.6(a), which shows that the flame consumes most of the low temperature mixture near the wall (for cases

with equivalence ratio > 0.5) before the flame is quenched with substantial unburned fuel in the crevice volume (figure 6.6(b)).

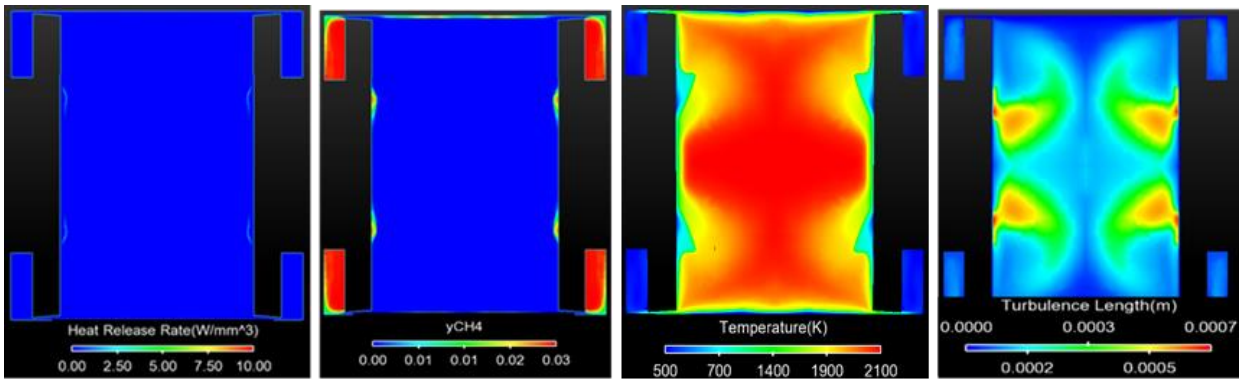

Figure 6.6 Contours of (a) Heat Release, (b) Mass Fraction of CH4, (c) Temperature and (d) Turbulence Length Scale at time corresponding to the peak pressure for CH4/Air (Φ = 0.5)

6.3.3. Lean Limit

An analysis was performed to understand the lean limit by using the combustion efficiency(χ) as a metric to define the lean limit. Combustion efficiency is defined as the ratio of the computed thermal energy to the initial chemical energy in the fuel/air mixture. ability of the system to convert the chemical energy assoicated with the fuel into the heat energy. Following Dumitrache et al. [37][38], the lean limit was characterized in terms of combustion efficiency(χ), which was obtained from the computed heat release. Total energy content of fuel ($E_{CH4/Air}$) is defined in terms of its lower heating value (LHV) as $E_{CH4/Air} = m_{CH4}LHV$ where m_{CH4} is the mass of methane present in the combustion chamber. The apparent heat release rate (from experiments) and integrated heat release rates (from computations) are used to compute the combustion efficiency as $\chi = Q_{total}/E_{CH4/Air}$, where Q_{total} is total heat release taken from the integration heat release rate.

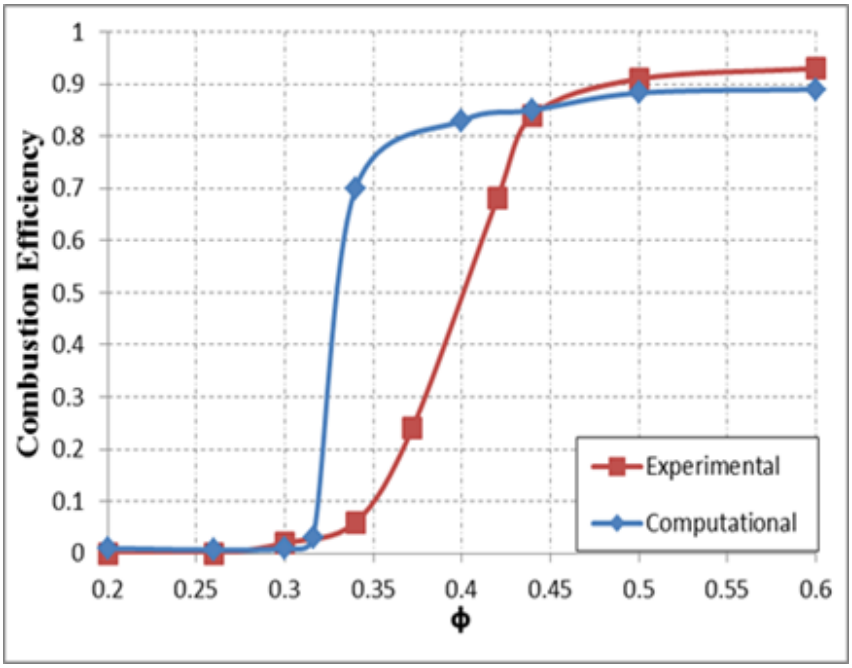

Figure 6.7 Combustion efficiencies for various equivalence ratios for characterizing lean limit

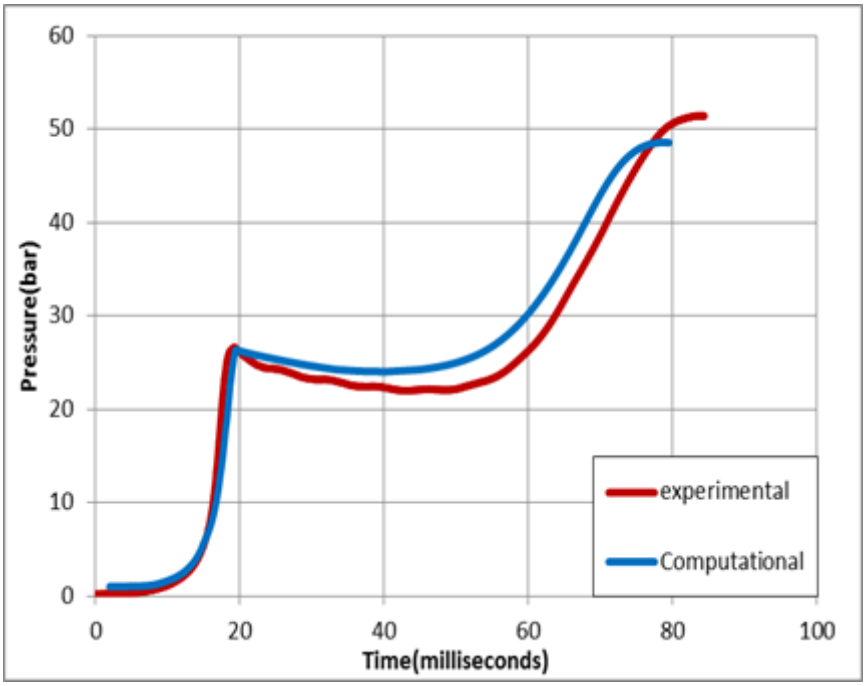

Figure 6.8 Sample pressure traces from experiment and computation for ignition of methane/air mixture at $\Phi = 0.5$

We see some differences in the combustion efficiency at $0.45 \geq \Phi \geq 0.3$ between experiments and computations as shown in figure 6.7. The discrepancy is likely a consequence of the heat

transfer model not adequately reproducing the heat loss to the cylinder walls observed in the experiment. The effect of the heat transfer on the combustion efficiency (and lean limit) is two-fold. First, as indicated by the pressure data in figure 6.8, the temperature in the adiabatic core at the spark ignition was likely lower in the experiments than in the model. Secondly, the flame quenching at the wall due to heat transfer from the flame to the wall is most likely not quantitatively accurate. More tuning of the heat transfer model in conjunction with additional experiments is necessary. Despite the slight quantitative differences in combustion efficiency vs. equivalence ratio as the mixture approaches the lean limit, the computations predicted no ignition for $\Phi < 0.31$, which is consistent with the experimental results.

6.3.4. Fuel Reactivity Study

Computational modeling was also performed for laser ignited n–heptane/isooctane/air mixtures to study the effect of fuel reactivity on knock propensity in the RCM/laser ignition system. The computational modeling approach used for these simulations was similar to that employed for the methane/air simulations. A 73 species reduced chemical kinetic mechanism for primary reference fuels developed by Wang, et al [40] was used for these simulations. A compressed temperature of 658 K was selected such that autoignition did not occur for stoichiometric isooctane/air at initial pressure of 1 bar which was found to be 658 K. A spark modeled as a hot spot of temperature was triggered at the center of the chamber acting as a spark. A set of simulations were conducted using the same initial conditions with increased n–heptane content.

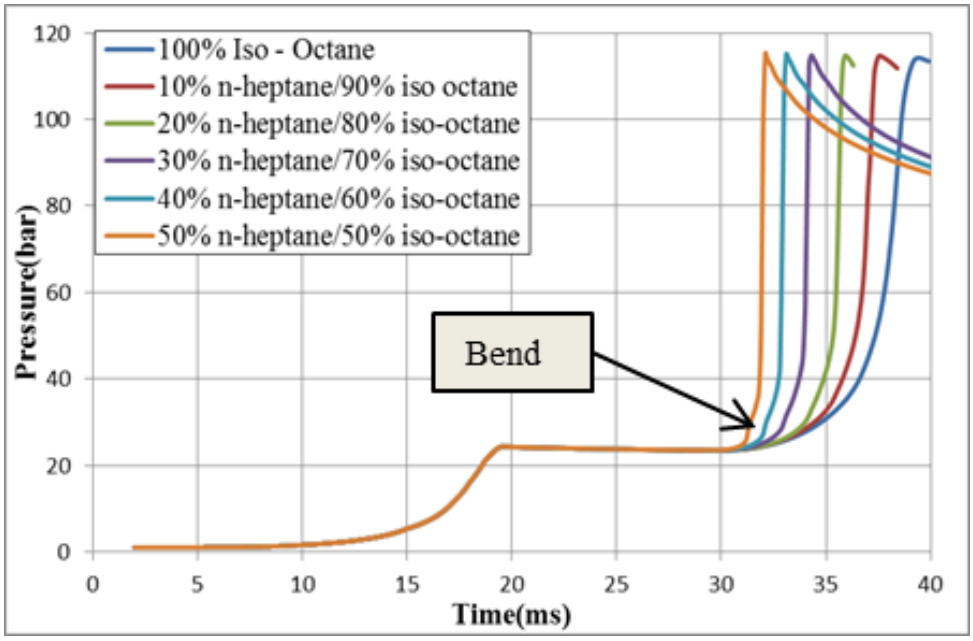

Figure 6.9 Computational pressure traces for spark ignited n-heptane/isooctane air mixtures in an RCM at Po = 1 bar, Tcomp = 658 K

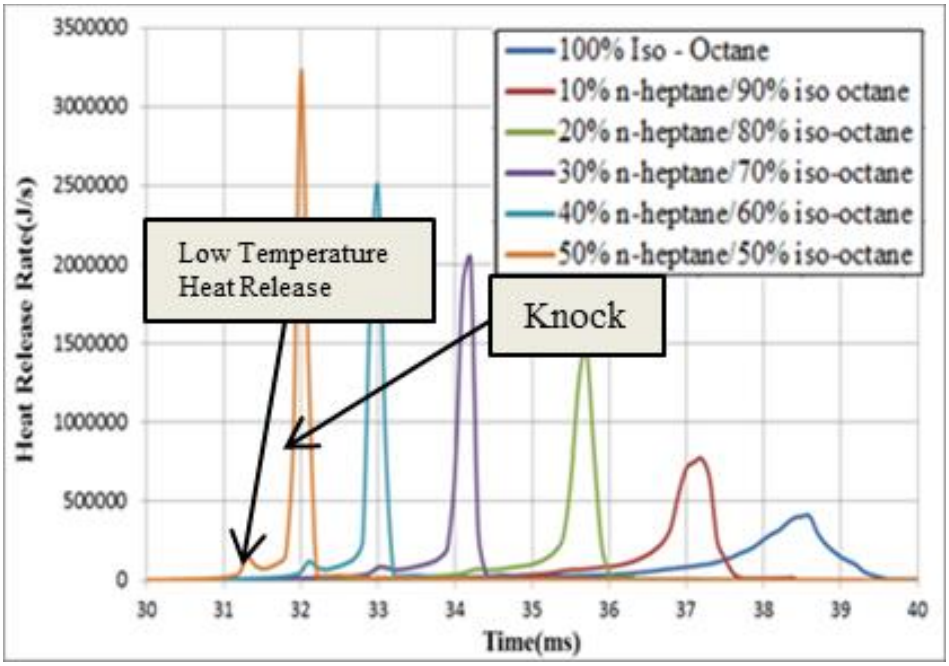

Figure 6.10 Computational heat release rates plots for spark ignited n-heptane/isooctane air mixtures in an RCM at Po = 1 bar, Tcomp = 658 K

As shown in the Fig. 6.9, as the concentration of the n-heptane is increased, the increase in chemical reactivity results in low temperature heat release (figure 6.10), and increased flame speed

(as evidenced by the increased pressure rise rate). For 100% iso-octane case, the unburned fuel is consumed solely by the propagating flame and a smooth rise in pressure along with a slow and distributed heat release rate. As the reactivity of the mixture is increased by adding n-heptane to the blend, a discrete change in slope is observed in the pressure trace, which is a result of autoignition of the end gases (i.e. knock). The timing at which the discrete change in slope occurs varies with the n-heptane content (i.e. octane number). A closer examination of the heat release rate plots shows evidence of increasing low temperature heat release with increasing fuel reactivity, which occurs prior to the high heat release of auto ignition event as has been observed in HCCI engines [39].

Figure 7 shows heat release contours for 50% n-heptane/50% iso-octane, which clearly shows homogeneous autoignition (i.e. knock) occurring in end gas upstream of the propagating flame. As seen in the sequence of images, evidence of low temperature heat release is observed at 0.031 s (figure 6.11(c)), which ignites a cool flame upstream of the propagating flame (figures 6.11(d) through 6.11(g)). As second low temperature heat release event is evident in figure 6.11(g), which ultimately transitions into homogenous autoignition in the end gas (figure 6.11(h)).

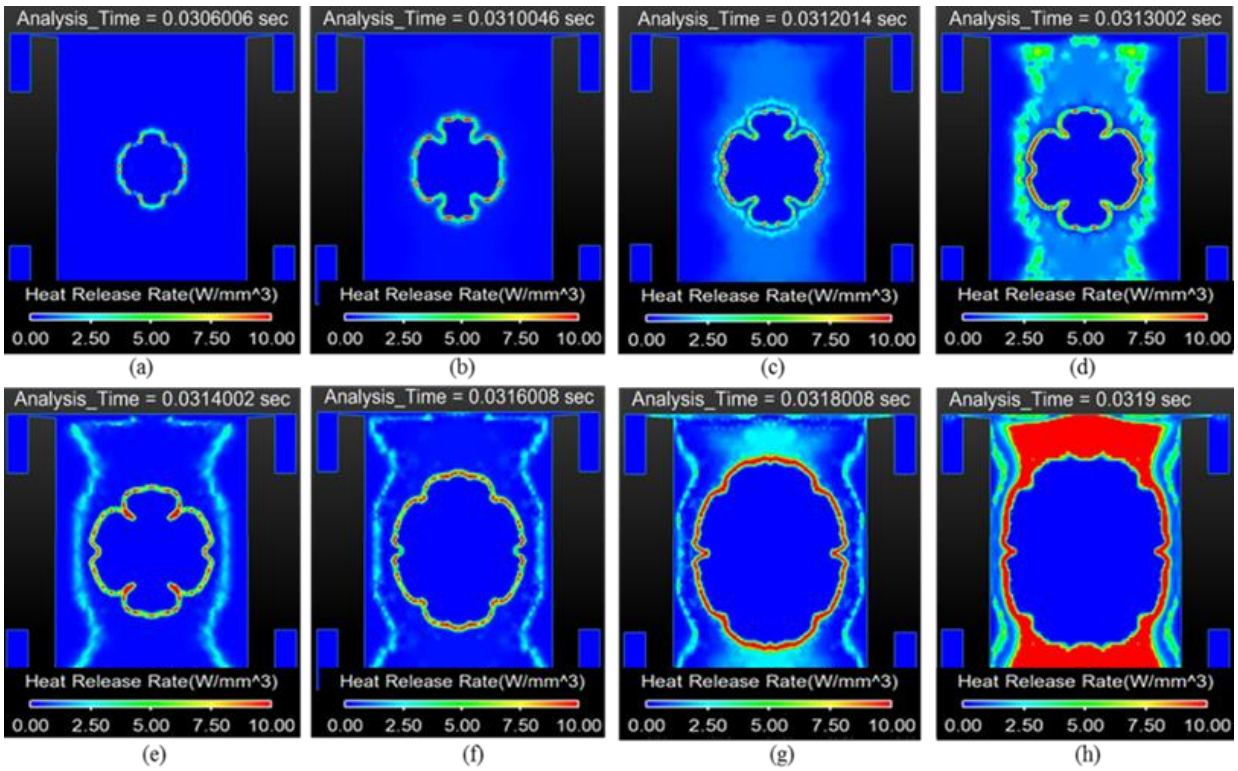

Figure 6.11 Computational heat release rate contours for laser ignited stoichiometric 50% n-heptane /50% isooctane/air in an RCM at P0 = 1 bar and T_{comp} = 658 K. The computations show low temperature heat release and cool flame propagation upstream of the laser ignited flame and homogeneous autoignition

6.4. Conclusion

The main motivation of this study was to investigate the laser induced ignition of hydrocarbon/air mixtures in RCM using CFD. The methane/air simulations compared favorably against experiments of Dumitrache, et al. [37] and showed that autoignition in the end gas did not occur. The methane/air simulations also revealed the interaction between the propagating flame and roll up vortices and their effect on the thermal boundary layer. After good agreement was obtained with the methane/air experiments, n-heptane/iso-octane/air simulations were performed, which revealed that as the reactivity of the fuel is increased autoignition (knock) is observed in the end gas. This investigation suggests that the RCM/laser ignition system represents a viable instrument to quantify knock propensity of fuels.

CHAPTER 7: DUAL FUEL DROPLET COMBUSTION IN A LEAN PREMIXED MIXTURE

7.1. Introduction

Combustion of two fuels of different relativity in internal combustion engine serves an ideal platform for reduction of pollutants, increasing the power output of engine, and improving the efficiency of engine. There is a major economic incentive of using natural gas in a dual fuel engine and maximizing the amount of natural gas in the dual fuel application because of its low cost per unit energy as compared to the diesel fuel. A detail study is required to understand the chemistry taking place in dual fuel engines as increasing concentration of natural gas results in knocking phenomenon which is still poorly understood. A detail computational study was performed by Andrew Hockett in his dissertation [34] shows the occurrence of knock in the engine chamber as the reactivity of fuel was increased by adding propane in the mixture along with the methane which are surrogates of natural gas. To understand the phenomenon properly and increase the substitution proportion of natural gas, a detail study is required of the phenomenon resulting in uncontrolled combustion in the dual fuel engine. Ignition/combustion of a droplet in a lean premixed mixture serves as an ideal platform for studying the dual fuel combustion because of its geometric simplicity which enables computations with detailed chemical kinetics with direct comparisons against the optical diagnostics. A Rapid compression machine serves as an ideal platform for droplet combustion in lean premixed mixture fuel droplet ignition under engine like conditions.

Prediction made by Energy Information Administration (EIA) highlights the energy consumption from the transportation sector to remain at 25% of the U.S total energy through 2040 [41]. It also highlights the fact that most of the energy will be provided by the internal combustion engines. It also predicts the increase in the natural gas use by 23%. [42] With climate change taking

place around the globe, there is growing attention given to the emissions coming from the internal combustion engines with strict regulation set by Environmental protection agency(EPA) on the emissions. Replacing the current fuel with some alternative fuels like natural gas will help to achieve substantial regulation norms. Natural gas has greater hydrogen to carbon ratio which helps in reducing the carbon dioxide emission by 25% while producing the same energy as diesel or gasoline. Also, in a dual fuel engine, a leaner mixture is used which reduces the combustion temperature and thus results in the reduction of the hot regions where soot is formed in case of diesel engines which runs on near stoichiometric conditions with reduction in the combustion temperature further reduces the NOx formation. Coupled with reduction in pollution, natural gas is less expensive compared to the diesel or gasoline on per unit energy basis which makes a dual fuel engine analysis a valuable study considering the environmental and economic aspect.

A small amount of diesel is sprayed in a premixed mixture of natural gas present in the combustion chamber of dual fuel engine via a high pressure liquid spray which subsequently breaks into small droplets. These droplets vaporize due the high pressure in the chamber resulting in a vapor cloud of gaseous fuel surrounding the liquid fuel. This cloud of vapor gets ignited which eventually results in a diffusion flame. This auto ignition of the diesel fuel causes a premixed flame which starts consuming the lean mixture of natural gas present in the chamber. The premixed flame along with the diffusion flame together contributes to the total heat release in a dual fuel engine. So, it is very important to understand the burning of spray or droplet in a lean premixed mixture of natural gas/air to develop better control over dual fuel combustion and also combustion processes which involves the ignition of spray or droplet.

The fuel cost saving increases with increasing concentration of natural gas in the chamber. But increasing in the natural gas concentration has a limitation as it causes uncontrolled fast

combustion in the chamber causing a large release of energy in short period of time. This results in a rapid pressure rise causing engine knock which is not desirable as it causes unacceptable engine noise, causes a high stress on the cylinder walls and leads in damaging the engine components. Exact mechanism resulting in knock is still not understood properly and hence the need to study the ignition/combustion of droplet in a lean mixture environment. Although the spray used in the engine does not break entirely into small droplets and combust as a set of separate droplets, combustion of an isolated single droplet in a lean premixed mixture of low reactive fuel reveals a lot of relevant chemistry and physics of dual fuel combustion process. Combustion/ignition of isolated droplets is studied since 1950[43] because of its geometric simplicity allowing the solution to analyzed analytically [44,45]. Till date, very few experiments are performed on droplets at engine like conditions of varying high pressure and temperature with most of the studies carried at moderate temperature and pressure. In case where high pressure/temperature combustion was carried, a constant steady flow field was used as those found in the constant volume chambers, or by using aerosol sprays which does not capture the relevant physics and chemistry effects as it does not allow isolation of a single droplet in the chamber. Very little research has been conducted for burning the droplet in a true engine like conditions where there is a rapid rise in the pressure and temperature.

To address these shortcomings in the literature, a detailed computational and experimental investigation of dual fuel, droplet base combustion in Rapid Compression Machine (RCM) is presented herein. RCM is an instrument typically designed for producing an ideal compression stroke of engine to study the auto ignition phenomenon in a controlled environment unlike found in the engine. RCM compression process is subjected to minimum heat loss and rapidly compresses premixed fuel/air mixtures to high pressure and temperature. Also, in RCM the

chamber gas is heated with no heating taking place along the walls which helps to neglect the wall reactions. An opposed piston assembly of the RCM allows for zero axial velocity at the center of RCM which provides a turbulence free environment ideal for droplet to stay spherical with minimum distortion due to fluid dynamic effects.

7.2. Previous Computational Modelling

Computational modelling of in-cylinder physics are carried out by many researchers all over the world for designing the engine components and understanding the combustion processes accurately as it takes into account the complex geometry of the engine such as piston bowl and can also predict the change in the combustion processes with change in the input parameters. Mansour et al. [46] used a single zone model with coupling between a Wiebe profile and detailed chemistry to predict the cycle pressure in pilot-injected dual fuel engine. Zhang et al. [47] used a multi-dimensional KIVA-3V code with spray physics, characteristic time combustion (CTC) model and the Shell ignition model for diesel auto –ignition for simulating a micro pilot dual fuel engine. Shell ignition model utilizes very small set of reactions and CTC model is based on reaction rates of only few species which are obtained using empirical relationship. Current work done by Andrew Hockett in his thesis dissertation [34] used a state-of-the-art in modelling the in cylinder dual fuel combustion which overcome the limitation in literature by simulating a conventional dual fuel combustion utilizing multi-dimensional CFD, advanced spray model, and a sufficiently detailed chemical kinetic mechanism. However, there is much of physics to be understood between the closely coupled premixed and diffusion flame which are present in these types of combustion.

To understand this physics accurately, droplet combustion under engine like condition serves as an ideal platform. Rapid compression machine provides an ideal environment for studying a well-defined, time dependent, non-premixed, laminar combustion problem which is essential for the developing and validating the models for the diffusive combustion processes as stated by Marchese et al [48].

7.3. Dual Fuel Droplet Combustion Model

The classical droplet combustion model is very important to understand as it can be used to develop a dual fuel droplet ignition model. In a classical droplet combustion model, an isolated droplet is subjected to a high temperature ambient of oxidizer containing only oxygen and inert gas. As the droplet is introduced in the hot ambient oxidizer, due to heating thermal expansion takes place resulting in initial increase in the size of the droplet. As the heating continues, the droplet continues to vaporize resulting in the decrease of the droplet size. At some distance away from the droplet surface, thermal runaway reaction start taking place as shown in figure 7.1(a). This reaction results in an auto ignition event causing a premixed flame which propagates towards the droplet surface consuming the fuel vapors as shown in figure 7.1(b). The flame continues to travel towards the droplet surface till it reaches at a distance where the fuel concentration become high and the concentration of the oxidizer become insufficient for the flame to propagate consuming the fuel vapors. Now, the flame motion ceases resulting in a premixed diffusion flame as shown in figure 7.1(d). At the flame front, the concentration of the fuel and oxidizer goes to zero as it establishes itself in a region of stoichiometric conditions of fuel and oxidizer. The flame continues to get oxidizer from the ambient far field and keeps getting fuel by continuously heating the droplet surface which causes it to vaporize and thus giving the necessary gaseous fuel for the

flame. This process continues till the droplet completely vaporizes and no fuel is available for the flame to withstand.

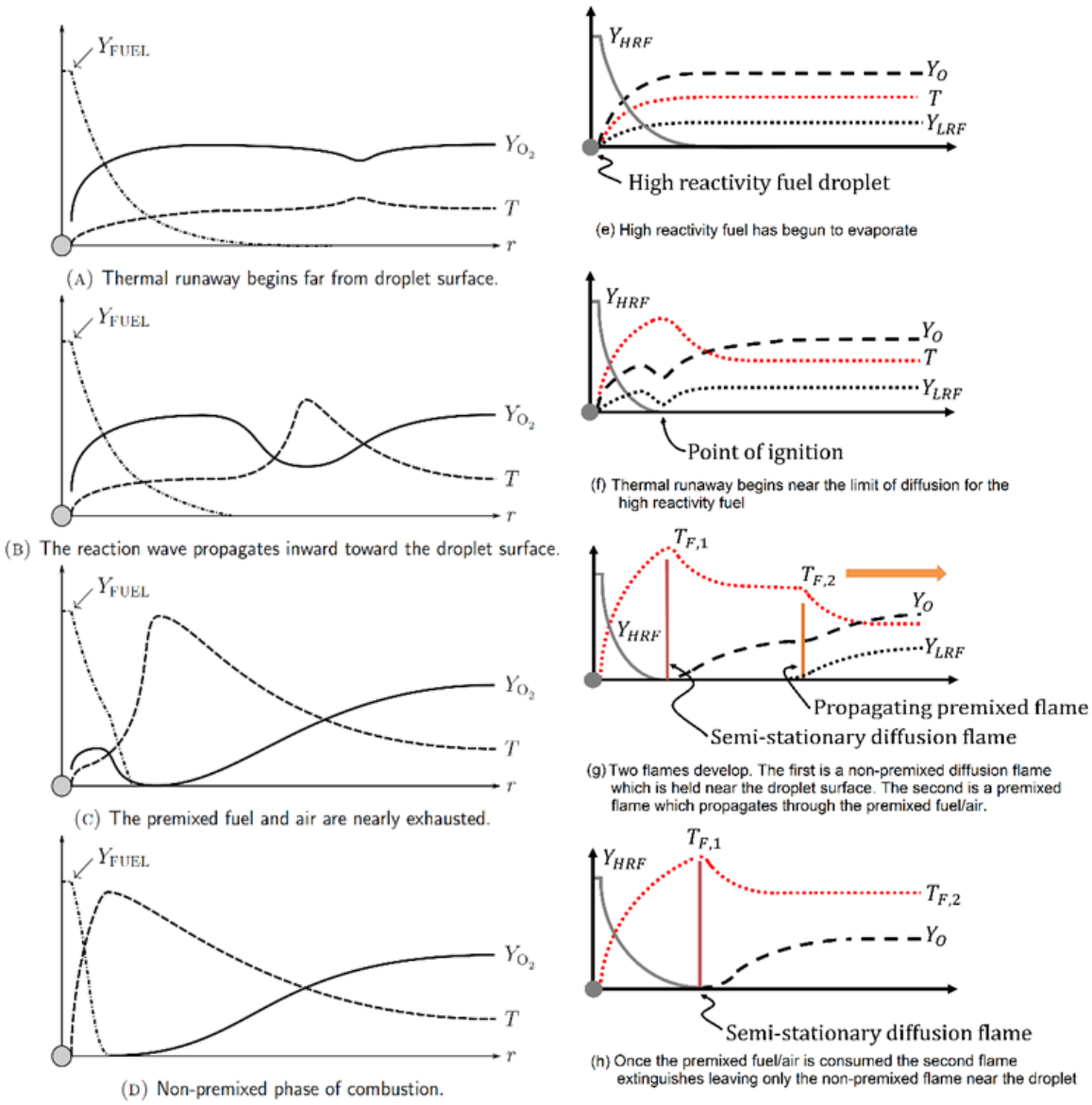

Figure 7.1 Representation of the classical droplet combustion work from [49] shown from (a-d) and the proposed dual fuel droplet combustion model shown from (e-h)

The dual fuel droplet theory follows the classical droplet theory with only difference seen is in the farfield condition where the hot ambient of oxidizer is replaced by a lean premixed mixture of

fuel and air. The fuel used in the far field is a low reactivity fuel (LRF) as compared to the droplet which is the high reactivity fuel (HRF). The reason of using the low reactivity fuel is to have an auto ignition event of the droplet to start the ignition process and consume the fuel present in the farfield. When a HRF droplet is subjected to the hot ambient of premixed LRF/air the droplet increases in size due to the thermal expansion. Due to continuous heating, the droplet loses the vapor to the surrounding causing a cloud of HRF vapor surrounding the droplet as shown in figure 7.1(e). At some distance away from the droplet surface, thermal runaway reaction takes place resulting in the auto ignition event of droplet as shown in figure 7.1(f). This autoignition causes to produce two flames in the system namely the premixed flame and a non-premixed diffusion flame. The premixed flame formed travels outwards consuming the lean LRF/air mixture and the premixed diffusion flame travels inwards towards the droplet surface consuming the high reactivity fuel as shown in figure 7.1(g). The premixed flame consuming the LRF can consume the entire fuel/air mixture provided that the LRF is above its flammability limit. The non-premixed diffusion flame keeps travelling towards the droplet surface till it reaches the region where the oxidizer concentration becomes insufficient for the flame to move inwards. This point of time, the flame ceases to travel and maintain itself at a stoichiometric condition where the fuel and oxidizer concentration goes to zero. The premixed flame extinguishes after consuming the lean premixed LRF/ air mixture and only diffusion flame remains in the system till all the HRF droplet is consumed as shown in figure 7.1(h).

7.4. Computational Modelling

A transient, three-dimensional analysis was carried out for droplet dual fuel combustion using Converge^{TM} CFD tool. Converge allows evaporation model only for the spray modelling and hence

it was difficult to model a single droplet evaporation and then subject the droplet to combustion. So, to solve the above problem, theoretical droplet evaporation theory was utilized. The droplet theory was subjected to the following assumptions:

1. The droplet evaporates in a quiescent, infinite medium.
2. The evaporation process is quasi steady.
3. The fuel is a single component liquid with zero solubility for gases.
4. Gases follow the ideal gas law.

Energy and mass conversation equations were used to determine the surface temperature. Once the surface temperature was determined, species distribution, temperature distribution and mass flow rate, velocity from the surface of droplet was determined. By assuming all the heat which the droplet surface receives is used to evaporate the droplet and no heat is used to raise the raise the temperature of the liquid droplet, heat transfer number of vaporization was derived by solving the energy equation which is defined as follows:

$$B_{h,v} = \frac{C_p(T - T_s)}{q_v} \tag{7.1}$$

where Cp is specific heat of the liquid fuel evaporating, T_s is the surface temperature of droplet, T is the unknown parameter which gives the temperature distribution around the droplet, q_v is the latent heat of vaporization of the liquid. The mass transfer number derived from mass conservation equation is defined as follows:

$$B_{m,v} = \frac{Y_{F,S} - Y_{F,\infty}}{1 - Y_{F,S}} \tag{7.2}$$

where $Y_{F,s}$ is the mass fraction of gaseous fuel at the surface of the droplet, $Y_{F,\infty}$ is the mass fraction of the evaporating species at far field which for the current study is assumed to be zero. For the study presented herein, a unity lewis number is considered which allowed us to combined the above two equations and solve them simultaneously to find the surface temperature, mass fraction distribution, temperature distribution in radial direction and also the mass flow rate or velocity at which the species is evaporated from the droplet surface. Assuming a vapor liquid equilibrium at the surface along the gas phase, using ideal gas assumption we have,

$$P_{A,i} = P_{SAT,A(T_S)} \tag{7.3}$$

which states that the partial pressure of the evaporating species($P_{A,i}$) is equal to the saturation pressure of that species at given liquid surface($P_{SAT,A(Ts)}$). For ideal gases, the partial pressure of the species divided by the total pressure is equal to the mole fraction of the mole fraction of the species is given as follows,

$$Y_{A,i} = \frac{MW_A}{MW_{mix}} X_{A,i} \tag{7.4}$$

where MW_A is the molecular weight of species A and MW_{mix} is the molecular weight of the entire mixture. Putting the above values into equations of mass and heat transfer number, we get a consistent equation in terms of the surface temperature. The surface temperature can be now iteratively solved by using fzero function of MATLAB. Once the surface temperature was determined, the next step was to solve the mass and heat transfer equations using the surface

temperature obtained above. The mass flow rate from the droplet surface was found using the equation shown below,

$$\dot{m} = \frac{4\pi k_g r_s}{C_p} \ln(1 + B_{m,v}) \tag{7.4}$$

where k_g is the thermal conductivity of gases present, r_s is the radius of the droplet. The thermal conductivity is found out by using Wilke's Approach of mixing gases which takes into considering the effect of all the gases surrounding the evaporating droplet. Finally, the velocity of the droplet vapors is found out using the equation as shown below,

$$\dot{m} = 4\pi r_s^2 \rho V_r \tag{7.5}$$

where ρ is the density of the gas phase evaporating species and V_r is the velocity. This completes the analysis of droplet evaporation using theoretical approach. The distribution of mass fraction, temperature of the evaporating droplet was found along the radial direction (radius). After this, the theoretical data obtained was exported to the Converge preprocessor to develop a model for droplet burning. Converge™ only uses Cartesian coordinate system and hence before exporting the mass fraction of fuel, oxidizer and temperature distribution which was available in spherical coordinate, a mathematical analysis was carried out to convert the spherical coordinate to cartesian coordinates. A mapping variable technique was used to map the data into the domain as shown in figure 7.2.

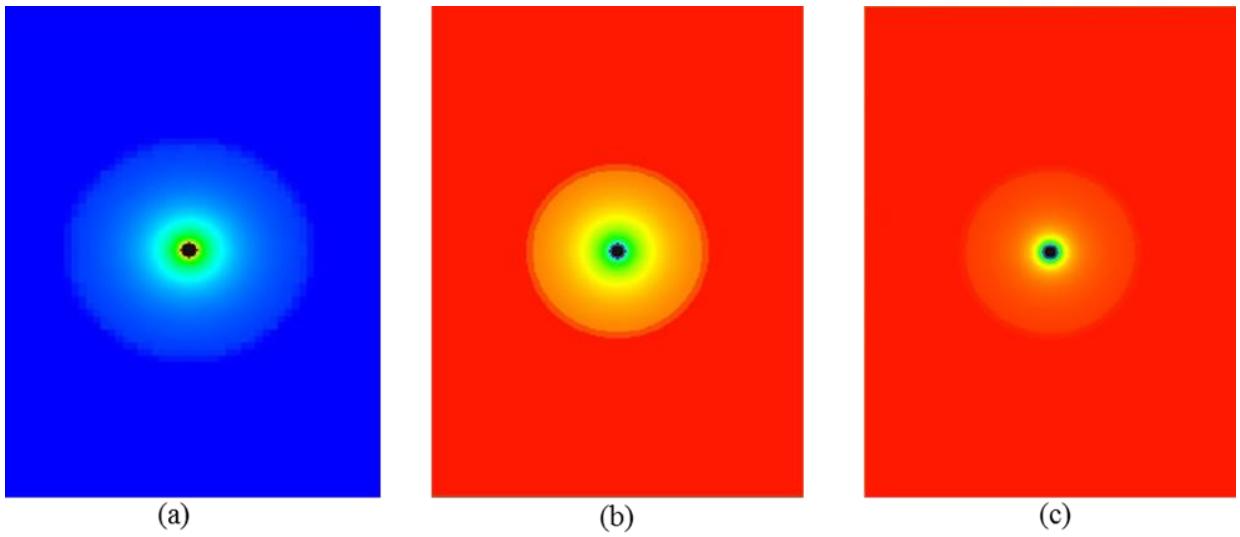

Figure 7.2 (a) Initial n-heptane concentration (b) initial natural gas concentration (c) Initial Temperature distribution

A three-dimensional modelling was carried out for dual fuel droplet ignition system. The initial conditions were set to high temperature and high pressure typically seen in a Rapid Compression Machine (RCM). A RCM has a uniform flow field with zero axial velocity at the center and an adiabatic core is established due to the new creviced design of RCM pistons. This makes the flow field around the droplet uniform with no disturbances around the droplet. This allowed us to model droplet ignition in a high temperature, high pressure uniform flow field environment which saved a lot of computational time as there was no need to model the piston motion as it doesn't not have any impact on the adiabatic core of the RCM.

To consider the vapors release from the droplet surface, droplet was modelled as a source term emitting vapors from the surface at velocity that was obtained using the equation 7.5. Boundary conditions for every other boundary were set as wall with law of wall as the heat transfer model. A SAGE combustion model was used to capture the combustion chemistry and turbulence model was employed to study the change in the flow field caused by the droplet burning. An adaptive mesh refinement was used to capture the temperature and velocity gradients coupled with

the spherical embedding along the droplet source term to resolve the species distribution with high accuracy and precision. Initial temperature of the domain was set to 765 K with pressure of 27 bars identical to the conditions found in RCM by using methane/heptane/air as the gases in the domain.

7.5. Results

First case was carried out at equivalence ratio of 0.5 in the far field which comprises of methane/air mixture and an n-heptane droplet vapor surrounded by the above far field at a temperature of 765K and a pressure of 27 bars. The initial species concentration and temperature distribution is as shown in the figure 7.3.

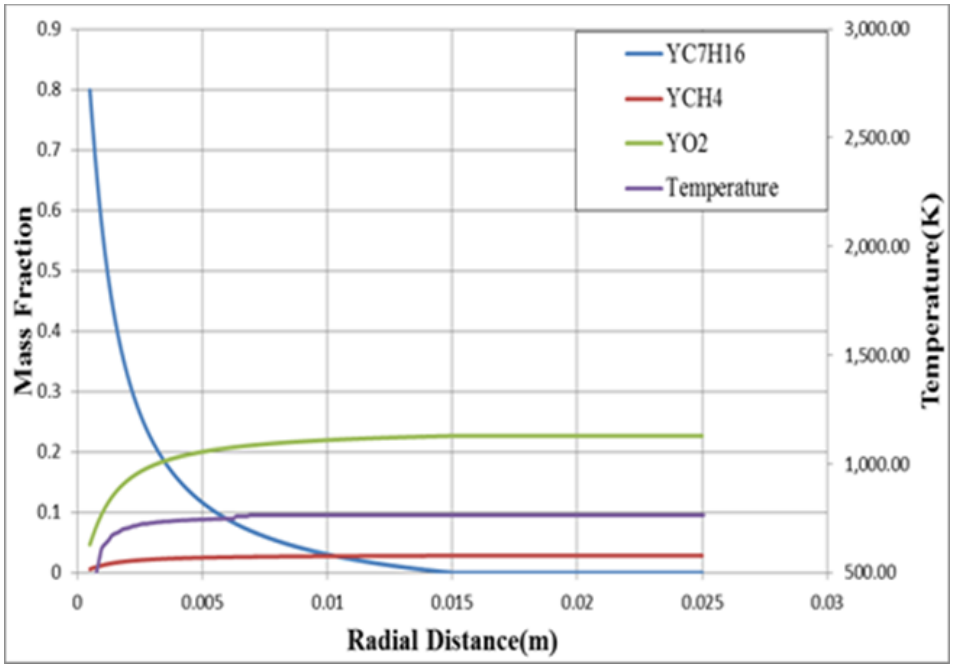

Figure 7.3 Initial Species and Temperature Distribution at time t = 0 sec

As discussed in the development theory of dual fuel droplet combustion, when the droplet is vaporizing, the vapors are heated up causing auto ignition of droplet resulting in a thermal runaway reaction taking place at some distance from the droplet surface as shown in figure 7.4.

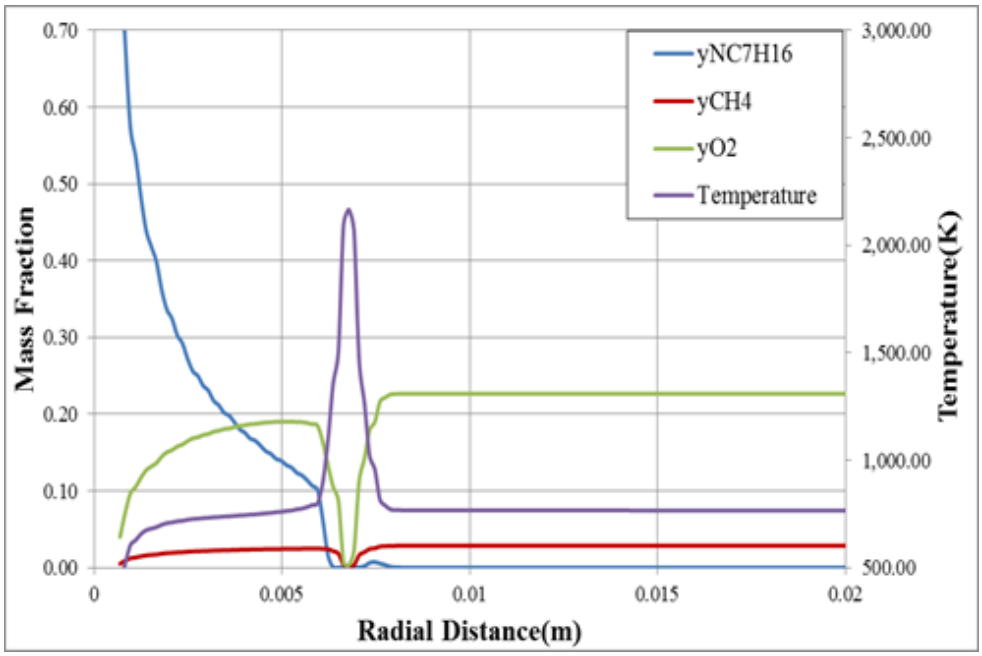

Figure 7.4 Species and Temperature Distribution at time of auto ignition

This auto ignition event causes enough energy for the low reactivity fuel to ignite. As a result of this, the first flame observed during the initial auto ignition splits into two flames.

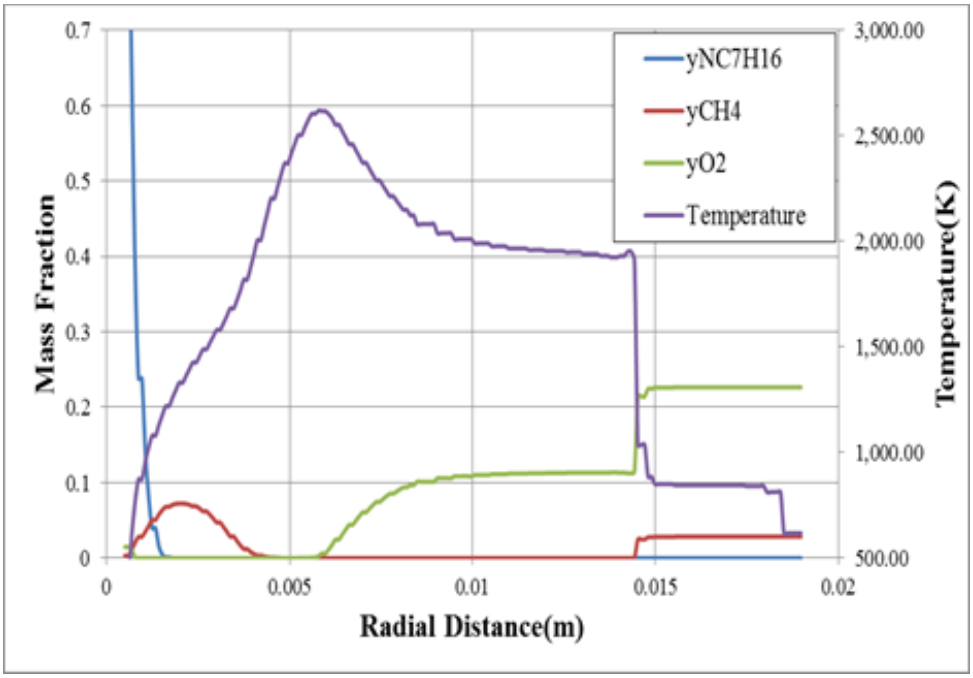

Figure 7.5 Species and Temperature distribution at time when diffusion flame and premixed flames are seen in the system

The first flame is a premixed flame propagating away from the droplet surface along the low reactivity fuel/air mixture as shown in the figures 7.5, 7,6, 7,7. This flame is seen to exist in the system since the given mixture was above flammability limit and thus was able to sustain the flame propagation. Also since the mixture is lean, enough oxygen is left in the domain for the standing diffusion flame. After some specific time period, the lean premixed flame completely disappears leaving only one diffusion flame in the system as shown in figure 7.6.

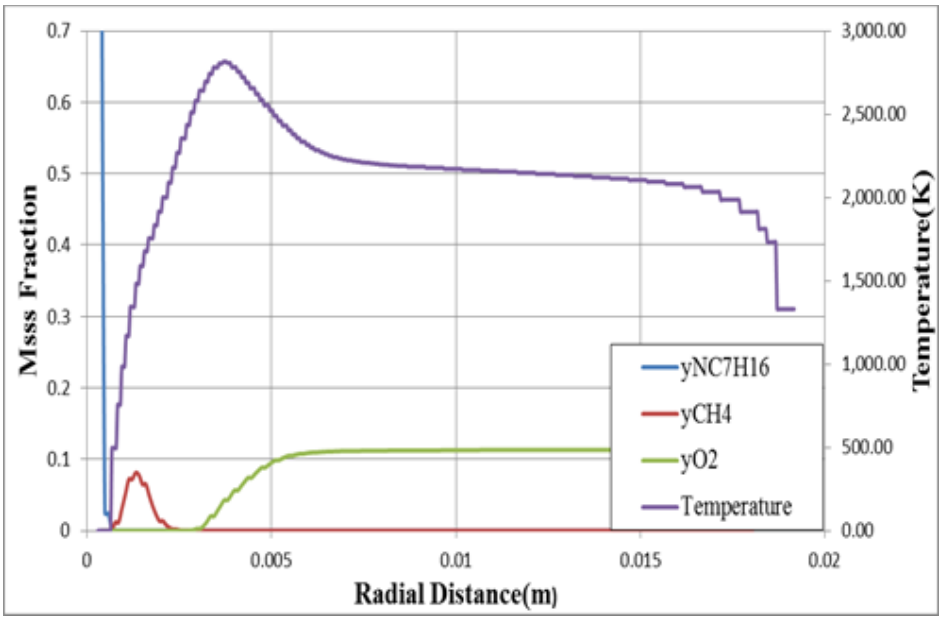

Figure 7.6 Species and temperature distribution showing the diffusion flame peak temperature with no premixed flame

Second flame which propagates towards the droplet surface in formed of a premixed diffusion flame travelling very close to the droplet surface enters a fuel rich region and the propagation ceases. This is the time when the premixed flame is converted into a classical non premixed diffusion flame front which is semi-stationary. At the flame position, the concentration of fuel and oxidizer goes to a theoretical value of zero as the flame establishes itself at stoichiometric condition. The non-premixed diffusion flame keeps getting the oxygen from the surrounding far field which is left as the low reactivity fuel/air is leaner and sufficient oxygen is left in the system to sustain the diffusion flame and the fuel is provided by the evaporating droplet due to the heat

transfer to the droplet surface as shown in figure 7.6. When the steady diffusion flame is established, the temperature near the droplet surface becomes very high. As a result of this, the gaseous vapors coming out of the droplet surface due to high temperature zone with no oxygen available undergoes thermal decomposition reaction producing a lot of smaller hydrocarbons like methane, ethane, propane, and so on as shown in figure 7.7.

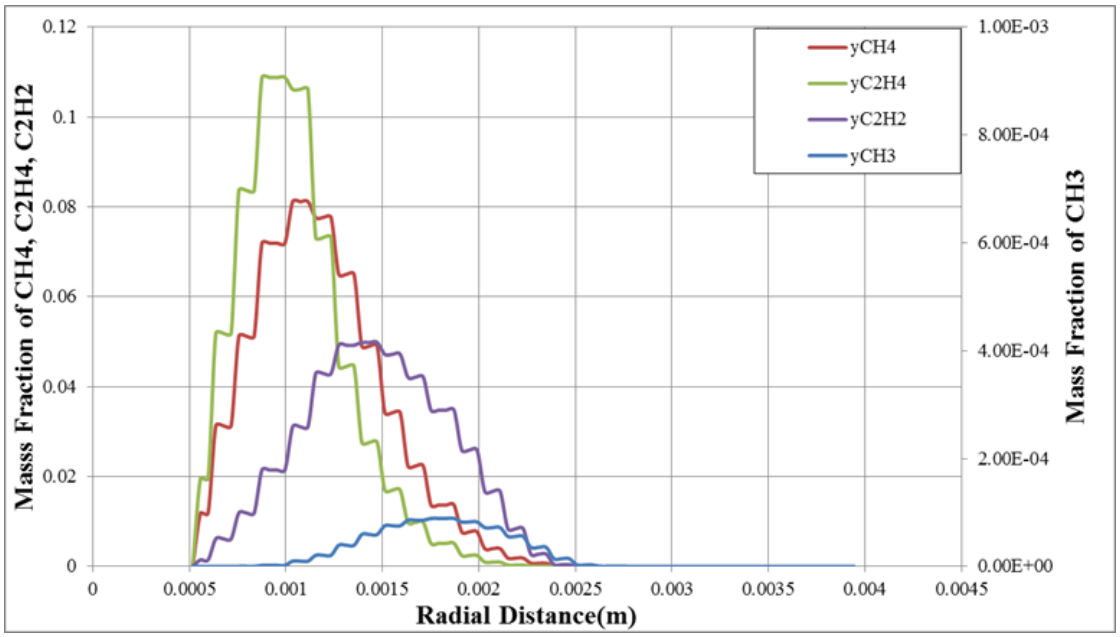

Figure 7.7 Mass fraction of smaller hydrocarbons caused due to the thermal decomposition of Heptane (HRF)

Finally, all the hydrocarbons produced break down into methyl radical near the flame front and gets consumed by the flame which makes the flame to sustain and diffusion flame is established. Figure 7.8 shows the results of computation of a 1 mm liquid n-heptane droplet ignited in a lean premixed CH4/air mixture at Φ=0.5. The figure shows a series of heat release contours at various times after TDC wherein the ambient temperature and pressure of the mixture is 765 K and 27 bar, respectively. As the droplet surface vaporizes, the vapors are heated up, and react with the ambient oxygen, causing autoignition of the droplet as shown in figure 7.8(b). The ignition event results in

a narrow temperature peak and local depletion of fuel and oxidizer at approximately 6 diameters from the droplet surface as shown in Fig. 7.8(b). This auto ignition event adds enough energy to the system for the lower reactivity CH4 fuel to ignite. As shown in figure 7.8(c-d), the localized autoignition event then bifurcates into two separate flames – an outwardly propagating premixed CH4/O2 flame and an inwardly propagating CH4/C7H16/O2 flame. The inwardly propagating flame then transitions into a stationary, non-premixed C7H16/O2 flame (figure 7.8(e-f)).

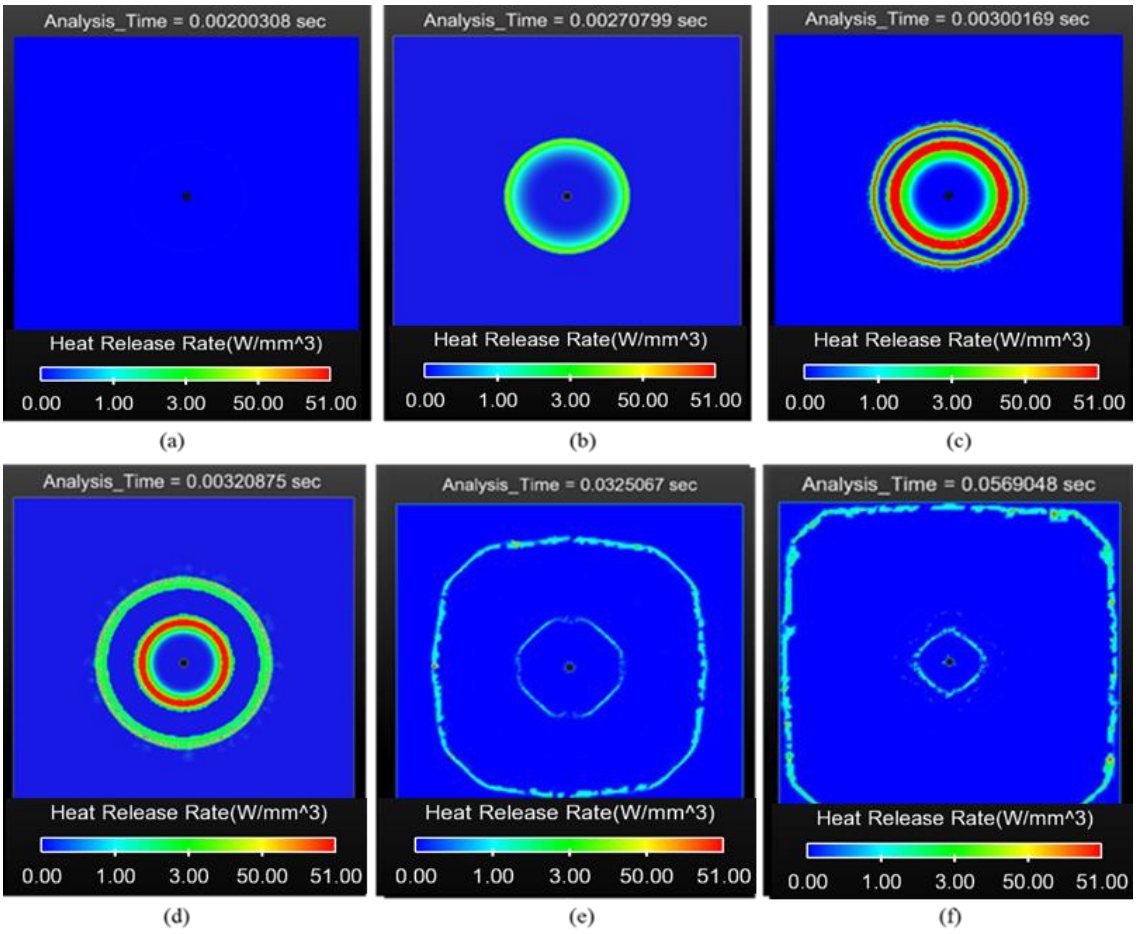

Figure 7.8 Heat release contours in the gas phase surrounding a 1 mm n-heptane droplet in a ϕ = 0.5 CH4/air mixture at 0.002 < t < 0.057 seconds after compression to To = 765 K, Po = 27 bar

Initially, the inwardly propagating premixed flame forms at some distance from the droplet surface and begin to travel inwards until it enters into the fuel rich region close to the droplet

surface at which point the propagation ceases. This occurs when the premixed flame seeks Φ=1.0 and is converted into a classical non-premixed diffusion flame front, which remains semi-stationary as shown in figure 7.8(f). At the location of the flame front, the concentration of fuel and oxidizer approach a theoretical value of zero as the flame establishes itself at stoichiometric conditions.

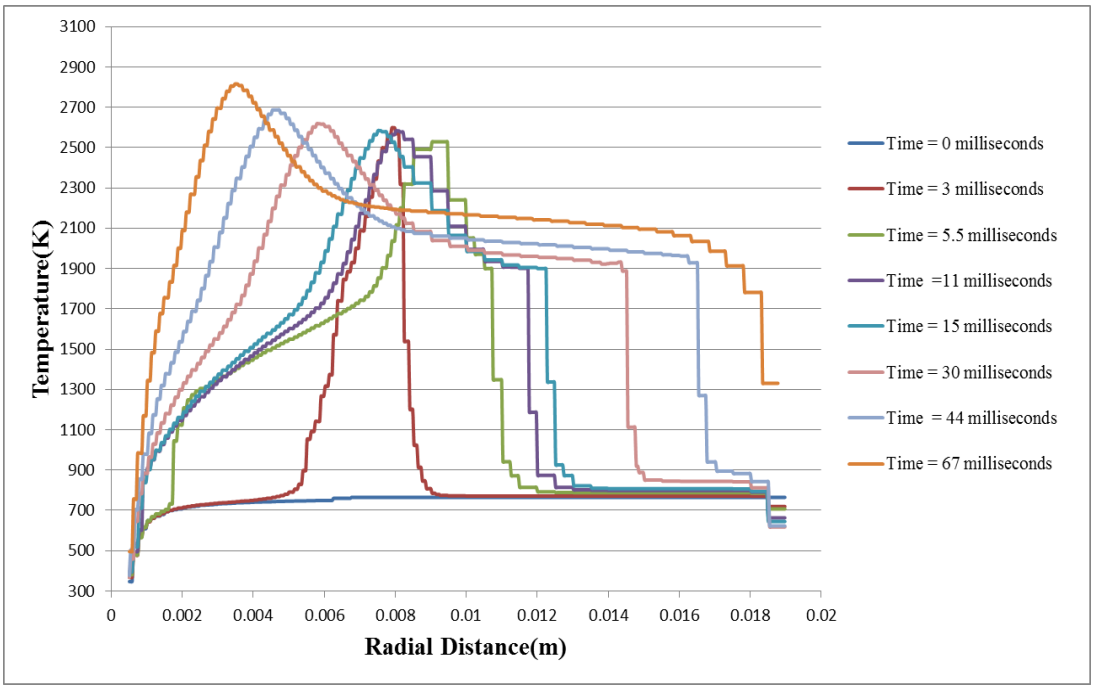

Figure 7.9 Temperature profiles in the gas phase surrounding a 1 mm heptane droplet in a $\phi = 0.5$ CH4/air mixture at $0.002 < t < 0.056$ seconds after compression to To = 765 K, Po = 27 bar.

Figure 7.9 is a plot of the gas phase temperature profiles at multiple times, which further illustrates the evolution of the position of the two flames. The figure reveals the initial inward movement of the diffusion flame and the outwardly propagating flame front of the premixed CH4/O2 flame as indicated by the sharp discontinuity in temperature across the flame front.

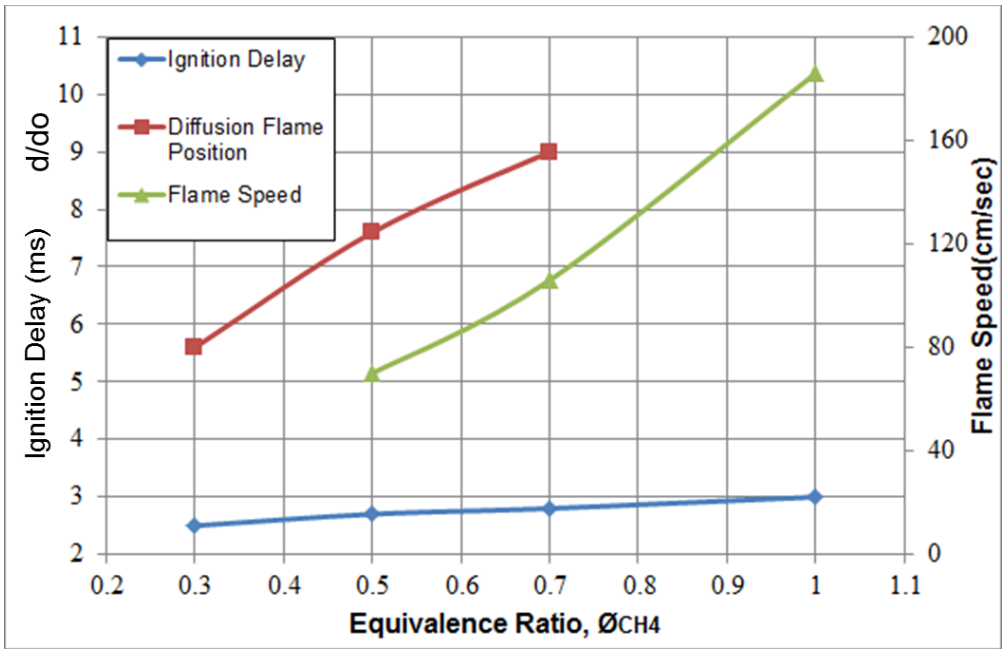

Figure 7.10 Parameter study of variation in flame speed, diffusion flame position and ignition delay with respect to equivalence ratios in far-field

As seen the figure 7.10, we see an effect of the changing equivalence ratio on the flame speed, position of diffusion flame and the change in the ignition delays of the high reactivity fuel. As the equivalence ratio in the farfield is increased, the premixed flame propagates faster consuming the low reactivity fuel/air mixture and increased in the flame speeds are observed. But increasing equivalence ratio of the far-field results in lesser oxygen availability after the premixed flame consumes the fuel/air charge. As less oxygen is available in the surrounding for higher equivalence ratio cases, diffusion flame establishes itself at a distance further away from the droplet surface as compared to lower equivalence ratio in the far-field. The change in the equivalence ratio in the far field also effects the ignition delay time of the high reactivity fuel droplet. As shown in the figure 7.10, as the equivalence ratio was increased we find increase in the ignition delay of the HRF.

CHAPTER 8: CONCLUSIONS AND FUTURE WORK

A computational study of the roll up vortices, homogenous autoignition and laser induced ignition of fuel/air mixtures, and dual fuel droplet ignition system is presented in the study. Motivation to study the roll up vortices was to study its effect on the flow field parameters like temperature, pressure, turbulences etc. Different crevice volumes of 3mm, 4mm, and 5 mm lengths were tested and a crevice volume of 5 mm length was found to ideal as it could keep all the low temperature mixture in the crevice volume with minimum mixing of the cold and hot fluid in the combustion chamber establishing the adiabatic core assumption to hold true.

Computational study of homogeneous autoignition was carried out in RCM with the motivation to validate the chemistry taking place in the RCM. First validation was carried out using iso-octane as the base fuel. A reduced chemical kinetic mechanism of 159 species and 805 reactions mechanism was developed to save the computational time which was validated against the ignition delay values of comprehensive chemical kinetic mechanism at various different values of temperature and pressure. The computational results obtained with CONVERGE^{TM} 3-D simulations and CHEMKIN 0-D simulations using the same experimental conditions were compared against the experimental results and a good agreement was achieved thus validating the chemistry in RCM. A 0-D and 3- D computational study using methane/air mixtures were also carried using CSU 86 and CSU 141 which where compared against the experimental data yielding a good agreement thus validating the chemical kinetics of CSU86 and CSU 141 mechanism and giving a second validation check of chemistry in the RCM.

Three-dimensional, transient computational study was carried for laser induced ignition of hydrocarbon /oxidizer mixtures with the motivation to study the laser induced ignition and get in-

depth details of the chemistry which the experiments were not able to capture. Simulation were carried out for methane/air mixtures at various equivalence ratios by modelling spark as hot spot of temperature for studying the flame propagation and lean limits. Simulations could capture the most of the relevant physics taking place near the piston and chamber walls which experiments were not able to capture. A good agreement was obtained comparing the lean limits found in experiments and computations which was phi = 0.45 for experiment and 0.43 for the computation considering combustion efficiency of 80%. With a good agreement between the computational and experimental results for methane/air laser ignition system, computational study of n-heptane/iso - octane/air using different blends were carried to characterize the knocking of end gas. Knocking of end gas was reported with increase in the n-heptane concentration in the blend (i.e. with increase in the octane number). A low temperature heat release was also reported which causes heating up of the end gas. The above sets of simulations prove the potential of RCM/laser system as a potential device to study the reactivity of fuels.

A dual fuel ignition system study was carried out computationally at various equivalence ratios in the far field which has methane/air mixture and has a heptane droplet at the center of the chamber. As predicted, the heptane droplet vaporizes due to hot ambience. As it being more reactivity, it auto ignites at some distance away from the droplet surface. This produces two flames in the systems namely the premixed flame propagating outwards and a diffusion flame which travel towards the droplet surface and maintain itself at stoichiometric conditions. Effect of the leaner and richer mixture in the far field on the position of diffusion flame has been reported which shows that as the mixture gets leaner, more oxygen is available for the diffusion flame causing the flame to move and stand closer to the droplet surface and at the same time causing the premixed flame to move slowly in the system. Also, the thermal breakdown was seen near the droplet surface

where the higher hydrocarbon (n- heptane) break into lower hydrocarbons like methane, ethane, propane etc. resulting in a flame to be established between the oxygen and the lower hydrocarbons.

Future work will be mainly focused on the three different combustion processes – homogeneous autoignition, spark induced ignition and dual fuel droplet ignition system. In case of homogenous autoignition study using RCM, a chemical kinetic mechanism can be developed incorporating the effects of fuel additives so as to test the potential of the fuel additives at certain conditions which experiments cannot produce and a detailed understanding of the fuel additive effects on the ignition delay and knocking can be established. For spark ignition of iso octane/n-heptane/air cases in RCM, experiments can be performed using RCM to validate the simulation results and its potential as a valuable tool to characterize the reactivity of fuel. Computational work of dual fuel ignition system was well understood using the computational approaches but it requires validation by performing experiments in RCM. Experiments will be performed at the same operating conditions as the computational model at various equivalence ratio of farfield. Some more computational study will also be conducted incorporating two droplets of high reactivity instead of one droplet to study the effect of the flame compression on the lean premixed fuel/air mixture present between them which may result in knocking. Experimental and computational results will be used to further validate the CSU 86 and CSU141 mechanism and necessary modifications will be made in the chemical mechanism scheme to widen the scope of the developed mechanism over wide ranges of temperature and pressure.

BIBLIOGRAPHY

[1] Vermeersch, M. L., Held, T. J., Stein, Y., and Dryer, F. L. (1991) Auto-Ignition Chemistry Studies of n-Butane in a Variable Pressure Flow Reactor. SAE Paper 912316.

[2] Kim, T. J., Yetter, R. A., and Dryer, F. L. (1994) New Results on Moist CO Oxidation: High Pressure, High Temperature Experiments and Comprehensive Kinetic Modeling. Proc. Combust. Inst., 25, 759-766.

[3] Dagaut, P., Reuillon, M., Cathonnet, M. (1995) Experimental Study of the Oxidation of n-Heptane in a Jet Stirred Reactor from Low to High Temperature and Pressures up to 40 Atm. Combust. Flame 101, 132-140.

[4] Sivaramakrishnan, R., Tranter, R.S., and Brezinsky, K. (2004) High-pressure, Hightemperature Oxidation of Toluene. Combust. Flame, 139, 340-350.

[5] Petersen, E., Davidson, D., Rohrig, M. and Hanson, R. (1996) High-pressure Shock-tube Measurements of Ignition Times in Stoichiometric H2/O2/Ar Mixtures. 20th International Symposium on Shock Waves, 941-946.

[6] Hu, H., and Keck, J. (1987) Autoignition of Adiabatically Compressed Combustible Gas Mixture. SAE 872110

[7] Griffiths, J. F., Halford-Maw, P. A., and Rose, D. J., (1993b) Fundamental Features of Hydrocarbon Autoignition in a Rapid Compression Machine. Combust. Flame, 95, 291-306.

[8] Tanaka, S., Ayala, F., and Keck, J. C. (2003b) A Reduced Chemical Kinetic Model for HCCI Combustion of Primary Reference Fuels in a Rapid Compression Machine. Combust. Flame, 133, 467-481.

[9] Daneshyar, H., Fuller, D. E., and Deckker, B. E. L. (1973) Vortex Motion Induced by the Piston of an Internal Combustion Engine. Int. J. Mech. Sci., 15, 381-390.

[10] Griffiths, J. F., Jiao, Q., Schreiber, A., Meyer, J., Knoche, K. F., and Kardylewski, W. (1993a) Experimental and Numerical Studies of Ditertiary Butyl Peroxide Combustion at High Pressure in a Rapid Compression Machine. Combust. Flame, 93, 303-315.

[11] Lee, D., and Hochgreb, S. (1998a) Rapid Compression Machine: Heat Transfer and Suppression of Corner Vortex. Combust. Flame, 114, 531-545.

[12] Clarkson, J., Griffiths, J. F., Macnamara, J. P., and Whitaker, B. J. (2001) Temperature Fields During the Development of Combustion in a Rapid Compression Machine. Combust. Flame, 125, 1162-1175.

[13] Convergent Science Inc., CONVERGE 2.2.0 Theory Manual, 2013.

[14] B. Launder and D. Spalding, "The Numerical Computation of Turbulent Flows," *Computer Methods in Applied Mechanics and Engineering*, 1974.

[15] A. Amsden, "KIVA 3-V: A Block Structured KIVA Program for Engines with Vertical or Canted Valves," Los Alamos National Laboratory Report No. LA-13313-MS, 1997.

[16] A. Babajimopoulos, D. Assanis, D. Flowers, S. Aceves and R. Hessel, "A fully coupled computational fluid dynamics and multi-zone model with detailed chemical kinetics

for the simulation of premixed charge compression ignition engines," Int. J. Engine Research, vol. 6, p. 497, 2005.

[17] Heywood, J. B., Internal Combustion Engine Fundamentals, McGraw Hill, Inc., 1988.

[18] J. Griffiths, Q. Jiao, W. Kordylewski, M. Schreiber, J. Jeyer and K. Knoche, "Experimental and numerical studies of ditertiary butyl peroxide combustion at high pressures in a rapid compression machine," Combustion and Flame, vol. 93, no. 3, pp. 303-315, 1993.

[19] P. Desgroux, L. Gasnot and L. Sochet, "Instantaneous temperature measurement in a rapid-compression machine using laser Rayleigh scattering," Applied Physics B, vol. 61, no. 1, pp. 69-72, 1995.

[20] G. Kukkadapu, K. Kumar, C. Sung, M. Mehl and W. Pitz, "Autoignition of gasoline and its surrogates in a rapid compression machine," Proceedings of the Combustion Institute, vol. 34, no. 1, pp. 345-352, 2013.

[21] S. Goldsborough, A chemical kinetically based ignition delay correlation for iso-octane covering a wide range of conditions including the NTC region, vol. 156, Combustion and Flame, 2009, pp. 1248-1262.

[22] G. Mittal and S. Sung, "Aerodynamics inside a rapid compression machine," Combustion and Flame , vol. 145, no. 1-2, pp. 160-180, 2006.

[23] C. Sung and H. Curran, "Using rapid compression machines for chemical kinetic studies," Progress in Energy and Combustion Science, no. dx.doi.org/10.1016/j.pecs.2014.04.001, 2014.

[24] M. Donovan, X. He, B. Zigler, T. Palmer, M. Woldridge and A. Atreya, "Demonstration of a free-piston rapid compression facility for the study of high temperature combustion phenomena," Combustion and Flame, vol. 137, pp. 351-365, 2004.

[25] M. Mehl, H. J. Curran, W. J. Pitz and C. K. Westbrook, "Chemical kinetic modeling of component mixtures relevant to gasoline," European Combustion Meeting, Vienna, Austria, 2009.

[26] S. S. Goldsborough, "A chemical kinetically based ignition delay correlation for iso-octane covering a wide range of conditions including the NTC region," Combustion and Flame, vol. 156, pp. 1248-1262, 2009.

[27] Andrew Boissure, Dissertation, Colorado State University, 2016

[28] H. Curran, P. Gaffuri, W. Pitz and C. Westbrook, "A Comprehensive Modeling Study of n-Heptane Oxidation," *Combustion and Flame*, vol. 114, pp. 149-177, 1998.

[29] B. Launder and D. Spalding, 'The Numerical Computation of Turbulent Flows," *Computer Methods in Applied Mechanics and Engineering*, 1974.

[30] Zsély, I. G., Nagy, T., Simmie, J. M., & Curran, H. J. (2011). Reduction of a detailed kinetic model for the ignition of methane/propane mixtures at gas turbine conditions using simulation error minimization methods. Combustion and Flame, 158(8), 1469-1479. DOI: 10.1016/j.combustflame.2010.12.011

[31] Mehl M., W.J. Pitz, C.K. Westbrook, H.J. Curran, "Kinetic Modeling of Gasoline Surrogate Components and Mixtures Under Engine Conditions", Proceedings of the Combustion Institute 33:193-200 (2011).

[32] N. Donato, C. Aul, E. Petersen, C. Zinner, H. Curran, G. Bourque Ignition and Oxidation of 50/50 Butane Isomer Blends Journal of Engineering for Gas Turbines and Power May 2010, Vol. 132 / 051502.

[33] Andrew Hockett, Greg Hampson, and Anthony J. Marchese," Development and Validation of a Reduced Chemical Kinetic Mechanism for Computational Fluid Dynamics Simulations of Natural Gas/Diesel Dual-Fuel Engines, Energy Fuels, 2016, 30 (3), pp 2414–2427

[34] Hockett, A. (2015). hD. Dissertation, Colorado State University.

[35] Hockett, A. G., Hampson, G. and Marchese, A. J. (2016). Reduced Chemical Kinetic Mechanism for CFD Simulations of Natural Gas/Diesel Dual Fuel Engines: Mechanism Development and Comparisons with Engine Experiments. Energy and Fuels, 30 (3), pp. 2414-2427.

[36] Hockett, A. G., Hampson, G. and Marchese, A. J. (2017). Natural Gas/Diesel RCCI CFD Simulations using Multi-component Fuel Surrogates. International Journal of Powertrains, In Press.

[37] C. Dumitrache, A. Boissiere, M. Baumgardner, A. Marchese, A. Yalin, A. Maria, and J. Roucis, "Laser Ignition of Methane-Air Mixtures: An Investigation of the Lean Limit and Minimum Ignition Energy," in Laser Ignition Conference, OSA Technical Digest (online) (Optical Society of America, 2015), paper W3A.4.

[38] Dumitrache, C., Baumgardner, M.E., Boissiere, A., Maria, A., Roucis, J., Marchese, A.J. and Yalin, A. (2016). A Study of Laser Induced Ignition of Methane-Air Mixtures

inside a Rapid Compression Ma-chine. Proc. Combust. Inst., DOI: 10.1016/j.proci.2016.05.033.

[39] Baumgardner M., Marchese, A. J. and Sarathy, M. (2013). Autoignition Characterization of Primary Reference Fuels and n-Heptane/n-Butanol mixtures in a Constant Volume Combustion Device and Homogeneous Charge Compression Ignition Engine. Energy and Fuels, 27 (12), pp. 7778-7779.

[40] Wang, H., Yao, M., Reitz, R.D. (2013). Development of a Reduced Primary Reference Fuel (PRF) Mechanism for IC Engine Combustion Simulations, Energy and Fuels, 27:7843-53.

[41] NSF Grant Proposal

[42] U.S. Energy Information Administration, "Annual Energy Outlook 2014 with Projections to 2040," DOE/EIA-0383(2014), 2014.

[43] G. Godsave, "Studies of the combustion of drops in a fuel spray—the burning of single drops of fuel," *Symposium (International) on Combustion*, vol. 4, no. 1, pp. 818-830, 1953.

[44] C. Law, "Recent advances in droplet vaporization and combustion," *Progress in Energy and Combustion Science*, vol. 8, no. 3, pp. 171-201, 1982.

[45] S. Sazhin, "Advanced models of fuel droplet heating and evaporation," *Progress in Energy and Combustion Science,* vol. 32, no. 2, pp. 162-214, 2006.

[46] C. Mansour, A. Bounif, A. Aris and F. Gillard, "Gas–Diesel (dual-fuel) modeling in diesel engine environment," *International Journal of Thermal Sciences,* vol. 40, no. 4, pp. 409-424, 2001.

[47] Y. Zhang, S. Kong and R. Reitz, "Modeling and Simulation of a Dual Fuel (Diesel/Natural Gas) Engine With Multidimensional CFD," *SAE Technical Paper 2003-01-0755*, 2003.

[48] A. Marchese, F. Dryer and V. Nayagam, "Numerical modeling of isolated n-alkane droplet flames: initial comparisons with ground and space-based microgravity experiments," *Combustion and Flame*, vol. 116, no. 3, pp. 432-459, 1999.

[49] T. Grumstrup, "NOx Formation in Methyl Ester, Alcohol, and Alkane Droplet," *Colorado State University, PhD Dissertation*, 2014.

[50] R. G. Gilbert, K. Luther and J. Troe, "Theory of Thermal Unimolecular Reactions in the Fall-off Range. II. Weak Collision Rate Constants," Ber. Bunsenges. Phys. Chem., vol. 87, no. 2, p. 169, 1983.

[51] Reaction Design, "CHEMKIN 10131: CHEMKIN Theory Manual," Reaction Design, San Diego, 2013.

APPENDIX A: A 159 species and 805 reactions reduced mechanism for Iso-octane

The following is the complete list of the chemical reactions and species that are found in the mechanism developed for carrying the computational study of homogenous autoignition of iso – octane as descried in the Chapter 5. Arrhenius form is used to represent the reaction rate constants associated with the given reactions are as shown below. Some of the reactions include the third body efficiency and Troe [50] pressure dependent reaction rates. CHEMKIN® theory manual [51] can be used to find out more information about the expressions used for reaction rates and format of mechanism. This mechanism was developed using Henry Curran's comprehensive iso-octane mechanism called iso –octane version 3 comprising of 893 species and 3600 reactions [25] with the method of direct relationship graph error propagation and sensitivity analysis as described in Chapter 3.

ELEMENTS CONSIDERED	ATOMIC WEIGHT
1. C	12.0112
2. H	1.00797
3. N	14.0067
4. O	15.9994
5. AR	39.9480
6. HE	4.00260

SPECIES CONSIDERED	PHASE	CHARGE	MOLECULAR WEIGHT	TEMPERATURE LOW	TEMPERATURE HIGH	ELEMENT COUNT C	H	N	O	AR	HE
1. H	G	0	1.0080E+00	300	5000	0	1	0	0	0	0
2. H2	G	0	2.0159E+00	300	5000	0	2	0	0	0	0
3. O	G	0	1.5999E+01	300	5000	0	0	0	1	0	0
4. O2	G	0	3.1999E+01	300	5000	0	0	0	2	0	0
5. OH	G	0	1.7007E+01	300	5000	0	1	0	1	0	0
6. H2O	G	0	1.8015E+01	300	5000	0	2	0	1	0	0
7. N2	G	0	2.8013E+01	300	5000	0	0	2	0	0	0
8. HO2	G	0	3.3007E+01	200	3500	0	1	0	2	0	0
9. H2O2	G	0	3.4015E+01	300	5000	0	2	0	2	0	0
10. AR	G	0	3.9948E+01	300	5000	0	0	0	0	1	0
11. CO	G	0	2.8011E+01	300	5000	1	0	0	1	0	0
12. CO2	G	0	4.4010E+01	300	5000	1	0	0	2	0	0
13. CH2O	G	0	3.0026E+01	300	5000	1	2	0	1	0	0
14. HCO	G	0	2.9019E+01	300	5000	1	1	0	1	0	0
15. HOCHO	G	0	4.6026E+01	300	5000	1	2	0	2	0	0
16. HOCH2O	G	0	4.7034E+01	300	5000	1	3	0	2	0	0
17. CH3OH	G	0	3.2042E+01	300	5000	1	4	0	1	0	0
18. CH2OH	G	0	3.1034E+01	300	5000	1	3	0	1	0	0
19. CH3O	G	0	3.1034E+01	300	5000	1	3	0	1	0	0
20. CH3O2H	G	0	4.8042E+01	300	5000	1	4	0	2	0	0
21. CH3O2	G	0	4.7034E+01	300	5000	1	3	0	2	0	0
22. CH4	G	0	1.6043E+01	300	5000	1	4	0	0	0	0
23. CH3	G	0	1.5035E+01	300	5000	1	3	0	0	0	0
24. C2H5	G	0	2.9062E+01	300	5000	2	5	0	0	0	0
25. C2H4	G	0	2.8054E+01	300	5000	2	4	0	0	0	0
26. C2H3	G	0	2.7046E+01	300	5000	2	3	0	0	0	0
27. C2H2	G	0	2.6038E+01	300	5000	2	2	0	0	0	0
28. C2H	G	0	2.5030E+01	300	5000	2	1	0	0	0	0
29. CH3CHO	G	0	4.4054E+01	300	5000	2	4	0	1	0	0
30. CH3CO	G	0	4.3046E+01	300	5000	2	3	0	1	0	0
31. CH2CHO	G	0	4.3046E+01	300	5000	2	3	0	1	0	0
32. CH2CO	G	0	4.2038E+01	300	5000	2	2	0	1	0	0
33. HCCO	G	0	4.1030E+01	300	4000	2	1	0	1	0	0
34. C2H3O1-2	G	0	4.3046E+01	300	5000	2	3	0	1	0	0
35. CH3COCH3	G	0	5.8081E+01	300	5000	3	6	0	1	0	0
36. CH3COCH2	G	0	5.7073E+01	300	5000	3	5	0	1	0	0
37. CH3COCH2O2	G	0	8.9072E+01	300	5000	3	5	0	3	0	0
38. CH3COCH2O2H	G	0	9.0079E+01	300	5000	3	6	0	3	0	0
39. CH3COCH2O	G	0	7.3072E+01	300	5000	3	5	0	2	0	0
40. C3H8	G	0	4.4097E+01	300	5000	3	8	0	0	0	0
41. IC3H7	G	0	4.3089E+01	300	5000	3	7	0	0	0	0
42. NC3H7	G	0	4.3089E+01	300	5000	3	7	0	0	0	0
43. C3H6	G	0	4.2081E+01	300	5000	3	6	0	0	0	0
44. C3H5-A	G	0	4.1073E+01	300	5000	3	5	0	0	0	0
45. C3H5-T	G	0	4.1073E+01	300	5000	3	5	0	0	0	0
46. C3H4-P	G	0	4.0065E+01	300	4000	3	4	0	0	0	0
47. C3H4-A	G	0	4.0065E+01	300	4000	3	4	0	0	0	0
48. C3H3	G	0	3.9057E+01	300	4000	3	3	0	0	0	0
49. C3H5O	G	0	5.7073E+01	300	5000	3	5	0	1	0	0
50. IC3H7O2H	G	0	7.6096E+01	300	5000	3	8	0	2	0	0
51. IC3H7O2	G	0	7.5088E+01	300	5000	3	7	0	2	0	0
52. IC3H7O	G	0	5.9089E+01	300	5000	3	7	0	1	0	0
53. C4H8-1	G	0	5.6108E+01	300	5000	4	8	0	0	0	0
54. PC4H9	G	0	5.7116E+01	300	5000	4	9	0	0	0	0
55. C4H71-3	G	0	5.5100E+01	300	5000	4	7	0	0	0	0
56. C4H72-2	G	0	5.5100E+01	300	5000	4	7	0	0	0	0
57. C4H6	G	0	5.4092E+01	300	5000	4	6	0	0	0	0
58. IC4H9	G	0	5.7116E+01	300	5000	4	9	0	0	0	0
59. TC4H9	G	0	5.7116E+01	300	5000	4	9	0	0	0	0
60. IC4H8	G	0	5.6108E+01	300	5000	4	8	0	0	0	0
61. IC4H7	G	0	5.5100E+01	300	5000	4	7	0	0	0	0
62. TC4H9O2	G	0	8.9115E+01	300	5000	4	9	0	2	0	0
63. IC4H9O2	G	0	8.9115E+01	300	5000	4	9	0	2	0	0
64. IC4H8O	G	0	7.2108E+01	300	5000	4	8	0	1	0	0
65. IC4H9O	G	0	7.3116E+01	300	5000	4	9	0	1	0	0
66. TC4H9O	G	0	7.3116E+01	300	5000	4	9	0	1	0	0
67. TC4H9O2H	G	0	9.0123E+01	300	5000	4	10	0	2	0	0
68. IC4H7O	G	0	7.1100E+01	300	5000	4	7	0	1	0	0
69. IC3H7CHO	G	0	7.2108E+01	300	5000	4	8	0	1	0	0
70. TC3H6CHO	G	0	7.1100E+01	300	5000	4	7	0	1	0	0
71. IC3H7CO	G	0	7.1100E+01	300	5000	4	7	0	1	0	0
72. IC4H7OH	G	0	7.2108E+01	300	5000	4	8	0	1	0	0
73. IC4H6OH	G	0	7.1100E+01	300	5000	4	7	0	1	0	0
74. IC3H5CHO	G	0	7.0092E+01	300	5000	4	6	0	1	0	0
75. IC3H5CO	G	0	6.9084E+01	300	5000	4	5	0	1	0	0
76. TC3H6OCHO	G	0	8.7099E+01	300	5000	4	7	0	2	0	0

77. IC3H6CO	G	0	7.0092E+01	300	5000	4	6	0	1	0	0
78. IC4H7OOH	G	0	8.8107E+01	300	5000	4	8	0	2	0	0
79. TC3H6O2HCO	G	0	1.0310E+02	300	5000	4	7	0	3	0	0
80. CH2CCH2OH	G	0	5.7073E+01	300	5000	3	5	0	1	0	0
81. CC5H10	G	0	7.0135E+01	300	5000	5	10	0	0	0	0
82. CC5H9-B	G	0	6.9127E+01	300	5000	5	9	0	0	0	0
83. CH3CHCHO	G	0	5.7073E+01	300	5000	3	5	0	1	0	0
84. BC6H12	G	0	8.4163E+01	300	5000	6	12	0	0	0	0
85. CC6H12	G	0	8.4163E+01	300	5000	6	12	0	0	0	0
86. CC6H11-B	G	0	8.3155E+01	300	5000	6	11	0	0	0	0
87. C5H10-1	G	0	7.0135E+01	300	5000	5	10	0	0	0	0
88. C5H10-2	G	0	7.0135E+01	300	5000	5	10	0	0	0	0
89. C5H92-4	G	0	6.9127E+01	300	5000	5	9	0	0	0	0
90. C5H11-2	G	0	7.1143E+01	300	5000	5	11	0	0	0	0
91. YC7H15	G	0	9.9198E+01	300	5000	7	15	0	0	0	0
92. XC7H14	G	0	9.8190E+01	300	5000	7	14	0	0	0	0
93. YC7H14	G	0	9.8190E+01	300	5000	7	14	0	0	0	0
94. XC7H13-Z	G	0	9.7182E+01	300	5000	7	13	0	0	0	0
95. YC7H13-Y2	G	0	9.7182E+01	300	5000	7	13	0	0	0	0
96. XC7H13O-Z	G	0	1.1318E+02	300	5000	7	13	0	1	0	0
97. YC7H15O2	G	0	1.3120E+02	300	5000	7	15	0	2	0	0
98. YC7H15O2H	G	0	1.3220E+02	300	5000	7	16	0	2	0	0
99. YC7H15O	G	0	1.1520E+02	300	5000	7	15	0	1	0	0
100. YC7H14OOH-Y2	G	0	1.3120E+02	300	5000	7	15	0	2	0	0
101. ACC6H10	G	0	8.2147E+01	300	5000	6	10	0	0	0	0
102. ACC6H9-D	G	0	8.1139E+01	300	5000	6	9	0	0	0	0
103. NEOC5H11	G	0	7.1143E+01	300	5000	5	11	0	0	0	0
104. NEOC5H11O2H	G	0	1.0415E+02	300	5000	5	12	0	2	0	0
105. NEOC5H11O2	G	0	1.0314E+02	300	5000	5	11	0	2	0	0
106. NEOC5H11O	G	0	8.7143E+01	300	5000	5	11	0	1	0	0
107. NEOC5H10OOH	G	0	1.0314E+02	300	5000	5	11	0	2	0	0
108. NEOC5H10OOH-O2	G	0	1.3514E+02	300	5000	5	11	0	4	0	0
109. NEOC5H9Q2-N	G	0	1.3514E+02	300	5000	5	11	0	4	0	0
110. NEOC5KET	G	0	1.1813E+02	300	5000	5	10	0	3	0	0
111. NEOC5KETOX	G	0	1.0113E+02	300	5000	5	9	0	2	0	0
112. TC4H9CHO	G	0	8.6135E+01	300	5000	5	10	0	1	0	0
113. C4H7CHO2-2	G	0	8.4119E+01	300	5000	5	8	0	1	0	0
114. C4H7CO2-2	G	0	8.3111E+01	300	5000	5	7	0	1	0	0
115. IC3H6CHCHO	G	0	8.4119E+01	300	5000	5	8	0	1	0	0
116. PC7H15	G	0	9.9198E+01	300	5000	7	15	0	0	0	0
117. OC7H14	G	0	9.8190E+01	300	5000	7	14	0	0	0	0
118. PC7H15O2	G	0	1.3120E+02	300	5000	7	15	0	2	0	0
119. PC7H15O2H	G	0	1.3220E+02	300	5000	7	16	0	2	0	0
120. PC7H15O	G	0	1.1520E+02	300	5000	7	15	0	1	0	0
121. IC8H18	G	0	1.1423E+02	300	5000	8	18	0	0	0	0
122. AC8H17	G	0	1.1322E+02	300	5000	8	17	0	0	0	0
123. BC8H17	G	0	1.1322E+02	300	5000	8	17	0	0	0	0
124. CC8H17	G	0	1.1322E+02	300	5000	8	17	0	0	0	0
125. DC8H17	G	0	1.1322E+02	300	5000	8	17	0	0	0	0
126. AC8H17O2	G	0	1.4522E+02	300	5000	8	17	0	2	0	0
127. BC8H17O2	G	0	1.4522E+02	300	5000	8	17	0	2	0	0
128. CC8H17O2	G	0	1.4522E+02	300	5000	8	17	0	2	0	0
129. DC8H17O2	G	0	1.4522E+02	300	5000	8	17	0	2	0	0
130. AC8H17O2H	G	0	1.4623E+02	300	5000	8	18	0	2	0	0
131. BC8H17O2H	G	0	1.4623E+02	300	5000	8	18	0	2	0	0
132. CC8H17O2H	G	0	1.4623E+02	300	5000	8	18	0	2	0	0
133. DC8H17O2H	G	0	1.4623E+02	300	5000	8	18	0	2	0	0
134. AC8H17O	G	0	1.2922E+02	300	5000	8	17	0	1	0	0
135. BC8H17O	G	0	1.2922E+02	300	5000	8	17	0	1	0	0
136. CC8H17O	G	0	1.2922E+02	300	5000	8	17	0	1	0	0
137. DC8H17O	G	0	1.2922E+02	300	5000	8	17	0	1	0	0
138. AC8H16OOH-A	G	0	1.4522E+02	300	5000	8	17	0	2	0	0
139. AC8H16OOH-B	G	0	1.4522E+02	300	5000	8	17	0	2	0	0
140. AC8H16OOH-C	G	0	1.4522E+02	300	5000	8	17	0	2	0	0
141. BC8H16OOH-A	G	0	1.4522E+02	300	5000	8	17	0	2	0	0
142. DC8H16OOH-B	G	0	1.4522E+02	300	5000	8	17	0	2	0	0
143. IC8ETERAA	G	0	1.2822E+02	300	5000	8	16	0	1	0	0
144. IC8ETERAB	G	0	1.2822E+02	300	5000	8	16	0	1	0	0
145. IC8ETERAC	G	0	1.2822E+02	300	5000	8	16	0	1	0	0
146. IC8ETERBD	G	0	1.2822E+02	300	5000	8	16	0	1	0	0
147. AC8H16OOH-AO2	G	0	1.7722E+02	300	5000	8	17	0	4	0	0
148. AC8H16OOH-BO2	G	0	1.7722E+02	300	5000	8	17	0	4	0	0
149. BC8H16OOH-AO2	G	0	1.7722E+02	300	5000	8	17	0	4	0	0
150. DC8H16OOH-BO2	G	0	1.7722E+02	300	5000	8	17	0	4	0	0
151. IC8KETAA	G	0	1.6021E+02	300	5000	8	16	0	3	0	0
152. IC8KETAB	G	0	1.6021E+02	300	5000	8	16	0	3	0	0
153. IC8KETBA	G	0	1.6021E+02	300	5000	8	16	0	3	0	0
154. IC8KETDB	G	0	1.6021E+02	300	5000	8	16	0	3	0	0
155. DC6H12CHO-D	G	0	1.1318E+02	300	5000	7	13	0	1	0	0
156. IC3H7COC3H6-T	G	0	1.1318E+02	300	5000	7	13	0	1	0	0
157. IC3H6CHCOCH3	G	0	9.8146E+01	300	5000	6	10	0	1	0	0
158. AC3H5CHCOCH3	G	0	9.7138E+01	300	5000	6	9	0	1	0	0
159. IC3H6CHCOCH2	G	0	9.7138E+01	300	5000	6	9	0	1	0	0

REACTIONS CONSIDERED	(k = A T**b exp(-E/RT)) A	b	E
1. H+O2=O+OH	3.55E+15	-0.4	16600.0

```
    Reverse Arrhenius coefficients:                1.03E+13   -0.0     -133.0
 2. O+H2=H+OH                                      5.08E+04    2.7     6292.0
    Reverse Arrhenius coefficients:                2.64E+04    2.7     4880.0
 3. OH+H2=H+H2O                                    2.16E+08    1.5     3430.0
    Reverse Arrhenius coefficients:                2.29E+09    1.4    18320.0
 4. O+H2O=OH+OH                                    2.97E+06    2.0    13400.0
    Reverse Arrhenius coefficients:                1.45E+05    2.1    -2904.0
 5. H2+M=H+H+M                                     4.58E+19   -1.4   104400.0
    H2              Enhanced by    2.500E+00
    H2O             Enhanced by    1.200E+01
    CO              Enhanced by    1.900E+00
    CO2             Enhanced by    3.800E+00
    Reverse Arrhenius coefficients:                1.14E+20   -1.7      820.0
 6. O2+M=O+O+M                                     4.42E+17   -0.6   118900.0
    H2              Enhanced by    2.500E+00
    H2O             Enhanced by    1.200E+01
    AR              Enhanced by    8.300E-01
    CO              Enhanced by    1.900E+00
    CO2             Enhanced by    3.800E+00
    CH4             Enhanced by    2.000E+00
    Reverse Arrhenius coefficients:                6.16E+15   -0.5        0.0
 7. OH+M=O+H+M                                     9.78E+17   -0.7   102100.0
    H2              Enhanced by    2.500E+00
    H2O             Enhanced by    1.200E+01
    AR              Enhanced by    7.500E-01
    CO              Enhanced by    1.500E+00
    CO2             Enhanced by    2.000E+00
    CH4             Enhanced by    2.000E+00
    Reverse Arrhenius coefficients:                4.71E+18   -1.0        0.0
 8. H2O+M=H+OH+M                                   1.91E+23   -1.8   118500.0
    H2              Enhanced by    7.300E-01
    H2O             Enhanced by    1.200E+01
    AR              Enhanced by    3.800E-01
    CH4             Enhanced by    2.000E+00
    Reverse Arrhenius coefficients:                4.50E+22   -2.0        0.0
 9. H+O2(+M)=HO2(+M)                               1.48E+12    0.6        0.0
    Low pressure limit:  0.34820E+17 -0.41100E+00 -0.11150E+04
    TROE centering:      0.50000E+00  0.10000E-29  0.10000E+31  0.10000E+11
    H2              Enhanced by    1.300E+00
    H2O             Enhanced by    1.400E+01
    AR              Enhanced by    6.700E-01
    CO              Enhanced by    1.900E+00
    CO2             Enhanced by    3.800E+00
    CH4             Enhanced by    2.000E+00
10. HO2+H=H2+O2                                    1.66E+13    0.0      823.0
    Reverse Arrhenius coefficients:                3.17E+12    0.3    55510.0
11. HO2+H=OH+OH                                    7.08E+13    0.0      295.0
    Reverse Arrhenius coefficients:                2.03E+10    0.7    36840.0
12. HO2+O=OH+O2                                    3.25E+13    0.0        0.0
    Reverse Arrhenius coefficients:                3.22E+12    0.3    53280.0
13. HO2+OH=H2O+O2                                  1.97E+10    1.0     -328.4
    Reverse Arrhenius coefficients:                3.99E+10    1.2    69250.0
14. H2O2+O2=HO2+HO2                                1.14E+16   -0.3    49730.0
    Reverse Arrhenius coefficients:                1.03E+14    0.0    11040.0
    Declared duplicate reaction...
15. H2O2+O2=HO2+HO2                                2.14E+13   -0.3    37280.0
    Reverse Arrhenius coefficients:                1.94E+11    0.0    -1409.0
    Declared duplicate reaction...
16. H2O2(+M)=OH+OH(+M)                             2.95E+14    0.0    48430.0
    Low pressure limit:  0.12020E+18  0.00000E+00  0.45500E+05
    TROE centering:      0.50000E+00  0.10000E-29  0.10000E+31  0.10000E+11
    H2              Enhanced by    2.500E+00
    H2O             Enhanced by    1.200E+01
    AR              Enhanced by    6.400E-01
    CO              Enhanced by    1.900E+00
    CO2             Enhanced by    3.800E+00
    CH4             Enhanced by    2.000E+00
17. H2O2+H=H2O+OH                                  2.41E+13    0.0     3970.0
    Reverse Arrhenius coefficients:                1.26E+08    1.3    71410.0
18. H2O2+H=H2+HO2                                  2.15E+10    1.0     6000.0
    Reverse Arrhenius coefficients:                3.72E+07    1.7    22000.0
19. H2O2+O=OH+HO2                                  9.55E+06    2.0     3970.0
    Reverse Arrhenius coefficients:                8.57E+03    2.7    18560.0
20. H2O2+OH=H2O+HO2                                2.00E+12    0.0      427.2
    Reverse Arrhenius coefficients:                3.66E+10    0.6    31320.0
    Declared duplicate reaction...
21. H2O2+OH=H2O+HO2                                1.70E+18    0.0    29410.0
    Reverse Arrhenius coefficients:                3.12E+16    0.6    60300.0
    Declared duplicate reaction...
22. CO+O(+M)=CO2(+M)                               1.80E+10    0.0     2384.0
    Low pressure limit:  0.13500E+25 -0.27880E+01  0.41910E+04
    H2              Enhanced by    2.000E+00
    O2              Enhanced by    6.000E+00
    H2O             Enhanced by    6.000E+00
    AR              Enhanced by    5.000E-01
    CO              Enhanced by    1.500E+00
    CO2             Enhanced by    3.500E+00
    CH4             Enhanced by    2.000E+00
23. CO+O2=CO2+O                                    1.05E+12    0.0    42540.0
    Reverse Arrhenius coefficients:                8.04E+15   -0.8    51230.0
24. CO+OH=CO2+H                                    2.23E+05    1.9    -1158.0
    Reverse Arrhenius coefficients:                5.90E+11    0.7    24260.0
25. CO+HO2=CO2+OH                                  3.01E+13    0.0    23000.0
    Reverse Arrhenius coefficients:                2.28E+16   -0.5    84970.0
26. HCO+M=H+CO+M                                   4.75E+11    0.7    14870.0
```

```
    H2              Enhanced by    2.000E+00
    H2O             Enhanced by    1.200E+01
    CO              Enhanced by    1.500E+00
    CO2             Enhanced by    2.000E+00
    CH4             Enhanced by    2.000E+00
    Reverse Arrhenius coefficients:                3.58E+10    1.0     -457.3
27. HCO+O2=CO+HO2                                  7.58E+12    0.0      410.0
    Reverse Arrhenius coefficients:                1.20E+12    0.3    33950.0
28. HCO+H=CO+H2                                    7.34E+13    0.0        0.0
    Reverse Arrhenius coefficients:                2.21E+12    0.7    88230.0
29. HCO+O=CO+OH                                    3.02E+13    0.0        0.0
    Reverse Arrhenius coefficients:                4.72E+11    0.6    86820.0
30. HCO+O=CO2+H                                    3.00E+13    0.0        0.0
    Reverse Arrhenius coefficients:                1.24E+18   -0.6   112200.0
31. HCO+OH=CO+H2O                                  1.02E+14    0.0        0.0
    Reverse Arrhenius coefficients:                3.26E+13    0.6   103100.0
32. HCO+CH3=CH4+CO                                 2.65E+13    0.0        0.0
    Reverse Arrhenius coefficients:                7.29E+14    0.2    89770.0
33. HCO+HO2=CH2O+O2                                2.50E+14   -0.1    13920.0
    Reverse Arrhenius coefficients:                8.07E+15    0.0    53420.0
34. HCO+HO2=CO2+H+OH                               3.00E+13    0.0        0.0
    Warning...all REV parameters are zero...          0.00000E+00 0.00000E+00 0.00000E+00
            this reaction will be treated as irreversible
35. CH2O+CO=HCO+HCO                                9.19E+13    0.4    73040.0
    Reverse Arrhenius coefficients:                1.80E+13    0.0        0.0
36. HCO+HCO=H2+CO+CO                               3.00E+12    0.0        0.0
    Warning...all REV parameters are zero...          0.00000E+00 0.00000E+00 0.00000E+00
            this reaction will be treated as irreversible
37. HCO+H(+M)=CH2O(+M)                             1.09E+12    0.5     -260.0
    Low pressure limit:  0.13500E+25 -0.25700E+01  0.14250E+04
    TROE centering:      0.78240E+00  0.27100E+03  0.27550E+04  0.65700E+04
    H2              Enhanced by    2.000E+00
    H2O             Enhanced by    6.000E+00
    AR              Enhanced by    7.000E-01
    CO              Enhanced by    1.500E+00
    CO2             Enhanced by    2.000E+00
    CH4             Enhanced by    2.000E+00
38. CO+H2(+M)=CH2O(+M)                             4.30E+07    1.5    79600.0
    Low pressure limit:  0.50700E+28 -0.34200E+01  0.84348E+05
    TROE centering:      0.93200E+00  0.19700E+03  0.15400E+04  0.10300E+05
    H2              Enhanced by    2.000E+00
    H2O             Enhanced by    6.000E+00
    AR              Enhanced by    7.000E-01
    CO              Enhanced by    1.500E+00
    CO2             Enhanced by    2.000E+00
    CH4             Enhanced by    2.000E+00
39. CH2O+OH=HCO+H2O                                7.82E+07    1.6    -1055.0
    Reverse Arrhenius coefficients:                4.90E+06    1.8    29030.0
40. CH2O+H=HCO+H2                                  5.74E+07    1.9     2740.0
    Reverse Arrhenius coefficients:                3.39E+05    2.2    17930.0
41. CH2O+O=HCO+OH                                  6.26E+09    1.1     2260.0
    Reverse Arrhenius coefficients:                1.92E+07    1.4    16040.0
42. CH2O+CH3=HCO+CH4                               3.83E+01    3.4     4312.0
    Reverse Arrhenius coefficients:                2.06E+02    3.2    21040.0
43. CH2O+HO2=HCO+H2O2                              7.10E-03    4.5     6580.0
    Reverse Arrhenius coefficients:                2.43E-02    4.1     5769.0
44. HOCH2O=CH2O+OH                                 2.06E+21   -2.3    25730.0
    Reverse Arrhenius coefficients:                4.50E+15   -1.1        0.0
45. HOCH2O=HOCHO+H                                 1.00E+14    0.0    14900.0
    Reverse Arrhenius coefficients:                1.12E+15   -0.3    11500.0
46. HOCHO=CO+H2O                                   2.45E+12    0.0    60470.0
    Reverse Arrhenius coefficients:                2.26E+03    2.1    52890.0
47. HOCHO=CO2+H2                                   2.95E+09    0.0    48520.0
    Reverse Arrhenius coefficients:                6.77E+05    1.0    51470.0
48. HOCHO=HCO+OH                                   3.47E+22   -1.5   110700.0
    Reverse Arrhenius coefficients:                1.00E+14    0.0        0.0
49. HOCHO+OH=H2O+CO2+H                             2.62E+06    2.1      916.0
    Warning...all REV parameters are zero...          0.00000E+00 0.00000E+00 0.00000E+00
            this reaction will be treated as irreversible
50. HOCHO+OH=H2O+CO+OH                             1.85E+07    1.5     -962.0
    Warning...all REV parameters are zero...          0.00000E+00 0.00000E+00 0.00000E+00
            this reaction will be treated as irreversible
51. HOCHO+H=H2+CO2+H                               4.24E+06    2.1     4868.0
    Warning...all REV parameters are zero...          0.00000E+00 0.00000E+00 0.00000E+00
            this reaction will be treated as irreversible
52. HOCHO+H=H2+CO+OH                               6.03E+13   -0.3     2988.0
    Warning...all REV parameters are zero...          0.00000E+00 0.00000E+00 0.00000E+00
            this reaction will be treated as irreversible
53. HOCHO+CH3=CH4+CO+OH                            3.90E-07    5.8     2200.0
    Warning...all REV parameters are zero...          0.00000E+00 0.00000E+00 0.00000E+00
            this reaction will be treated as irreversible
54. HOCHO+HO2=H2O2+CO+OH                           1.00E+12    0.0    11920.0
    Warning...all REV parameters are zero...          0.00000E+00 0.00000E+00 0.00000E+00
            this reaction will be treated as irreversible
55. HOCHO+O=CO+OH+OH                               1.77E+18   -1.9     2975.0
    Warning...all REV parameters are zero...          0.00000E+00 0.00000E+00 0.00000E+00
            this reaction will be treated as irreversible
56. CH3O(+M)=CH2O+H(+M)                            6.80E+13    0.0    26170.0
    Low pressure limit:  0.18670E+26 -0.30000E+01  0.24307E+05
    TROE centering:      0.90000E+00  0.25000E+04  0.13000E+04  0.10000+100
    H2              Enhanced by    2.000E+00
    H2O             Enhanced by    6.000E+00
    CO              Enhanced by    1.500E+00
    CO2             Enhanced by    2.000E+00
    CH4             Enhanced by    2.000E+00
```

```
57. CH3O+O2=CH2O+HO2                                  4.38E-19    9.5    -5501.0
    Reverse Arrhenius coefficients:                   1.42E-20    9.8    21080.0
58. CH2O+CH3O=CH3OH+HCO                               6.62E+11    0.0     2294.0
    Reverse Arrhenius coefficients:                   8.39E+10    0.1    17710.0
59. CH4+CH3O=CH3+CH3OH                                6.12E+02    2.9     8248.0
    Reverse Arrhenius coefficients:                   1.44E+01    3.1     6935.0
60. CH3O+CH3=CH2O+CH4                                 1.20E+13    0.0        0.0
    Reverse Arrhenius coefficients:                   6.75E+13    0.2    82810.0
61. CH3O+H=CH2O+H2                                    2.00E+13    0.0        0.0
    Reverse Arrhenius coefficients:                   1.23E+11    0.7    81270.0
62. CH3O+HO2=CH2O+H2O2                                3.01E+11    0.0        0.0
    Reverse Arrhenius coefficients:                   1.07E+12   -0.0    65270.0
63. CH2O+H(+M)=CH2OH(+M)                              5.40E+11    0.5     3600.0
    Low pressure limit:  0.12700E+33 -0.48200E+01  0.65300E+04
    TROE centering:      0.71870E+00  0.10300E+03  0.12910E+04  0.41600E+04
    H2              Enhanced by    2.000E+00
    H2O             Enhanced by    6.000E+00
    CO              Enhanced by    1.500E+00
    CO2             Enhanced by    2.000E+00
    CH4             Enhanced by    2.000E+00
64. CH2OH+O2=CH2O+HO2                                 1.51E+15   -1.0        0.0
    Reverse Arrhenius coefficients:                   1.98E+14   -0.6    20060.0
    Declared duplicate reaction...
65. CH2OH+O2=CH2O+HO2                                 2.41E+14    0.0     5017.0
    Reverse Arrhenius coefficients:                   3.15E+13    0.4    25080.0
    Declared duplicate reaction...
66. CH2OH+H=CH2O+H2                                   6.00E+12    0.0        0.0
    Reverse Arrhenius coefficients:                   1.50E+11    0.8    74750.0
67. CH2OH+HO2=CH2O+H2O2                               1.20E+13    0.0        0.0
    Reverse Arrhenius coefficients:                   1.73E+14    0.1    58750.0
68. CH2OH+HCO=CH2O+CH2O                               1.80E+14    0.0        0.0
    Reverse Arrhenius coefficients:                   7.60E+14    0.5    59560.0
69. CH2OH+CH3O=CH2O+CH3OH                             2.40E+13    0.0        0.0
    Reverse Arrhenius coefficients:                   1.28E+13    0.6    74980.0
70. CH2OH+CH2O=CH3OH+HCO                              1.88E+04    2.7     4208.0
    Reverse Arrhenius coefficients:                   9.63E+03    2.9    13110.0
71. OH+CH2OH=H2O+CH2O                                 2.40E+13    0.0        0.0
    Reverse Arrhenius coefficients:                   6.35E+12    0.7    89640.0
72. O+CH2OH=OH+CH2O                                   4.20E+13    0.0        0.0
    Reverse Arrhenius coefficients:                   5.44E+11    0.7    73340.0
73. CH2O+CH3OH=CH2OH+CH2OH                            6.50E+12    0.7    68460.0
    Reverse Arrhenius coefficients:                   3.00E+12    0.0        0.0
74. CH2OH+HO2=HOCH2O+OH                               1.00E+13    0.0        0.0
    Reverse Arrhenius coefficients:                   8.17E+13   -0.0    33470.0
75. CH3OH(+M)=CH3+OH(+M)                              1.90E+16    0.0    91730.0
    Low pressure limit:  0.29500E+45 -0.73500E+01  0.95460E+05
    TROE centering:      0.41400E+00  0.27900E+03  0.54590E+04  0.10000E+11
76. CH3OH(+M)=CH2OH+H(+M)                             2.69E+16   -0.1    98940.0
    Low pressure limit:  0.23400E+41 -0.63300E+01  0.10310E+06
    TROE centering:      0.77300E+00  0.69300E+03  0.53330E+04  0.10000E+11
77. CH3OH+H=CH3O+H2                                   3.60E+12    0.0     6095.0
    Reverse Arrhenius coefficients:                   1.68E+11    0.2     5868.0
78. CH3OH+H=CH2OH+H2                                  1.20E+06    2.4     2583.0
    Reverse Arrhenius coefficients:                   1.39E+04    2.5     8871.0
79. CH3OH+O=CH2OH+OH                                  3.88E+05    2.5     3080.0
    Reverse Arrhenius coefficients:                   2.32E+03    2.6     7956.0
80. CH3OH+OH=CH3O+H2O                                 5.13E+05    2.1     2450.0
    Reverse Arrhenius coefficients:                   2.53E+05    2.2    17120.0
81. CH3OH+OH=CH2OH+H2O                                1.44E+06    2.0     -839.0
    Reverse Arrhenius coefficients:                   1.76E+05    2.0    20340.0
82. CH3OH+O2=CH2OH+HO2                                2.05E+13    0.0    44900.0
    Reverse Arrhenius coefficients:                   1.24E+12   -0.2    -3501.0
83. CH3OH+HO2=CH2OH+H2O2                              1.08E+04    2.5    10530.0
    Reverse Arrhenius coefficients:                   7.20E+04    2.0      819.0
84. CH3OH+CH3=CH2OH+CH4                               3.19E+01    3.2     7172.0
    Reverse Arrhenius coefficients:                   3.35E+02    2.8    15000.0
85. CH3O+CH3OH=CH2OH+CH3OH                            3.00E+11    0.0     4074.0
    Reverse Arrhenius coefficients:                   7.42E+10   -0.1    10590.0
86. CH3OH+CH2O=CH3O+CH3O                              7.98E+12    0.5    81490.0
    Reverse Arrhenius coefficients:                   6.03E+13    0.0        0.0
87. CH3+H(+M)=CH4(+M)                                 1.27E+16   -0.6      383.0
    Low pressure limit:  0.24770E+34 -0.47600E+01  0.24440E+04
    TROE centering:      0.78300E+00  0.74000E+02  0.29400E+04  0.69600E+04
    H2              Enhanced by    2.000E+00
    H2O             Enhanced by    6.000E+00
    AR              Enhanced by    7.000E-01
    CO              Enhanced by    1.500E+00
    CO2             Enhanced by    2.000E+00
    CH4             Enhanced by    2.000E+00
88. CH4+H=CH3+H2                                      6.14E+05    2.5     9587.0
    Reverse Arrhenius coefficients:                   6.73E+02    2.9     8047.0
89. CH4+OH=CH3+H2O                                    5.83E+04    2.6     2190.0
    Reverse Arrhenius coefficients:                   6.78E+02    2.9    15540.0
90. CH4+O=CH3+OH                                      1.02E+09    1.5     8600.0
    Reverse Arrhenius coefficients:                   5.80E+05    1.9     5648.0
91. CH4+HO2=CH3+H2O2                                  1.13E+01    3.7    21010.0
    Reverse Arrhenius coefficients:                   7.17E+00    3.5     3468.0
92. CH3+OH=CH2O+H2                                    8.00E+09    0.5    -1755.0
    Reverse Arrhenius coefficients:                   1.07E+12    0.3    68210.0
93. CH3+OH=CH3O+H                                     6.94E+07    1.3    11200.0
    Reverse Arrhenius coefficients:                   1.50E+12    0.5     -110.0
94. CH3+OH=CH2OH+H                                    3.09E+07    1.6     4506.0
    Reverse Arrhenius coefficients:                   1.65E+11    0.7     -284.0
95. CH3+HO2=CH3O+OH                                   1.00E+12    0.3     -687.5
    Reverse Arrhenius coefficients:                   6.19E+12    0.1    24550.0
```

```
 96. CH3+HO2=CH4+O2                                  1.16E+05    2.2    -3022.0
     Reverse Arrhenius coefficients:                 2.02E+07    2.1    53210.0
 97. CH3+O=CH2O+H                                    5.54E+13    0.1     -136.0
     Reverse Arrhenius coefficients:                 3.83E+15   -0.1    68410.0
 98. CH3+O2=CH3O+O                                   7.55E+12    0.0    28320.0
     Reverse Arrhenius coefficients:                 4.72E+14   -0.5      288.0
 99. CH3+O2=CH2O+OH                                  2.64E+00    3.3     8105.0
     Reverse Arrhenius coefficients:                 5.28E-01    3.5    59920.0
100. CH3+O2(+M)=CH3O2(+M)                            7.81E+09    0.9        0.0
     Low pressure limit:  0.68500E+25 -0.30000E+01  0.00000E+00
     TROE centering:      0.60000E+00  0.10000E+04  0.70000E+02  0.17000E+04
101. CH3O2+CH2O=CH3O2H+HCO                           1.99E+12    0.0    11660.0
     Reverse Arrhenius coefficients:                 1.32E+14   -0.9     9259.0
102. CH4+CH3O2=CH3+CH3O2H                            1.81E+11    0.0    18480.0
     Reverse Arrhenius coefficients:                 2.23E+12   -0.7     -655.0
103. CH3OH+CH3O2=CH2OH+CH3O2H                        1.81E+12    0.0    13710.0
     Reverse Arrhenius coefficients:                 2.35E+14   -1.0     2404.0
104. CH3O2+CH3=CH3O+CH3O                             5.08E+12    0.0    -1411.0
     Reverse Arrhenius coefficients:                 1.97E+12    0.2    28070.0
105. CH3O2+HO2=CH3O2H+O2                             2.47E+11    0.0    -1570.0
     Reverse Arrhenius coefficients:                 5.30E+14   -0.8    35520.0
106. CH3O2+CH3O2=CH2O+CH3OH+O2                       3.11E+14   -1.6    -1051.0
     Warning...all REV parameters are zero...           0.00000E+00 0.00000E+00 0.00000E+00
              this reaction will be treated as irreversible
107. CH3O2+CH3O2=O2+CH3O+CH3O                        1.40E+16   -1.6     1860.0
     Warning...all REV parameters are zero...           0.00000E+00 0.00000E+00 0.00000E+00
              this reaction will be treated as irreversible
108. CH3O2+H=CH3O+OH                                 9.60E+13    0.0        0.0
     Reverse Arrhenius coefficients:                 1.72E+09    1.0    40780.0
109. CH3O2+O=CH3O+O2                                 3.60E+13    0.0        0.0
     Reverse Arrhenius coefficients:                 2.23E+11    0.6    57520.0
110. CH3O2+OH=CH3OH+O2                               6.00E+13    0.0        0.0
     Reverse Arrhenius coefficients:                 1.54E+13    0.4    59160.0
111. CH3O2H=CH3O+OH                                  6.31E+14    0.0    42300.0
     Reverse Arrhenius coefficients:                 2.51E+06    1.9    -2875.0
112. C2H4+H(+M)=C2H5(+M)                             1.08E+12    0.5     1822.0
     Low pressure limit:  0.12000E+43 -0.76200E+01  0.69700E+04
     TROE centering:      0.97500E+00  0.21000E+03  0.98400E+03  0.43740E+04
     H2              Enhanced by    2.000E+00
     H2O             Enhanced by    6.000E+00
     AR              Enhanced by    7.000E-01
     CO              Enhanced by    1.500E+00
     CO2             Enhanced by    2.000E+00
     CH4             Enhanced by    2.000E+00
113. H2+CH3O2=H+CH3O2H                               1.50E+14    0.0    26030.0
     Reverse Arrhenius coefficients:                 1.69E+18   -1.1     8434.0
114. C2H5+C2H3=C2H4+C2H4                             6.86E+11    0.1    -4300.0
     Reverse Arrhenius coefficients:                 4.82E+14    0.0    71530.0
115. CH3+C2H5=CH4+C2H4                               1.18E+04    2.5    -2921.0
     Reverse Arrhenius coefficients:                 2.39E+06    2.4    66690.0
116. C2H5+H=CH3+CH3                                  9.69E+13    0.0      220.0
     Reverse Arrhenius coefficients:                 2.03E+09    1.0    10510.0
117. C2H5+H=C2H4+H2                                  2.00E+12    0.0        0.0
     Reverse Arrhenius coefficients:                 4.44E+11    0.4    68070.0
118. C2H5+O=CH3CHO+H                                 1.10E+14    0.0        0.0
     Reverse Arrhenius coefficients:                 1.03E+17   -0.5    77420.0
119. C2H5+O2=C2H4+HO2                                7.56E+14   -1.0     4749.0
     Reverse Arrhenius coefficients:                 8.80E+14   -1.0    18130.0
     Declared duplicate reaction...
120. C2H5+O2=C2H4+HO2                                4.00E-01    3.9    13620.0
     Reverse Arrhenius coefficients:                 4.66E-01    3.9    27000.0
     Declared duplicate reaction...
121. C2H5+O2=CH3CHO+OH                               8.26E+02    2.4     5285.0
     Reverse Arrhenius coefficients:                 2.25E+03    2.3    65970.0
122. C2H3O1-2=CH3CO                                  8.50E+14    0.0    14000.0
     Reverse Arrhenius coefficients:                 1.00E+14    0.0    48710.0
123. C2H3O1-2=CH2CHO                                 1.00E+14    0.0    14000.0
     Reverse Arrhenius coefficients:                 1.24E+15   -0.4    44010.0
124. CH3CHO=CH3+HCO                                  7.69E+20   -1.3    86950.0
     Reverse Arrhenius coefficients:                 1.75E+13    0.0        0.0
125. CH3CHO+H=CH3CO+H2                               2.37E+13    0.0     3642.0
     Reverse Arrhenius coefficients:                 1.64E+10    0.6    17600.0
126. CH3CHO+O=CH3CO+OH                               5.94E+12    0.0     1868.0
     Reverse Arrhenius coefficients:                 2.13E+09    0.6    14410.0
127. CH3CHO+OH=CH3CO+H2O                             3.37E+12    0.0     -619.0
     Reverse Arrhenius coefficients:                 2.47E+10    0.5    28230.0
128. CH3CHO+O2=CH3CO+HO2                             3.01E+13    0.0    39150.0
     Reverse Arrhenius coefficients:                 1.09E+11    0.3    -1588.0
129. CH3CHO+CH3=CH3CO+CH4                            7.08E-04    4.6     1966.0
     Reverse Arrhenius coefficients:                 4.47E-04    4.8    17460.0
130. CH3CHO+HO2=CH3CO+H2O2                           3.01E+12    0.0    11920.0
     Reverse Arrhenius coefficients:                 1.20E+12   -0.1     9877.0
131. CH3O2+CH3CHO=CH3O2H+CH3CO                       3.01E+12    0.0    11920.0
     Reverse Arrhenius coefficients:                 2.34E+13   -0.5     8282.0
132. CH3CHO+OH=CH3+HOCHO                             3.00E+15   -1.1        0.0
     Reverse Arrhenius coefficients:                 2.37E+16   -1.3    23750.0
133. CH3CHO+OH=CH2CHO+H2O                            1.72E+05    2.4      815.0
     Reverse Arrhenius coefficients:                 1.33E+05    2.5    24950.0
134. CH3CO(+M)=CH3+CO(+M)                            3.00E+12    0.0    16720.0
     Low pressure limit:  0.12000E+16  0.00000E+00  0.12518E+05
135. CH3CO+H=CH2CO+H2                                2.00E+13    0.0        0.0
     Reverse Arrhenius coefficients:                 1.04E+13    0.2    60560.0
136. CH3CO+O=CH2CO+OH                                2.00E+13    0.0        0.0
     Reverse Arrhenius coefficients:                 5.38E+12    0.2    59140.0
137. CH3CO+CH3=CH2CO+CH4                             5.00E+13    0.0        0.0
```

```
     Reverse Arrhenius coefficients:               2.36E+16   -0.2    62100.0
138. CH2CHO=CH2CO+H                                4.07E+15   -0.3    50600.0
     Reverse Arrhenius coefficients:               5.00E+13    0.0    12300.0
139. CH2CHO+O2=CH2O+CO+OH                          8.95E+13   -0.6    10120.0
     Warning...all REV parameters are zero...          0.00000E+00 0.00000E+00 0.00000E+00
               this reaction will be treated as irreversible
140. CH2CO+H=CH3+CO                                1.10E+13    0.0     3400.0
     Reverse Arrhenius coefficients:               2.40E+12    0.0    40200.0
141. CH2CO+H=HCCO+H2                               2.00E+14    0.0     8000.0
     Reverse Arrhenius coefficients:               1.43E+11    0.5     4520.0
142. CH2CO+O=HCCO+OH                               1.00E+13    0.0     8000.0
     Reverse Arrhenius coefficients:               3.72E+09    0.5     3108.0
143. CH2CO+OH=HCCO+H2O                             1.00E+13    0.0     2000.0
     Reverse Arrhenius coefficients:               7.60E+10    0.4    13410.0
144. CH2CO+OH=CH2OH+CO                             2.00E+12    0.0    -1010.0
     Reverse Arrhenius coefficients:               8.17E+09    0.5    24530.0
145. HCCO+OH=H2+CO+CO                              1.00E+14    0.0        0.0
     Warning...all REV parameters are zero...          0.00000E+00 0.00000E+00 0.00000E+00
               this reaction will be treated as irreversible
146. HCCO+O=H+CO+CO                                8.00E+13    0.0        0.0
     Warning...all REV parameters are zero...          0.00000E+00 0.00000E+00 0.00000E+00
               this reaction will be treated as irreversible
147. HCCO+O2=OH+CO+CO                              4.20E+10    0.0      850.0
     Warning...all REV parameters are zero...          0.00000E+00 0.00000E+00 0.00000E+00
               this reaction will be treated as irreversible
148. C2H3+H(+M)=C2H4(+M)                           1.36E+14    0.2      660.0
     Low pressure limit:  0.14000E+31 -0.38600E+01  0.33200E+04
     TROE centering:      0.78200E+00  0.20750E+03  0.26630E+04  0.60950E+04
     H2              Enhanced by    2.000E+00
     H2O             Enhanced by    6.000E+00
     AR              Enhanced by    7.000E-01
     CO              Enhanced by    1.500E+00
     CO2             Enhanced by    2.000E+00
     CH4             Enhanced by    2.000E+00
149. C2H4(+M)=C2H2+H2(+M)                          8.00E+12    0.4    88770.0
     Low pressure limit:  0.15800E+52 -0.93000E+01  0.97800E+05
     TROE centering:      0.73500E+00  0.18000E+03  0.10350E+04  0.54170E+04
     H2              Enhanced by    2.000E+00
     H2O             Enhanced by    6.000E+00
     AR              Enhanced by    7.000E-01
     CO              Enhanced by    1.500E+00
     CO2             Enhanced by    2.000E+00
     CH4             Enhanced by    2.000E+00
150. C2H4+H=C2H3+H2                                5.07E+07    1.9    12950.0
     Reverse Arrhenius coefficients:               1.60E+04    2.4     5190.0
151. C2H4+O=CH3+HCO                                8.56E+06    1.9      183.0
     Reverse Arrhenius coefficients:               3.30E+02    2.6    26140.0
152. C2H4+O=CH2CHO+H                               4.99E+06    1.9      183.0
     Reverse Arrhenius coefficients:               1.54E+09    1.2    18780.0
153. C2H4+OH=C2H3+H2O                              1.80E+06    2.0     2500.0
     Reverse Arrhenius coefficients:               6.03E+03    2.4     9632.0
154. C2H4+CH3=C2H3+CH4                             6.62E+00    3.7     9500.0
     Reverse Arrhenius coefficients:               1.91E+00    3.8     3280.0
155. C2H4+O2=C2H3+HO2                              4.00E+13    0.0    58200.0
     Reverse Arrhenius coefficients:               6.63E+10    0.2    -4249.0
156. C2H4+CH3O=C2H3+CH3OH                          1.20E+11    0.0     6750.0
     Reverse Arrhenius coefficients:               8.14E+08    0.3     -783.0
157. C2H4+CH3O2=C2H3+CH3O2H                        2.23E+12    0.0    17190.0
     Reverse Arrhenius coefficients:               7.93E+12   -0.6    -8167.0
158. C2H2+H(+M)=C2H3(+M)                           5.60E+12    0.0     2400.0
     Low pressure limit:  0.38000E+41 -0.72700E+01  0.72200E+04
     TROE centering:      0.75100E+00  0.98500E+02  0.13020E+04  0.41670E+04
     H2              Enhanced by    2.000E+00
     H2O             Enhanced by    6.000E+00
     AR              Enhanced by    7.000E-01
     CO              Enhanced by    1.500E+00
     CO2             Enhanced by    2.000E+00
     CH4             Enhanced by    2.000E+00
159. C2H3+O2=C2H2+HO2                              2.12E-06    6.0     9484.0
     Reverse Arrhenius coefficients:               1.09E-05    5.9    24030.0
160. C2H3+O2=CH2O+HCO                              8.50E+28   -5.3     6500.0
     Reverse Arrhenius coefficients:               3.99E+27   -4.9    93450.0
161. C2H3+O2=CH2CHO+O                              5.50E+14   -0.6     5260.0
     Reverse Arrhenius coefficients:               3.00E+18   -1.4    16300.0
162. CH3+C2H3=CH4+C2H2                             3.92E+11    0.0        0.0
     Reverse Arrhenius coefficients:               3.50E+14   -0.2    70780.0
163. C2H3+H=C2H2+H2                                9.64E+13    0.0        0.0
     Reverse Arrhenius coefficients:               9.43E+13    0.3    69240.0
164. C2H3+OH=C2H2+H2O                              5.00E+12    0.0        0.0
     Reverse Arrhenius coefficients:               5.18E+13    0.1    84130.0
165. C2H+H(+M)=C2H2(+M)                            1.00E+17    0.0        0.0
     Low pressure limit:  0.37500E+34 -0.48000E+01  0.19000E+04
     TROE centering:      0.64600E+00  0.13200E+03  0.13150E+04  0.55660E+04
     H2              Enhanced by    2.000E+00
     H2O             Enhanced by    6.000E+00
     AR              Enhanced by    7.000E-01
     CO              Enhanced by    1.500E+00
     CO2             Enhanced by    2.000E+00
     CH4             Enhanced by    2.000E+00
166. C2H2+O2=HCCO+OH                               2.00E+08    1.5    30100.0
     Reverse Arrhenius coefficients:               2.04E+06    1.5    32270.0
167. O+C2H2=C2H+OH                                 4.60E+19   -1.4    28950.0
     Reverse Arrhenius coefficients:               3.02E+15   -0.6    -1782.0
168. C2H2+O=HCCO+H                                 1.35E+07    2.0     1900.0
     Reverse Arrhenius coefficients:               4.76E+07    1.6    20800.0
```

```
169. C2H2+OH=C2H+H2O                                3.37E+07    2.0    14000.0
     Reverse Arrhenius coefficients:                4.52E+04    2.7     -428.0
170. C2H2+OH=CH2CO+H                                3.24E+13    0.0    12000.0
     Reverse Arrhenius coefficients:                3.06E+17   -0.8    35790.0
171. C2H2+OH=CH3+CO                                 4.83E-04    4.0    -2000.0
     Reverse Arrhenius coefficients:                3.49E-06    4.6    52120.0
172. CH3COCH3(+M)=CH3CO+CH3(+M)                     7.11E+21   -1.6    84680.0
     Low pressure limit:  0.70130E+90 -0.20380E+02  0.10715E+06
     TROE centering:      0.86300E+00  0.10000E+11  0.41640E+03  0.32900E+10
173. CH3COCH3+OH=CH3COCH2+H2O                       1.25E+05    2.5      445.0
     Reverse Arrhenius coefficients:                8.62E+04    2.3    24710.0
174. CH3COCH3+H=CH3COCH2+H2                         9.80E+05    2.4     5160.0
     Reverse Arrhenius coefficients:                6.37E+04    2.4    14530.0
175. CH3COCH3+O=CH3COCH2+OH                         5.13E+11    0.2     4890.0
     Reverse Arrhenius coefficients:                1.73E+10    0.1    12850.0
176. CH3COCH3+CH3=CH3COCH2+CH4                      3.96E+11    0.0     9784.0
     Reverse Arrhenius coefficients:                2.35E+13   -0.5    20690.0
177. CH3COCH3+CH3O=CH3COCH2+CH3OH                   4.34E+11    0.0     6460.0
     Reverse Arrhenius coefficients:                6.06E+11   -0.3    16060.0
178. CH3COCH3+O2=CH3COCH2+HO2                       6.03E+13    0.0    48500.0
     Reverse Arrhenius coefficients:                2.06E+13   -0.4     3181.0
179. CH3COCH3+HO2=CH3COCH2+H2O2                     1.70E+13    0.0    20460.0
     Reverse Arrhenius coefficients:                6.40E+14   -0.8    13830.0
180. CH3COCH3+CH3O2=CH3COCH2+CH3O2H                 1.70E+13    0.0    20460.0
     Reverse Arrhenius coefficients:                1.24E+16   -1.2    12230.0
181. CH3COCH2=CH2CO+CH3                             1.00E+14    0.0    31000.0
     Reverse Arrhenius coefficients:                1.00E+11    0.0     6000.0
182. CH3COCH2O2=CH3COCH2+O2                         2.02E+15   -1.0    24460.0
     Reverse Arrhenius coefficients:                1.20E+11    0.0    -1100.0
183. CH3COCH3+CH3COCH2O2=CH3COCH2+CH3COCH2O2H       1.00E+11    0.0     5000.0
     Reverse Arrhenius coefficients:                2.00E+10    0.0    10000.0
184. CH2O+CH3COCH2O2=HCO+CH3COCH2O2H                1.29E+11    0.0     9000.0
     Reverse Arrhenius coefficients:                2.51E+10    0.0    10100.0
185. HO2+CH3COCH2O2=CH3COCH2O2H+O2                  1.00E+12    0.0        0.0
     Warning...all REV parameters are zero...          0.00000E+00 0.00000E+00 0.00000E+00
               this reaction will be treated as irreversible
186. CH3COCH2O2H=CH3COCH2O+OH                       1.00E+16    0.0    43000.0
     Reverse Arrhenius coefficients:                4.24E+08    1.7    -4342.0
187. CH3COCH2O=CH3CO+CH2O                           3.73E+20   -2.2    17260.0
     Reverse Arrhenius coefficients:                1.00E+11    0.0    11900.0
188. C3H8(+M)=CH3+C2H5(+M)                          1.29E+37   -5.8    97380.0
     Low pressure limit:  0.56400E+75 -0.15740E+02  0.98714E+05
     TROE centering:      0.31000E+00  0.50000E+02  0.30000E+04  0.90000E+04
     H2              Enhanced by    2.000E+00
     H2O             Enhanced by    6.000E+00
     AR              Enhanced by    7.000E-01
     CO              Enhanced by    1.500E+00
     CO2             Enhanced by    2.000E+00
     CH4             Enhanced by    2.000E+00
189. C3H8=NC3H7+H                                   3.75E+17   -0.4   101200.0
     Reverse Arrhenius coefficients:                1.00E+14    0.0        0.0
190. C3H8=IC3H7+H                                   2.38E+18   -0.7    98680.0
     Reverse Arrhenius coefficients:                1.00E+14    0.0        0.0
191. C3H8+O2=IC3H7+HO2                              2.00E+13    0.0    49640.0
     Reverse Arrhenius coefficients:                1.76E+09    0.6     -169.0
192. C3H8+O2=NC3H7+HO2                              6.00E+13    0.0    52290.0
     Reverse Arrhenius coefficients:                3.35E+10    0.3      -59.0
193. H+C3H8=H2+IC3H7                                1.30E+06    2.4     4471.0
     Reverse Arrhenius coefficients:                2.19E+01    3.3     9351.0
194. H+C3H8=H2+NC3H7                                1.33E+06    2.5     6756.0
     Reverse Arrhenius coefficients:                1.42E+02    3.2     9096.0
195. C3H8+O=IC3H7+OH                                5.49E+05    2.5     3140.0
     Reverse Arrhenius coefficients:                4.79E+00    3.4     6608.0
196. C3H8+O=NC3H7+OH                                3.71E+06    2.4     5505.0
     Reverse Arrhenius coefficients:                2.05E+02    3.0     6433.0
197. C3H8+OH=NC3H7+H2O                              1.05E+10    1.0     1586.0
     Reverse Arrhenius coefficients:                1.19E+07    1.5    18820.0
198. C3H8+OH=IC3H7+H2O                              4.67E+07    1.6      -35.0
     Reverse Arrhenius coefficients:                8.33E+03    2.5    19740.0
199. C3H8+HO2=IC3H7+H2O2                            5.88E+04    2.5    14860.0
     Reverse Arrhenius coefficients:                5.72E+02    2.8     3742.0
200. C3H8+HO2=NC3H7+H2O2                            8.10E+04    2.5    16690.0
     Reverse Arrhenius coefficients:                5.00E+03    2.4     3030.0
201. CH3+C3H8=CH4+IC3H7                             6.40E+04    2.2     7520.0
     Reverse Arrhenius coefficients:                9.82E+02    2.7    13940.0
202. CH3+C3H8=CH4+NC3H7                             9.04E-01    3.6     7154.0
     Reverse Arrhenius coefficients:                8.79E-02    3.8    11030.0
203. IC3H7+C3H8=NC3H7+C3H8                          3.00E+10    0.0    12900.0
     Reverse Arrhenius coefficients:                3.00E+10    0.0    12900.0
204. C2H3+C3H8=C2H4+IC3H7                           1.00E+11    0.0    10400.0
     Reverse Arrhenius coefficients:                1.31E+11    0.0    17800.0
205. C2H3+C3H8=C2H4+NC3H7                           1.00E+11    0.0    10400.0
     Reverse Arrhenius coefficients:                1.31E+11    0.0    17800.0
206. C3H8+C3H5-A=NC3H7+C3H6                         7.94E+11    0.0    20500.0
     Reverse Arrhenius coefficients:                5.37E+16   -1.3    13400.0
207. C3H8+C3H5-A=IC3H7+C3H6                         7.94E+11    0.0    16200.0
     Reverse Arrhenius coefficients:                5.37E+16   -1.3     9095.0
208. C3H8+CH3O=NC3H7+CH3OH                          3.00E+11    0.0     7000.0
     Reverse Arrhenius coefficients:                1.22E+10    0.0     9182.0
209. C3H8+CH3O=IC3H7+CH3OH                          3.00E+11    0.0     7000.0
     Reverse Arrhenius coefficients:                1.22E+10    0.0     9182.0
210. CH3O2+C3H8=CH3O2H+NC3H7                        8.10E+04    2.5    16690.0
     Reverse Arrhenius coefficients:                9.72E+04    2.0     1435.0
211. CH3O2+C3H8=CH3O2H+IC3H7                        5.88E+04    2.5    14860.0
     Reverse Arrhenius coefficients:                1.11E+04    2.3     2147.0
```

```
212. IC3H7O2+C3H8=IC3H7O2H+NC3H7                  1.70E+13    0.0    20460.0
     Reverse Arrhenius coefficients:              2.09E+13   -0.5     5000.0
213. IC3H7O2+C3H8=IC3H7O2H+IC3H7                  2.00E+12    0.0    17000.0
     Reverse Arrhenius coefficients:              3.88E+11   -0.2     4080.0
214. IC3H7=H+C3H6                                 6.92E+13   -0.0    37690.0
     Reverse Arrhenius coefficients:              2.64E+13    0.0     2160.0
215. IC3H7+H=C2H5+CH3                             2.00E+13    0.0        0.0
     Reverse Arrhenius coefficients:              4.34E+07    1.2     8620.0
216. IC3H7+O2=C3H6+HO2                            4.50E-19    0.0     5020.0
     Reverse Arrhenius coefficients:              2.00E-19    0.0    17500.0
217. IC3H7+OH=C3H6+H2O                            2.41E+13    0.0        0.0
     Reverse Arrhenius coefficients:              2.98E+12    0.6    83820.0
218. IC3H7+O=CH3COCH3+H                           4.82E+13    0.0        0.0
     Reverse Arrhenius coefficients:              1.29E+16   -0.2    79380.0
219. IC3H7+O=CH3CHO+CH3                           4.82E+13    0.0        0.0
     Reverse Arrhenius coefficients:              1.28E+11    0.8    86480.0
220. NC3H7=CH3+C2H4                               9.97E+40   -8.6    41430.0
     Reverse Arrhenius coefficients:              1.90E+34   -7.0    17100.0
221. NC3H7=H+C3H6                                 8.78E+39   -8.1    46580.0
     Reverse Arrhenius coefficients:              2.07E+37   -7.4    12020.0
222. NC3H7+O2=C3H6+HO2                            3.00E-19    0.0     3000.0
     Reverse Arrhenius coefficients:              2.00E-19    0.0    17500.0
223. C3H6=C2H3+CH3                                2.73E+62  -13.3   123200.0
     Reverse Arrhenius coefficients:              6.82E+53  -11.8    20550.0
224. C3H6=C3H5-A+H                                2.01E+61  -13.3   118500.0
     Reverse Arrhenius coefficients:              2.04E+61  -13.5    30610.0
225. C3H6=C3H5-T+H                                5.62E+71  -16.6   139300.0
     Reverse Arrhenius coefficients:              4.26E+68  -16.2    30080.0
226. C3H6+O=C2H5+HCO                              1.58E+07    1.8    -1216.0
     Reverse Arrhenius coefficients:              9.19E+01    2.7    23110.0
227. C3H6+O=CH2CO+CH3+H                           2.50E+07    1.8       76.0
     Warning...all REV parameters are zero...          0.00000E+00 0.00000E+00 0.00000E+00
               this reaction will be treated as irreversible
228. C3H6+O=C3H5-A+OH                             5.24E+11    0.7     5884.0
     Reverse Arrhenius coefficients:              1.10E+11    0.7    20150.0
229. C3H6+O=C3H5-T+OH                             6.03E+10    0.7     7632.0
     Reverse Arrhenius coefficients:              9.48E+06    1.4      576.0
230. C3H6+OH=C3H5-A+H2O                           3.12E+06    2.0     -298.0
     Reverse Arrhenius coefficients:              1.34E+07    1.9    30270.0
231. C3H6+OH=C3H5-T+H2O                           1.11E+06    2.0     1451.0
     Reverse Arrhenius coefficients:              3.56E+03    2.6    10700.0
232. C3H6+HO2=C3H5-A+H2O2                         2.70E+04    2.5    12340.0
     Reverse Arrhenius coefficients:              6.34E+06    1.8    12010.0
233. C3H6+HO2=C3H5-T+H2O2                         9.00E+03    2.5    23590.0
     Reverse Arrhenius coefficients:              1.58E+03    2.5     1941.0
234. C3H6+H=C3H5-A+H2                             1.73E+05    2.5     2492.0
     Reverse Arrhenius coefficients:              7.02E+04    2.5    18170.0
235. C3H6+H=C3H5-T+H2                             4.05E+05    2.5     9794.0
     Reverse Arrhenius coefficients:              1.23E+02    3.2     4150.0
236. C3H6+H=C2H4+CH3                              2.30E+13    0.0     2547.0
     Reverse Arrhenius coefficients:              7.27E+07    1.3    11200.0
237. C3H6+O2=C3H5-A+HO2                           4.00E+12    0.0    39900.0
     Reverse Arrhenius coefficients:              8.51E+12   -0.3      887.0
238. C3H6+O2=C3H5-T+HO2                           1.40E+12    0.0    60700.0
     Reverse Arrhenius coefficients:              2.22E+09    0.3      369.0
239. C3H6+CH3=C3H5-A+CH4                          2.21E+00    3.5     5675.0
     Reverse Arrhenius coefficients:              8.18E+02    3.1    22890.0
240. C3H6+CH3=C3H5-T+CH4                          8.40E-01    3.5    11660.0
     Reverse Arrhenius coefficients:              2.32E-01    3.7     7552.0
241. C3H6+CH3O2=C3H5-A+CH3O2H                     3.24E+11    0.0    14900.0
     Reverse Arrhenius coefficients:              2.00E+10    0.0    15000.0
242. C3H6+IC3H7O2=C3H5-A+IC3H7O2H                 3.24E+11    0.0    14900.0
     Reverse Arrhenius coefficients:              2.00E+10    0.0    15000.0
243. C3H5-A=C2H2+CH3                              2.40E+48   -9.9    82080.0
     Reverse Arrhenius coefficients:              2.61E+46   -9.8    36950.0
244. C3H5-A=C3H4-A+H                              4.19E+13    0.2    61930.0
     Reverse Arrhenius coefficients:              2.40E+11    0.7     3007.0
245. C3H5-A+HO2=C3H5O+OH                          7.00E+12    0.0    -1000.0
     Reverse Arrhenius coefficients:              1.60E+12    0.1    11660.0
246. C3H5-A+CH3O2=C3H5O+CH3O                      7.00E+12    0.0    -1000.0
     Reverse Arrhenius coefficients:              1.99E+15   -0.7    17020.0
247. C3H5-A+H=C3H4-A+H2                           1.23E+03    3.0     2582.0
     Reverse Arrhenius coefficients:              2.82E+00    3.8    47220.0
248. C3H5-A+CH3=C3H4-A+CH4                        1.00E+11    0.0        0.0
     Reverse Arrhenius coefficients:              4.92E+12    0.1    47780.0
249. C3H5-A+C2H5=C2H4+C3H6                        4.00E+11    0.0        0.0
     Reverse Arrhenius coefficients:              6.94E+16   -1.3    52800.0
250. C3H5-A+C2H3=C2H4+C3H4-A                      1.00E+12    0.0        0.0
     Reverse Arrhenius coefficients:              1.62E+13    0.1    48190.0
251. C3H4-A+C3H6=C3H5-A+C3H5-A                    4.75E+08    0.7    28700.0
     Reverse Arrhenius coefficients:              8.43E+10    0.0     -262.0
252. C3H5-A+O2=C3H4-A+HO2                         2.18E+21   -2.9    30760.0
     Reverse Arrhenius coefficients:              2.61E+19   -2.4    20710.0
253. C3H5-A+O2=CH2CHO+CH2O                        7.14E+15   -1.2    21050.0
     Reverse Arrhenius coefficients:              4.94E+16   -1.4    88620.0
254. C3H5-A+O2=C2H2+CH2O+OH                       9.72E+29   -5.7    21450.0
     Warning...all REV parameters are zero...          0.00000E+00 0.00000E+00 0.00000E+00
               this reaction will be treated as irreversible
255. C3H5-T=C2H2+CH3                              2.16E+40   -8.3    45110.0
     Reverse Arrhenius coefficients:              1.61E+40   -8.6    20330.0
256. C3H5-T=C3H4-A+H                              3.51E+14   -0.4    40890.0
     Reverse Arrhenius coefficients:              8.50E+12    0.0     2000.0
257. C3H5-T=C3H4-P+H                              1.08E+15   -0.6    38490.0
     Reverse Arrhenius coefficients:              6.50E+12    0.0     2000.0
258. C3H5-T+O2=C3H4-A+HO2                         1.89E+30   -5.6    15540.0
```

```
     Reverse Arrhenius coefficients:               3.04E+31   -5.9    26810.0
259. C3H5-T+O2=CH3COCH2+O                          3.81E+17   -1.4     5580.0
     Reverse Arrhenius coefficients:               2.00E+11    0.0    17500.0
260. C3H5-T+O2=CH2O+CH3CO                          3.71E+25   -4.0     7043.0
     Reverse Arrhenius coefficients:               1.87E+27   -4.4   101200.0
261. C3H5-T+H=C3H4-P+H2                            3.33E+12    0.0        0.0
     Reverse Arrhenius coefficients:               2.14E+16   -0.9    71050.0
262. C3H5-T+CH3=C3H4-P+CH4                         1.00E+11    0.0        0.0
     Reverse Arrhenius coefficients:               1.68E+16   -0.9    71530.0
263. C3H4-A+M=C3H3+H+M                             1.14E+17    0.0    70000.0
     Reverse Arrhenius coefficients:               1.80E+15   -0.4    10610.0
264. C3H4-A=C3H4-P                                 1.20E+15    0.0    92400.0
     Reverse Arrhenius coefficients:               3.22E+18   -1.0    96590.0
265. C3H4-A+O2=C3H3+HO2                            4.00E+13    0.0    39160.0
     Reverse Arrhenius coefficients:               3.17E+11   -0.1      311.0
266. C3H4-A+OH=CH2CO+CH3                           3.12E+12    0.0     -397.0
     Reverse Arrhenius coefficients:               1.81E+17   -1.4    36070.0
267. C3H4-A+OH=C3H3+H2O                            1.00E+07    2.0     1000.0
     Reverse Arrhenius coefficients:               1.60E+05    2.2    31730.0
268. C3H4-A+O=C2H4+CO                              7.80E+12    0.0     1600.0
     Reverse Arrhenius coefficients:               3.27E+08    1.3   121900.0
269. C3H4-A+O=C2H2+CH2O                            3.00E-03    4.6    -4243.0
     Reverse Arrhenius coefficients:               2.32E+02    3.2    81190.0
270. C3H4-A+H=C3H3+H2                              2.00E+07    2.0     5000.0
     Reverse Arrhenius coefficients:               3.02E+04    2.3    20840.0
271. C3H4-A+CH3=C3H3+CH4                           3.67E-02    4.0     6830.0
     Reverse Arrhenius coefficients:               5.06E-02    3.8    24210.0
272. C3H4-A+C3H5-A=C3H3+C3H6                       2.00E+11    0.0     7700.0
     Reverse Arrhenius coefficients:               2.64E+19   -2.7    42140.0
273. C3H4-A+C2H=C3H3+C2H2                          1.00E+13    0.0        0.0
     Reverse Arrhenius coefficients:               1.42E+16   -1.4    53820.0
274. C3H4-P+M=C3H3+H+M                             1.14E+17    0.0    70000.0
     Reverse Arrhenius coefficients:               6.71E+11    0.6     6420.0
275. C3H4-P=C2H+CH3                                4.20E+16    0.0   100000.0
     Reverse Arrhenius coefficients:               1.02E+12    0.6    -1600.0
276. C3H4-P+O2=C3H3+HO2                            2.00E+13    0.0    41600.0
     Reverse Arrhenius coefficients:               6.37E+11   -0.2     1021.0
277. C3H4-P+HO2=C2H4+CO+OH                         3.00E+12    0.0    19000.0
     Reverse Arrhenius coefficients:               1.00E+00    0.0        0.0
278. C3H4-P+OH=C3H3+H2O                            1.00E+07    2.0     1000.0
     Reverse Arrhenius coefficients:               6.44E+05    2.0    30000.0
279. C3H4-P+OH=CH2CO+CH3                           5.00E-04    4.5    -1000.0
     Reverse Arrhenius coefficients:               1.08E-02    4.1    31280.0
280. C3H4-P+O=C2H3+HCO                             3.20E+12    0.0     2010.0
     Reverse Arrhenius coefficients:               2.55E+12   -0.4    32350.0
281. C3H4-P+O=HCCO+CH3                             9.60E+08    1.0        0.0
     Reverse Arrhenius coefficients:               1.43E+04    1.8    26990.0
282. C3H4-P+O=C3H3+OH                              7.65E+08    1.5     8600.0
     Reverse Arrhenius coefficients:               2.18E+08    1.3    22470.0
283. C3H4-P+H=C3H3+H2                              2.00E+07    2.0     5000.0
     Reverse Arrhenius coefficients:               1.22E+05    2.1    19110.0
284. C3H4-P+CH3=C3H3+CH4                           1.50E+00    3.5     5600.0
     Reverse Arrhenius coefficients:               8.31E+00    3.2    21250.0
285. C3H4-P+C2H=C3H3+C2H2                          1.00E+12    0.0        0.0
     Reverse Arrhenius coefficients:               5.30E+11   -0.4    49630.0
286. C3H4-P+C2H3=C3H3+C2H4                         1.00E+12    0.0     7700.0
     Reverse Arrhenius coefficients:               9.54E+11   -0.4    52450.0
287. C3H4-P+C3H5-A=C3H3+C3H6                       1.00E+12    0.0     7700.0
     Reverse Arrhenius coefficients:               4.93E+16   -1.7    37950.0
288. C3H3+O=CH2O+C2H                               1.00E+13    0.0        0.0
     Reverse Arrhenius coefficients:               5.45E+14    0.0    31610.0
289. C3H3+O2=CH2CO+HCO                             3.01E+10    0.0     2870.0
     Reverse Arrhenius coefficients:               4.88E+11    0.0    59470.0
290. C3H3+CH3=C2H5+C2H                             4.30E+15   -0.8    45630.0
     Reverse Arrhenius coefficients:               1.81E+13    0.0        0.0
291. C3H4-A+HO2=C2H4+CO+OH                         1.00E+12    0.0    14000.0
     Reverse Arrhenius coefficients:               1.00E+00    0.0        0.0
292. C3H4-A+HO2=C3H3+H2O2                          3.00E+13    0.0    14000.0
     Reverse Arrhenius coefficients:               1.55E+16   -1.4    44000.0
293. C2H2+CH3=C3H4-P+H                             4.23E+08    1.1    12090.0
     Reverse Arrhenius coefficients:               1.00E+14    0.0     4000.0
294. C2H2+CH3=C3H4-A+H                             6.74E+19   -2.1    31590.0
     Reverse Arrhenius coefficients:               6.41E+25   -3.3    21770.0
295. IC3H7+HO2=IC3H7O+OH                           7.00E+12    0.0    -1000.0
     Reverse Arrhenius coefficients:               1.05E+16   -0.6    27320.0
296. CH3O2+IC3H7=CH3O+IC3H7O                       7.00E+12    0.0    -1000.0
     Reverse Arrhenius coefficients:               6.57E+14   -0.3    31560.0
297. IC3H7O2=IC3H7+O2                              3.13E+22   -2.2    38160.0
     Reverse Arrhenius coefficients:               7.54E+12    0.0        0.0
298. IC3H7O2+CH2O=IC3H7O2H+HCO                     5.60E+12    0.0    13600.0
     Reverse Arrhenius coefficients:               8.00E+11    0.0    10000.0
299. IC3H7O2+CH3CHO=IC3H7O2H+CH3CO                 2.80E+12    0.0    13600.0
     Reverse Arrhenius coefficients:               1.00E+12    0.0    10000.0
300. IC3H7O2+HO2=IC3H7O2H+O2                       1.75E+10    0.0    -3275.0
     Reverse Arrhenius coefficients:               3.86E+13   -0.8    33610.0
301. C2H4+IC3H7O2=C2H3+IC3H7O2H                    1.13E+13    0.0    30430.0
     Reverse Arrhenius coefficients:               3.00E+12    0.0    11500.0
302. CH3OH+IC3H7O2=CH2OH+IC3H7O2H                  6.30E+12    0.0    19360.0
     Reverse Arrhenius coefficients:               1.00E+09    0.0    10000.0
303. CH4+IC3H7O2=CH3+IC3H7O2H                      1.12E+13    0.0    24640.0
     Reverse Arrhenius coefficients:               7.43E+11    0.0     5500.0
304. IC3H7O2+CH3O2=IC3H7O+CH3O+O2                  1.40E+16   -1.6     1860.0
     Warning...all REV parameters are zero...          0.00000E+00 0.00000E+00 0.00000E+00
               this reaction will be treated as irreversible
305. H2+IC3H7O2=H+IC3H7O2H                         3.01E+13    0.0    26030.0
```

```
     Reverse Arrhenius coefficients:                4.80E+13    0.0     7950.0
306. IC3H7O2+IC3H7O2=O2+IC3H7O+IC3H7O               1.40E+16   -1.6     1860.0
     Warning...all REV parameters are zero...          0.00000E+00 0.00000E+00 0.00000E+00
               this reaction will be treated as irreversible
307. IC3H7O2+CH3=IC3H7O+CH3O                        7.00E+12    0.0    -1000.0
     Reverse Arrhenius coefficients:                1.14E+11    0.7    26720.0
308. IC3H7O2+IC3H7=IC3H7O+IC3H7O                    7.00E+12    0.0    -1000.0
     Reverse Arrhenius coefficients:                2.78E+13    0.3    29800.0
309. IC3H7O2+C3H5-A=IC3H7O+C3H5O                    7.00E+12    0.0    -1000.0
     Reverse Arrhenius coefficients:                4.24E+09    0.9    14140.0
310. IC3H7O2H=IC3H7O+OH                             9.45E+15    0.0    42600.0
     Reverse Arrhenius coefficients:                1.55E+06    2.4    -4132.0
311. IC3H7O=CH3+CH3CHO                              5.33E+19   -1.7    17140.0
     Reverse Arrhenius coefficients:                1.00E+11    0.0     9256.0
312. IC3H7O=CH3COCH3+H                              8.66E+14   -0.5    20080.0
     Reverse Arrhenius coefficients:                2.00E+12    0.0     7270.0
313. IC3H7O+O2=CH3COCH3+HO2                         9.09E+09    0.0      390.0
     Reverse Arrhenius coefficients:                1.00E+11    0.0    32000.0
314. C3H5O=C2H3+CH2O                                1.46E+20   -2.0    35090.0
     Reverse Arrhenius coefficients:                1.50E+11    0.0    10600.0
315. IC3H7O2=C3H6+HO2                               1.01E+43   -9.4    41490.0
     Reverse Arrhenius coefficients:                1.95E+33   -7.3    16670.0
316. PC4H9=C2H5+C2H4                                3.50E+12    0.5    29470.0
     Reverse Arrhenius coefficients:                1.32E+04    2.5     6130.0
317. PC4H9=C4H8-1+H                                 2.62E+12    0.3    35700.0
     Reverse Arrhenius coefficients:                2.50E+11    0.5     2620.0
318. PC4H9+O2=C4H8-1+HO2                            2.00E-18    0.0     5000.0
     Reverse Arrhenius coefficients:                2.00E-19    0.0    17500.0
319. C4H8-1=C3H5-A+CH3                              5.08E+19   -1.3    76510.0
     Reverse Arrhenius coefficients:                1.35E+13    0.0        0.0
320. C4H8-1=C2H3+C2H5                               2.88E+23   -2.0   101600.0
     Reverse Arrhenius coefficients:                9.00E+12    0.0        0.0
321. C4H8-1=H+C4H71-3                               3.72E+14   -0.1    85200.0
     Reverse Arrhenius coefficients:                5.00E+13    0.0        0.0
322. C4H8-1+O2=C4H71-3+HO2                          2.00E+13    0.0    37190.0
     Reverse Arrhenius coefficients:                4.65E+12    0.1     -168.0
323. C4H8-1+H=C4H71-3+H2                            3.38E+05    2.4      207.0
     Reverse Arrhenius coefficients:                4.32E+06    2.1    20330.0
324. C4H8-1+OH=C4H71-3+H2O                          2.76E+04    2.6    -1919.0
     Reverse Arrhenius coefficients:                1.53E+06    2.4    33360.0
325. C4H8-1+CH3=C4H71-3+CH4                         3.69E+00    3.3     4002.0
     Reverse Arrhenius coefficients:                1.23E+03    3.0    24610.0
326. C4H8-1+HO2=C4H71-3+H2O2                        4.82E+03    2.5    10530.0
     Reverse Arrhenius coefficients:                1.59E+06    2.0    14350.0
327. C4H8-1+CH3O2=C4H71-3+CH3O2H                    4.82E+03    2.5    10530.0
     Reverse Arrhenius coefficients:                3.30E+06    1.8    11330.0
328. C4H8-1+CH3O=C4H71-3+CH3OH                      4.00E+01    2.9     8609.0
     Reverse Arrhenius coefficients:                2.47E+02    2.7    27000.0
329. C4H8-1+C3H5-A=C4H71-3+C3H6                     7.90E+10    0.0    12400.0
     Reverse Arrhenius coefficients:                1.00E+11    0.0    17500.0
330. C4H8-1+C4H6=C4H71-3+C4H71-3                    2.35E+12    0.0    46720.0
     Reverse Arrhenius coefficients:                1.60E+12    0.0        0.0
331. C4H8-1+IC3H7O2=C4H71-3+IC3H7O2H                1.40E+12    0.0    14900.0
     Reverse Arrhenius coefficients:                3.16E+11    0.0    13000.0
332. C4H72-2=C3H4-P+CH3                             6.33E+10    0.5    30020.0
     Reverse Arrhenius coefficients:                1.00E+11    0.0     7800.0
333. C4H71-3=C4H6+H                                 1.20E+14    0.0    49300.0
     Reverse Arrhenius coefficients:                4.00E+13    0.0     1300.0
334. C4H71-3+C2H5=C4H8-1+C2H4                       2.59E+12    0.0     -131.0
     Reverse Arrhenius coefficients:                1.15E+13    0.1    49440.0
335. C4H71-3+CH3O=C4H8-1+CH2O                       2.41E+13    0.0        0.0
     Reverse Arrhenius coefficients:                2.48E+12    0.3    66330.0
336. C3H5-A+C4H71-3=C3H6+C4H6                       6.31E+12    0.0        0.0
     Reverse Arrhenius coefficients:                1.00E+10    0.0    50000.0
337. C4H71-3+O2=C4H6+HO2                            1.00E+09    0.0        0.0
     Reverse Arrhenius coefficients:                1.00E+11    0.0    17000.0
338. H+C4H71-3=C4H6+H2                              3.16E+13    0.0        0.0
     Reverse Arrhenius coefficients:                1.07E+13    0.0    56810.0
339. C2H3+C4H71-3=C2H4+C4H6                         3.98E+12    0.0        0.0
     Reverse Arrhenius coefficients:                1.16E+13    0.0    57710.0
340. C4H6=C2H3+C2H3                                 4.03E+19   -1.0    98150.0
     Reverse Arrhenius coefficients:                1.26E+13    0.0        0.0
341. C4H6+OH=C2H5+CH2CO                             1.00E+12    0.0        0.0
     Reverse Arrhenius coefficients:                3.73E+12    0.0    30020.0
342. C4H6+OH=CH2O+C3H5-A                            1.00E+12    0.0        0.0
     Reverse Arrhenius coefficients:                3.50E+06    0.0    71060.0
343. C4H6+OH=C2H3+CH3CHO                            1.00E+12    0.0        0.0
     Reverse Arrhenius coefficients:                5.44E+11    0.0    18550.0
344. C4H6+O=C2H4+CH2CO                              1.00E+12    0.0        0.0
     Reverse Arrhenius coefficients:                6.38E+11    0.0    94340.0
345. C4H6+O=CH2O+C3H4-A                             1.00E+12    0.0        0.0
     Reverse Arrhenius coefficients:                1.08E+12    0.0    79050.0
346. C2H3+C2H4=C4H6+H                               5.00E+11    0.0     7300.0
     Reverse Arrhenius coefficients:                1.00E+13    0.0     4700.0
347. IC4H9+HO2=IC4H9O+OH                            7.00E+12    0.0    -1000.0
     Reverse Arrhenius coefficients:                3.71E+15   -0.7    26540.0
348. TC4H9+HO2=TC4H9O+OH                            7.00E+12    0.0    -1000.0
     Reverse Arrhenius coefficients:                4.08E+18   -1.3    28650.0
349. CH3O2+IC4H9=CH3O+IC4H9O                        7.00E+12    0.0    -1000.0
     Reverse Arrhenius coefficients:                2.32E+14   -0.4    30780.0
350. CH3O2+TC4H9=CH3O+TC4H9O                        7.00E+12    0.0    -1000.0
     Reverse Arrhenius coefficients:                2.55E+17   -1.0    32890.0
351. IC4H9=IC4H8+H                                  3.37E+13    0.1    33660.0
     Reverse Arrhenius coefficients:                6.25E+11    0.5     2620.0
352. IC4H9=C3H6+CH3                                 9.50E+11    0.8    30700.0
```

```
     Reverse Arrhenius coefficients:               1.89E+03    2.7     6850.0
353. TC4H9=H+IC4H8                                 1.13E+12    0.7    36560.0
     Reverse Arrhenius coefficients:               1.06E+12    0.5     1230.0
354. TC4H9+O2=IC4H8+HO2                            8.37E-01    3.6    11960.0
     Reverse Arrhenius coefficients:               1.65E+00    3.3    25500.0
355. IC4H9+O2=IC4H8+HO2                            1.07E+00    3.7     9322.0
     Reverse Arrhenius coefficients:               4.16E-02    4.0    27150.0
356. IC4H9O2=IC4H9+O2                              6.64E+19   -1.6    36080.0
     Reverse Arrhenius coefficients:               2.26E+12    0.0        0.0
357. TC4H9O2=TC4H9+O2                              3.33E+24   -2.5    37870.0
     Reverse Arrhenius coefficients:               1.41E+13    0.0        0.0
358. IC3H7O2+IC4H9=IC3H7O+IC4H9O                   7.00E+12    0.0    -1000.0
     Reverse Arrhenius coefficients:               9.81E+12    0.2    29020.0
359. IC3H7O2+TC4H9=IC3H7O+TC4H9O                   7.00E+12    0.0    -1000.0
     Reverse Arrhenius coefficients:               1.08E+16   -0.5    31130.0
360. IC3H7O2+IC4H7=IC3H7O+IC4H7O                   7.00E+12    0.0    -1000.0
     Reverse Arrhenius coefficients:               9.04E+09    0.9    13300.0
361. TC4H9O2+C3H6=TC4H9O2H+C3H5-A                  3.24E+11    0.0    14900.0
     Reverse Arrhenius coefficients:               2.00E+10    0.0    15000.0
362. TC4H9O2+IC4H8=TC4H9O2H+IC4H7                  1.40E+12    0.0    14900.0
     Reverse Arrhenius coefficients:               3.16E+11    0.0    13000.0
363. IC3H7O2+IC4H8=IC3H7O2H+IC4H7                  1.40E+12    0.0    14900.0
     Reverse Arrhenius coefficients:               3.16E+11    0.0    13000.0
364. TC4H9O2+C4H8-1=TC4H9O2H+C4H71-3               1.40E+12    0.0    14900.0
     Reverse Arrhenius coefficients:               3.16E+11    0.0    13000.0
365. C2H4+TC4H9O2=C2H3+TC4H9O2H                    7.00E+11    0.0    17110.0
     Reverse Arrhenius coefficients:               1.00E+11    0.0    10000.0
366. TC4H9O2+CH4=TC4H9O2H+CH3                      1.13E+13    0.0    20460.0
     Reverse Arrhenius coefficients:               7.50E+08    0.0     1280.0
367. H2+TC4H9O2=H+TC4H9O2H                         3.01E+13    0.0    26030.0
     Reverse Arrhenius coefficients:               4.80E+13    0.0     7950.0
368. TC4H9O2+C3H8=TC4H9O2H+IC3H7                   2.00E+12    0.0    17000.0
     Reverse Arrhenius coefficients:               5.00E+11    0.0     6500.0
369. TC4H9O2+C3H8=TC4H9O2H+NC3H7                   1.70E+13    0.0    20460.0
     Reverse Arrhenius coefficients:               5.00E+11    0.0     6500.0
370. TC4H9O2+CH3OH=TC4H9O2H+CH2OH                  6.30E+12    0.0    19360.0
     Reverse Arrhenius coefficients:               1.00E+09    0.0    10000.0
371. TC4H9O2+CH3CHO=TC4H9O2H+CH3CO                 2.80E+12    0.0    13600.0
     Reverse Arrhenius coefficients:               1.00E+12    0.0    10000.0
372. TC4H9O2+HO2=TC4H9O2H+O2                       1.75E+10    0.0    -3275.0
     Reverse Arrhenius coefficients:               3.85E+13   -0.8    33620.0
373. TC4H9O2+H2O2=TC4H9O2H+HO2                     2.40E+12    0.0    10000.0
     Reverse Arrhenius coefficients:               2.40E+12    0.0    10000.0
374. TC4H9O2+CH2O=TC4H9O2H+HCO                     1.30E+11    0.0     9000.0
     Reverse Arrhenius coefficients:               2.50E+10    0.0    10100.0
375. IC4H9O2+CH3O2=IC4H9O+CH3O+O2                  1.40E+16   -1.6     1860.0
     Warning...all REV parameters are zero...                0.00000E+00 0.00000E+00 0.00000E+00
               this reaction will be treated as irreversible
376. TC4H9O2+CH3O2=TC4H9O+CH3O+O2                  1.40E+16   -1.6     1860.0
     Warning...all REV parameters are zero...                0.00000E+00 0.00000E+00 0.00000E+00
               this reaction will be treated as irreversible
377. IC4H9O2+IC4H9O2=O2+IC4H9O+IC4H9O              1.40E+16   -1.6     1860.0
     Warning...all REV parameters are zero...                0.00000E+00 0.00000E+00 0.00000E+00
               this reaction will be treated as irreversible
378. IC4H9O2+TC4H9O2=IC4H9O+TC4H9O+O2              1.40E+16   -1.6     1860.0
     Warning...all REV parameters are zero...                0.00000E+00 0.00000E+00 0.00000E+00
               this reaction will be treated as irreversible
379. TC4H9O2+TC4H9O2=O2+TC4H9O+TC4H9O              1.40E+16   -1.6     1860.0
     Warning...all REV parameters are zero...                0.00000E+00 0.00000E+00 0.00000E+00
               this reaction will be treated as irreversible
380. IC4H9O2+IC3H7O2=IC4H9O+IC3H7O+O2              1.40E+16   -1.6     1860.0
     Warning...all REV parameters are zero...                0.00000E+00 0.00000E+00 0.00000E+00
               this reaction will be treated as irreversible
381. TC4H9O2+IC3H7O2=TC4H9O+IC3H7O+O2              1.40E+16   -1.6     1860.0
     Warning...all REV parameters are zero...                0.00000E+00 0.00000E+00 0.00000E+00
               this reaction will be treated as irreversible
382. IC4H9O2+HO2=IC4H9O+OH+O2                      1.40E+16   -1.6     1860.0
     Warning...all REV parameters are zero...                0.00000E+00 0.00000E+00 0.00000E+00
               this reaction will be treated as irreversible
383. TC4H9O2+HO2=TC4H9O+OH+O2                      1.40E+16   -1.6     1860.0
     Warning...all REV parameters are zero...                0.00000E+00 0.00000E+00 0.00000E+00
               this reaction will be treated as irreversible
384. IC4H9O2+CH3=IC4H9O+CH3O                       7.00E+12    0.0    -1000.0
     Reverse Arrhenius coefficients:               5.72E+12    0.0    28020.0
385. IC4H9O2+IC3H7=IC4H9O+IC3H7O                   7.00E+12    0.0    -1000.0
     Reverse Arrhenius coefficients:               1.39E+15   -0.4    31100.0
386. IC4H9O2+IC4H9=IC4H9O+IC4H9O                   7.00E+12    0.0    -1000.0
     Reverse Arrhenius coefficients:               4.90E+14   -0.5    30320.0
387. IC4H9O2+TC4H9=IC4H9O+TC4H9O                   7.00E+12    0.0    -1000.0
     Reverse Arrhenius coefficients:               5.39E+17   -1.2    32430.0
388. IC4H9O2+C3H5-A=IC4H9O+C3H5O                   7.00E+12    0.0    -1000.0
     Reverse Arrhenius coefficients:               2.12E+11    0.2    15440.0
389. IC4H9O2+IC4H7=IC4H9O+IC4H7O                   7.00E+12    0.0    -1000.0
     Reverse Arrhenius coefficients:               4.51E+11    0.2    14600.0
390. TC4H9O2+CH3=TC4H9O+CH3O                       7.00E+12    0.0    -1000.0
     Reverse Arrhenius coefficients:               7.82E+11    0.2    28340.0
391. TC4H9O2+IC3H7=TC4H9O+IC3H7O                   7.00E+12    0.0    -1000.0
     Reverse Arrhenius coefficients:               1.90E+14   -0.2    31420.0
392. TC4H9O2+IC4H9=TC4H9O+IC4H9O                   7.00E+12    0.0    -1000.0
     Reverse Arrhenius coefficients:               6.70E+13   -0.3    30640.0
393. TC4H9O2+TC4H9=TC4H9O+TC4H9O                   7.00E+12    0.0    -1000.0
     Reverse Arrhenius coefficients:               7.37E+16   -1.0    32750.0
394. TC4H9O2+C3H5-A=TC4H9O+C3H5O                   7.00E+12    0.0    -1000.0
     Reverse Arrhenius coefficients:               2.90E+10    0.4    15760.0
395. TC4H9O2+IC4H7=TC4H9O+IC4H7O                   7.00E+12    0.0    -1000.0
```

```
     Reverse Arrhenius coefficients:               6.17E+10    0.4    14920.0
396. TC4H9O2H=TC4H9O+OH                            5.95E+15    0.0    42540.0
     Reverse Arrhenius coefficients:               6.68E+06    1.9    -2582.0
397. IC4H9O+HO2=IC3H7CHO+H2O2                      1.00E+12    0.0        0.0
     Reverse Arrhenius coefficients:               1.38E+13   -0.2    72130.0
398. IC4H9O+OH=IC3H7CHO+H2O                        1.81E+13    0.0        0.0
     Reverse Arrhenius coefficients:               4.21E+13    0.1   103600.0
399. IC4H9O+CH3=IC3H7CHO+CH4                       2.40E+13    0.0        0.0
     Reverse Arrhenius coefficients:               3.37E+14    0.1    88920.0
400. IC4H9O+O=IC3H7CHO+OH                          6.00E+12    0.0        0.0
     Reverse Arrhenius coefficients:               1.42E+12    0.1    86350.0
401. IC4H9O+H=IC3H7CHO+H2                          1.99E+13    0.0        0.0
     Reverse Arrhenius coefficients:               1.07E+13    0.1    88440.0
402. IC4H9O=IC3H7CHO+H                             4.00E+14    0.0    21500.0
     Reverse Arrhenius coefficients:               1.14E+10    1.1     2500.0
403. IC4H9O=CH2O+IC3H7                             2.00E+14    0.0    17500.0
     Reverse Arrhenius coefficients:               1.88E+02    2.8     4591.0
404. TC4H9O=CH3COCH3+CH3                           9.56E+22   -2.5    18650.0
     Reverse Arrhenius coefficients:               1.50E+11    0.0    11900.0
405. IC4H9O+O2=IC3H7CHO+HO2                        1.93E+11    0.0     1660.0
     Reverse Arrhenius coefficients:               7.03E+08    0.6    33200.0
406. TC4H9O+O2=IC4H8O+HO2                          8.10E+11    0.0     4700.0
     Reverse Arrhenius coefficients:               1.00E+11    0.0    32000.0
407. IC4H8O=IC3H7CHO                               4.18E+13    0.0    52720.0
     Reverse Arrhenius coefficients:               1.39E+10    0.6    72050.0
408. IC3H7CHO=TC3H6CHO+H                           2.30E+18   -0.9    92000.0
     Reverse Arrhenius coefficients:               2.00E+14    0.0        0.0
409. IC3H7CHO=IC3H7+HCO                            1.13E+17   -0.0    79760.0
     Reverse Arrhenius coefficients:               1.81E+13    0.0        0.0
410. IC3H7CHO+HO2=IC3H7CO+H2O2                     3.00E+12    0.0    11920.0
     Reverse Arrhenius coefficients:               7.99E+11   -0.1    10360.0
411. IC3H7CHO+HO2=TC3H6CHO+H2O2                    8.00E+10    0.0    11920.0
     Reverse Arrhenius coefficients:               3.37E+12   -0.4    11050.0
412. IC3H7CHO+CH3=IC3H7CO+CH4                      3.98E+12    0.0     8700.0
     Reverse Arrhenius coefficients:               2.32E+13   -0.1    25630.0
413. IC3H7CHO+O=IC3H7CO+OH                         7.18E+12    0.0     1389.0
     Reverse Arrhenius coefficients:               7.05E+11   -0.1    15740.0
414. IC3H7CHO+O2=IC3H7CO+HO2                       4.00E+13    0.0    37600.0
     Reverse Arrhenius coefficients:               1.62E+11    0.3    -3432.0
415. IC3H7CHO+OH=IC3H7CO+H2O                       2.69E+10    0.8     -340.0
     Reverse Arrhenius coefficients:               1.16E+10    0.8    31200.0
416. IC3H7CHO+OH=TC3H6CHO+H2O                      1.68E+12    0.0     -781.0
     Reverse Arrhenius coefficients:               1.19E+13   -0.1    29810.0
417. IC3H7CHO+H=IC3H7CO+H2                         2.60E+12    0.0     2600.0
     Reverse Arrhenius coefficients:               1.20E+09    0.6    17040.0
418. IC3H7CO=IC3H7+CO                              2.87E+20   -2.2    14970.0
     Reverse Arrhenius coefficients:               1.50E+11    0.0     4810.0
419. IC4H9O2=IC4H8+HO2                             2.27E+35   -7.2    39490.0
     Reverse Arrhenius coefficients:               3.00E+26   -5.3    21240.0
420. TC4H9O2=IC4H8+HO2                             7.61E+42   -9.4    41490.0
     Reverse Arrhenius coefficients:               6.34E+31   -7.2    17160.0
421. IC4H8=C3H5-T+CH3                              1.92E+66  -14.2   128100.0
     Reverse Arrhenius coefficients:               1.56E+56  -12.3    26100.0
422. IC4H8=IC4H7+H                                 3.07E+55  -11.5   114300.0
     Reverse Arrhenius coefficients:               1.43E+55  -11.7    26400.0
423. IC4H8+H=C3H6+CH3                              5.68E+33   -5.7    20000.0
     Reverse Arrhenius coefficients:               6.09E+26   -4.2    27200.0
424. IC4H8+H=IC4H7+H2                              3.40E+05    2.5     2492.0
     Reverse Arrhenius coefficients:               6.32E+04    2.5    18160.0
425. IC4H8+O=CH2CO+CH3+CH3                         3.33E+07    1.8       76.0
     Warning...all REV parameters are zero...         0.00000E+00 0.00000E+00 0.00000E+00
               this reaction will be treated as irreversible
426. IC4H8+O=IC3H6CO+H+H                           1.66E+07    1.8       76.0
     Warning...all REV parameters are zero...         0.00000E+00 0.00000E+00 0.00000E+00
               this reaction will be treated as irreversible
427. IC4H8+O=IC4H7+OH                              1.21E+11    0.7     7633.0
     Reverse Arrhenius coefficients:               1.16E+10    0.7    21890.0
428. IC4H8+CH3=IC4H7+CH4                           4.42E+00    3.5     5675.0
     Reverse Arrhenius coefficients:               7.50E+02    3.1    22890.0
429. IC4H8+HO2=IC4H7+H2O2                          1.93E+04    2.6    13910.0
     Reverse Arrhenius coefficients:               2.07E+06    1.9    13580.0
430. IC4H8+O2=IC4H7+HO2                            6.00E+12    0.0    39900.0
     Reverse Arrhenius coefficients:               5.85E+12   -0.3      883.0
431. IC4H8+C3H5-A=IC4H7+C3H6                       7.94E+11    0.0    20500.0
     Reverse Arrhenius coefficients:               4.40E+20   -1.3    60610.0
432. IC4H8+C3H5-T=IC4H7+C3H6                       7.94E+11    0.0    20500.0
     Reverse Arrhenius coefficients:               5.59E+20   -1.3    80170.0
433. IC4H8+OH=IC4H7+H2O                            5.20E+06    2.0     -298.0
     Reverse Arrhenius coefficients:               1.02E+07    1.9    30270.0
434. IC4H8+O=IC3H7+HCO                             1.58E+07    1.8    -1216.0
     Reverse Arrhenius coefficients:               4.54E+00    3.1    21690.0
435. IC4H8+CH3O2=IC4H7+CH3O2H                      1.93E+04    2.6    13910.0
     Reverse Arrhenius coefficients:               4.03E+07    1.5    11990.0
436. IC4H8+HO2=IC4H8O+OH                           1.29E+12    0.0    13340.0
     Reverse Arrhenius coefficients:               1.00E+12    0.0     7500.0
437. IC4H7+O2=IC3H5CHO+OH                          2.47E+13   -0.5    23020.0
     Reverse Arrhenius coefficients:               3.37E+13   -0.6    73010.0
438. IC4H7+O2=CH3COCH2+CH2O                        7.14E+15   -1.2    21050.0
     Reverse Arrhenius coefficients:               1.70E+12   -0.4    88250.0
439. IC4H7+O2=C3H4-A+CH2O+OH                       7.29E+29   -5.7    21450.0
     Warning...all REV parameters are zero...         0.00000E+00 0.00000E+00 0.00000E+00
               this reaction will be treated as irreversible
440. IC4H7+O=IC3H5CHO+H                            6.03E+13    0.0        0.0
     Reverse Arrhenius coefficients:               2.84E+16   -0.5    66730.0
441. IC4H7=C3H4-A+CH3                              1.23E+47   -9.7    74260.0
```

```
     Reverse Arrhenius coefficients:                1.65E+38   -7.8    22540.0
442. CH3O2+IC4H7=CH3O+IC4H7O                        7.00E+12    0.0    -1000.0
     Reverse Arrhenius coefficients:                2.14E+11    0.3    15060.0
443. IC4H7+HO2=IC4H7O+OH                            7.00E+12    0.0    -1000.0
     Reverse Arrhenius coefficients:                3.42E+12    0.1    10820.0
444. IC4H7O=C3H5-T+CH2O                             2.92E+21   -2.4    35590.0
     Reverse Arrhenius coefficients:                1.00E+11    0.0    12600.0
445. IC4H7O=IC4H6OH                                 1.39E+11    0.0    15600.0
     Reverse Arrhenius coefficients:                4.23E+11   -0.2    31670.0
446. IC4H7O=IC3H5CHO+H                              5.00E+13    0.0    29100.0
     Reverse Arrhenius coefficients:                6.67E+13   -0.1    18410.0
447. IC4H6OH+H2=IC4H7OH+H                           2.16E+04    2.4    18990.0
     Reverse Arrhenius coefficients:                5.61E+02    3.0     1399.0
448. IC4H6OH+HO2=IC4H7OH+O2                         5.57E+13   -0.3      862.0
     Reverse Arrhenius coefficients:                6.00E+13    0.0    39900.0
449. IC4H6OH+CH2O=IC4H7OH+HCO                       6.30E+08    1.9    18190.0
     Reverse Arrhenius coefficients:                2.10E+07    2.2    17730.0
450. IC4H6OH+IC4H8=IC4H7OH+IC4H7                    4.70E+02    3.3    19840.0
     Reverse Arrhenius coefficients:                2.81E-01    3.9     6521.0
451. IC4H7OH=IC4H6OH+H                              4.90E+16   -0.4    89850.0
     Reverse Arrhenius coefficients:                1.00E+14    0.0        0.0
452. IC4H7OH+HO2=IC4H6OH+H2O2                       7.64E+03    2.7    13930.0
     Reverse Arrhenius coefficients:                7.83E+05    2.0    13580.0
453. IC4H6OH=C3H4-A+CH2OH                           7.24E+19   -1.9    57050.0
     Reverse Arrhenius coefficients:                1.00E+11    0.0     9200.0
454. IC4H7O+O2=IC3H5CHO+HO2                         3.00E+10    0.0     1649.0
     Reverse Arrhenius coefficients:                6.31E+10   -0.1    38980.0
455. IC4H7O+HO2=IC3H5CHO+H2O2                       3.00E+11    0.0        0.0
     Reverse Arrhenius coefficients:                8.93E+14   -0.8    78500.0
456. IC4H7O+CH3=IC3H5CHO+CH4                        2.40E+13    0.0        0.0
     Reverse Arrhenius coefficients:                7.26E+16   -0.5    95290.0
457. IC4H7O+O=IC3H5CHO+OH                           6.00E+12    0.0        0.0
     Reverse Arrhenius coefficients:                3.05E+14   -0.5    92720.0
458. IC4H7O+OH=IC3H5CHO+H2O                         1.81E+13    0.0        0.0
     Reverse Arrhenius coefficients:                9.08E+15   -0.5   110000.0
459. IC4H7O+H=IC3H5CHO+H2                           1.99E+13    0.0        0.0
     Reverse Arrhenius coefficients:                2.30E+15   -0.5    94810.0
460. IC3H5CHO+OH=IC3H5CO+H2O                        2.69E+10    0.8     -340.0
     Reverse Arrhenius coefficients:                4.40E+10    0.8    36080.0
461. IC3H5CHO+HO2=IC3H5CO+H2O2                      1.00E+12    0.0    11920.0
     Reverse Arrhenius coefficients:                9.71E+12   -0.3    16880.0
462. IC3H5CHO+CH3=IC3H5CO+CH4                       3.98E+12    0.0     8700.0
     Reverse Arrhenius coefficients:                3.93E+13    0.0    30450.0
463. IC3H5CHO+O=IC3H5CO+OH                          7.18E+12    0.0     1389.0
     Reverse Arrhenius coefficients:                1.19E+12    0.0    20560.0
464. IC3H5CHO+O2=IC3H5CO+HO2                        2.00E+13    0.0    40700.0
     Reverse Arrhenius coefficients:                1.82E+11    0.3     5337.0
465. IC3H5CHO+H=IC3H5CO+H2                          2.60E+12    0.0     2600.0
     Reverse Arrhenius coefficients:                9.82E+11    0.0    23870.0
466. IC3H5CO=C3H5-T+CO                              1.28E+20   -1.9    34460.0
     Reverse Arrhenius coefficients:                1.51E+11    0.0     4809.0
467. TC3H6CHO+HO2=TC3H6OCHO+OH                      9.64E+12    0.0        0.0
     Reverse Arrhenius coefficients:                2.02E+17   -1.2    21010.0
468. TC3H6OCHO=CH3COCH3+HCO                         3.98E+13    0.0     9700.0
     Reverse Arrhenius coefficients:                2.17E+08    0.8    14240.0
469. TC3H6CHO=IC3H5CHO+H                            1.32E+14    0.0    39340.0
     Reverse Arrhenius coefficients:                1.30E+13    0.0     1200.0
470. TC3H6CHO=IC3H6CO+H                             4.09E+14   -0.1    42410.0
     Reverse Arrhenius coefficients:                1.30E+13    0.0     4800.0
471. TC3H6CHO+H2=IC3H7CHO+H                         2.16E+05    2.4    18990.0
     Reverse Arrhenius coefficients:                1.32E+05    2.5     3550.0
472. IC4H7OOH=IC4H7O+OH                             6.40E+15    0.0    45550.0
     Reverse Arrhenius coefficients:                1.00E+11    0.0        0.0
473. IC4H7OH=IC4H7O+H                               5.97E+16   -0.6   105900.0
     Reverse Arrhenius coefficients:                4.00E+13    0.0        0.0
474. IC4H7O+H2=IC4H7OH+H                            9.05E+06    2.0    17830.0
     Reverse Arrhenius coefficients:                7.16E+05    2.4    16310.0
475. IC4H7OH=IC4H7+OH                               7.31E+16   -0.4    79700.0
     Reverse Arrhenius coefficients:                3.00E+13    0.0        0.0
476. IC4H7O+CH2O=IC4H7OH+HCO                        1.15E+11    0.0     1280.0
     Reverse Arrhenius coefficients:                3.02E+11    0.0    18160.0
477. TC3H6CHO+CH2O=IC3H7CHO+HCO                     2.52E+08    1.9    18190.0
     Reverse Arrhenius coefficients:                1.23E+07    2.0    17420.0
478. TC3H6CHO+IC4H8=IC3H7CHO+IC4H7                  4.70E+02    3.3    19840.0
     Reverse Arrhenius coefficients:                6.61E+00    3.4     8672.0
479. IC3H6CO+OH=IC3H7+CO2                           1.73E+12    0.0    -1010.0
     Reverse Arrhenius coefficients:                2.58E+14   -0.4    55480.0
480. TC3H6O2HCO=CH3COCH3+CO+OH                      4.24E+18   -1.4     4800.0
     Warning...all REV parameters are zero...          0.00000E+00 0.00000E+00 0.00000E+00
               this reaction will be treated as irreversible
481. TC3H6CHO+O2=IC3H5CHO+HO2                       2.72E-19    0.0     7240.0
     Reverse Arrhenius coefficients:                1.39E+11   -0.2    17310.0
482. TC3H6CHO+O2=CH3COCH3+CO+OH                     3.62E-20    0.0        0.0
     Warning...all REV parameters are zero...          0.00000E+00 0.00000E+00 0.00000E+00
               this reaction will be treated as irreversible
483. TC3H6CHO+HO2=IC3H7CHO+O2                       3.68E+12    0.0     1310.0
     Reverse Arrhenius coefficients:                1.24E+14   -0.2    43350.0
484. TC3H6CHO+CH3=IC3H5CHO+CH4                      3.01E+12   -0.3     -131.0
     Reverse Arrhenius coefficients:                2.21E+15   -0.8    67900.0
485. IC4H7O+IC4H8=IC4H7OH+IC4H7                     2.70E+11    0.0     4000.0
     Reverse Arrhenius coefficients:                1.00E+10    0.0     9000.0
486. IC4H6OH+HO2=CH2CCH2OH+CH2O+OH                  1.45E+13    0.0        0.0
     Warning...all REV parameters are zero...          0.00000E+00 0.00000E+00 0.00000E+00
               this reaction will be treated as irreversible
487. IC4H7OH=CH2CCH2OH+CH3                          1.25E+20   -1.0    98570.0
```

```
     Reverse Arrhenius coefficients:               3.00E+13    0.0        0.0
488. CH2CCH2OH+O2=CH2OH+CO+CH2O                    4.34E+12    0.0        0.0
     Warning...all REV parameters are zero...          0.00000E+00 0.00000E+00 0.00000E+00
               this reaction will be treated as irreversible
489. CH2CCH2OH=C2H2+CH2OH                          2.16E+40   -8.3    45110.0
     Reverse Arrhenius coefficients:               1.61E+40   -8.6    20330.0
490. CH2CCH2OH=C3H4-A+OH                           6.70E+16   -1.1    42580.0
     Reverse Arrhenius coefficients:               8.50E+12    0.0     2000.0
491. CC5H10=C4H71-3+CH3                            1.30E+21   -1.6    76140.0
     Reverse Arrhenius coefficients:               1.00E+13    0.0        0.0
492. CC5H10+OH=IC4H9+CH2O                          2.00E+10    0.0     4000.0
     Reverse Arrhenius coefficients:               2.00E+13    0.0    20000.0
493. CC5H10+H=CC5H9-B+H2                           2.65E+06    2.2        0.0
     Reverse Arrhenius coefficients:               1.82E+07    2.1    22280.0
494. CC5H10+OH=CC5H9-B+H2O                         6.14E+02    3.2    -3500.0
     Reverse Arrhenius coefficients:               1.83E+04    3.1    33940.0
495. CC5H10+CH3=CC5H9-B+CH4                        4.61E+00    3.1     2330.0
     Reverse Arrhenius coefficients:               8.28E+02    3.0    25090.0
496. CC5H10+HO2=CC5H9-B+H2O2                       1.81E+03    2.5     7154.0
     Reverse Arrhenius coefficients:               3.20E+05    2.1    13130.0
497. CC5H10+CH3O2=CC5H9-B+CH3O2H                   1.81E+03    2.5     7154.0
     Reverse Arrhenius coefficients:               6.66E+05    1.9    10110.0
498. CC5H10+CH3O=CC5H9-B+CH3OH                     1.00E+01    2.9     5231.0
     Reverse Arrhenius coefficients:               3.31E+01    2.8    25790.0
499. BC6H12+OH=CH3COCH3+NC3H7                      1.00E+11    0.0    -4000.0
     Warning...all REV parameters are zero...          0.00000E+00 0.00000E+00 0.00000E+00
               this reaction will be treated as irreversible
500. CC6H12+OH=IC4H9+CH3CHO                        1.00E+11    0.0    -4000.0
     Warning...all REV parameters are zero...          0.00000E+00 0.00000E+00 0.00000E+00
               this reaction will be treated as irreversible
501. CC6H12+O=IC4H9+CH3CO                          1.00E+11    0.0    -1050.0
     Warning...all REV parameters are zero...          0.00000E+00 0.00000E+00 0.00000E+00
               this reaction will be treated as irreversible
502. BC6H12=CH3+CC5H9-B                            1.00E+16    0.0    71000.0
     Reverse Arrhenius coefficients:               1.00E+13    0.0        0.0
503. CC6H12=CH3+C5H92-4                            1.00E+16    0.0    71000.0
     Reverse Arrhenius coefficients:               1.00E+13    0.0        0.0
504. BC6H12+H=CC6H11-B+H2                          3.38E+05    2.4      207.0
     Reverse Arrhenius coefficients:               2.50E+06    2.3    21040.0
505. BC6H12+OH=CC6H11-B+H2O                        2.76E+04    2.6    -1919.0
     Reverse Arrhenius coefficients:               8.85E+05    2.5    34070.0
506. BC6H12+CH3=CC6H11-B+CH4                       3.69E+00    3.3     4002.0
     Reverse Arrhenius coefficients:               7.13E+02    3.2    25310.0
507. BC6H12+HO2=CC6H11-B+H2O2                      4.82E+03    2.5    10530.0
     Reverse Arrhenius coefficients:               9.16E+05    2.1    15050.0
508. BC6H12+CH3O2=CC6H11-B+CH3O2H                  4.82E+03    2.5    10530.0
     Reverse Arrhenius coefficients:               1.91E+06    1.9    12030.0
509. BC6H12+CH3O=CC6H11-B+CH3OH                    4.00E+01    2.9     8609.0
     Reverse Arrhenius coefficients:               1.43E+02    2.8    27710.0
510. CC6H12+H=CC6H11-B+H2                          2.65E+06    2.2        0.0
     Reverse Arrhenius coefficients:               9.15E+06    2.1    22250.0
511. CC6H12+OH=CC6H11-B+H2O                        6.14E+02    3.2    -3500.0
     Reverse Arrhenius coefficients:               9.18E+03    3.1    33910.0
512. CC6H12+CH3=CC6H11-B+CH4                       4.61E+00    3.1     2330.0
     Reverse Arrhenius coefficients:               4.16E+02    3.0    25060.0
513. CC6H12+HO2=CC6H11-B+H2O2                      1.81E+03    2.5     7154.0
     Reverse Arrhenius coefficients:               1.61E+05    2.1    13100.0
514. CC6H12+CH3O2=CC6H11-B+CH3O2H                  1.81E+03    2.5     7154.0
     Reverse Arrhenius coefficients:               3.35E+05    1.9    10080.0
515. CC6H12+CH3O=CC6H11-B+CH3OH                    1.00E+01    2.9     5231.0
     Reverse Arrhenius coefficients:               1.66E+01    2.8    25750.0
516. C5H10-1+OH=PC4H9+CH2O                         2.00E+10    0.0    -4000.0
     Reverse Arrhenius coefficients:               3.00E+11    0.0    20400.0
517. C5H10-2+OH=NC3H7+CH3CHO                       2.00E+10    0.0    -4000.0
     Reverse Arrhenius coefficients:               2.00E+13    0.0    20000.0
518. C5H10-2+O=C3H6+CH3CHO                         1.00E+10    0.0        0.0
     Reverse Arrhenius coefficients:               1.00E+12    0.0    81000.0
519. C5H10-1+O=PC4H9+HCO                           1.00E+11    0.0        0.0
     Warning...all REV parameters are zero...          0.00000E+00 0.00000E+00 0.00000E+00
               this reaction will be treated as irreversible
520. C5H10-1+O=NC3H7+CH3CO                         1.00E+11    0.0        0.0
     Warning...all REV parameters are zero...          0.00000E+00 0.00000E+00 0.00000E+00
               this reaction will be treated as irreversible
521. C5H10-1+OH=NC3H7+CH3CHO                       1.00E+11    0.0        0.0
     Warning...all REV parameters are zero...          0.00000E+00 0.00000E+00 0.00000E+00
               this reaction will be treated as irreversible
522. C5H10-2+H=C5H92-4+H2                          3.38E+05    2.4      207.0
     Reverse Arrhenius coefficients:               4.36E+06    2.1    20330.0
523. C5H10-2+O=C5H92-4+OH                          9.90E+05    2.4     1210.0
     Reverse Arrhenius coefficients:               5.62E+06    2.2    19240.0
524. C5H10-2+OH=C5H92-4+H2O                        2.76E+04    2.6    -1919.0
     Reverse Arrhenius coefficients:               1.55E+06    2.4    33360.0
525. C5H10-2+CH3=C5H92-4+CH4                       3.69E+00    3.3     4002.0
     Reverse Arrhenius coefficients:               1.24E+03    3.0    24610.0
526. C5H10-2+O2=C5H92-4+HO2                        2.20E+12    0.0    37220.0
     Reverse Arrhenius coefficients:               5.16E+11    0.1     -136.0
527. C5H10-2+HO2=C5H92-4+H2O2                      4.82E+03    2.5    10530.0
     Reverse Arrhenius coefficients:               1.60E+06    2.0    14350.0
528. C5H10-2+CH3O2=C5H92-4+CH3O2H                  4.82E+03    2.5    10530.0
     Reverse Arrhenius coefficients:               3.33E+06    1.8    11330.0
529. C5H10-2+CH3O=C5H92-4+CH3OH                    4.00E+01    2.9     8609.0
     Reverse Arrhenius coefficients:               2.49E+02    2.7    27010.0
530. C5H11-2=C3H6+C2H5                             2.00E+13    0.0    29100.0
     Reverse Arrhenius coefficients:               4.00E+10    0.0     7500.0
531. C5H11-2=C5H10-1+H                             5.00E+12    0.0    40400.0
```

```
     Reverse Arrhenius coefficients:               7.90E+12    0.0     2900.0
532. C5H11-2=C5H10-2+H                             5.00E+12    0.0    37900.0
     Reverse Arrhenius coefficients:               2.50E+12    0.0     1200.0
533. YC7H15=IC3H7+IC4H8                            2.22E+20   -2.1    32470.0
     Reverse Arrhenius coefficients:               5.00E+10    0.0     9200.0
534. YC7H15=XC7H14+H                               1.44E+13    0.2    37690.0
     Reverse Arrhenius coefficients:               2.60E+13    0.0     1200.0
535. YC7H15=YC7H14+H                               3.09E+13    0.0    36390.0
     Reverse Arrhenius coefficients:               2.60E+13    0.0     2500.0
536. YC7H15+O2=XC7H14+HO2                          6.00E-29    0.0     5020.0
     Reverse Arrhenius coefficients:               2.00E-29    0.0    17500.0
537. YC7H15+O2=YC7H14+HO2                          3.00E-29    0.0     3000.0
     Reverse Arrhenius coefficients:               2.00E-29    0.0    17500.0
538. XC7H14=IC3H7+IC4H7                            2.21E+24   -2.4    74670.0
     Reverse Arrhenius coefficients:               1.28E+14   -0.3        0.0
539. YC7H14=CH3+CC6H11-B                           4.47E+22   -2.1    75430.0
     Reverse Arrhenius coefficients:               1.93E+14   -0.3        0.0
540. YC7H15+HO2=YC7H15O+OH                         7.00E+12    0.0    -1000.0
     Reverse Arrhenius coefficients:               2.41E+18   -1.3    28400.0
541. YC7H15+CH3O2=YC7H15O+CH3O                     7.00E+12    0.0    -1000.0
     Reverse Arrhenius coefficients:               1.51E+17   -1.0    32640.0
542. XC7H14+OH=CH3COCH3+IC4H9                      2.00E+10    0.0    -4000.0
     Warning...all REV parameters are zero...          0.00000E+00 0.00000E+00 0.00000E+00
               this reaction will be treated as irreversible
543. YC7H14+OH=CH3COCH3+IC4H9                      2.00E+10    0.0    -4000.0
     Warning...all REV parameters are zero...          0.00000E+00 0.00000E+00 0.00000E+00
               this reaction will be treated as irreversible
544. XC7H14+O=CH2O+CC6H12                          2.00E+10    0.0    -1050.0
     Warning...all REV parameters are zero...          0.00000E+00 0.00000E+00 0.00000E+00
               this reaction will be treated as irreversible
545. YC7H14+O=CH3COCH3+IC4H8                       2.00E+10    0.0    -1050.0
     Warning...all REV parameters are zero...          0.00000E+00 0.00000E+00 0.00000E+00
               this reaction will be treated as irreversible
546. XC7H14+H=XC7H13-Z+H2                          3.38E+05    2.4      207.0
     Reverse Arrhenius coefficients:               4.42E+06    2.1    20370.0
547. XC7H14+OH=XC7H13-Z+H2O                        2.76E+04    2.6    -1919.0
     Reverse Arrhenius coefficients:               1.57E+06    2.4    33400.0
548. XC7H14+CH3=XC7H13-Z+CH4                       3.69E+00    3.3     4002.0
     Reverse Arrhenius coefficients:               1.26E+03    3.0    24640.0
549. XC7H14+HO2=XC7H13-Z+H2O2                      4.82E+03    2.5    10530.0
     Reverse Arrhenius coefficients:               1.62E+06    2.0    14380.0
550. XC7H14+CH3O2=XC7H13-Z+CH3O2H                  4.82E+03    2.5    10530.0
     Reverse Arrhenius coefficients:               3.38E+06    1.8    11360.0
551. XC7H14+CH3O=XC7H13-Z+CH3OH                    4.00E+01    2.9     8609.0
     Reverse Arrhenius coefficients:               2.52E+02    2.7    27040.0
552. YC7H14+H=XC7H13-Z+H2                          3.46E+05    2.5     2492.0
     Reverse Arrhenius coefficients:               9.75E+06    2.1    20050.0
553. YC7H14+H=YC7H13-Y2+H2                         2.65E+06    2.2        0.0
     Reverse Arrhenius coefficients:               1.84E+07    2.1    22290.0
554. YC7H14+OH=XC7H13-Z+H2O                        6.24E+06    2.0     -298.0
     Reverse Arrhenius coefficients:               7.61E+08    1.6    32420.0
555. YC7H14+OH=YC7H13-Y2+H2O                       6.14E+02    3.2    -3500.0
     Reverse Arrhenius coefficients:               1.84E+04    3.1    33940.0
556. XC7H13-Z=ACC6H10+CH3                          2.84E+16   -0.8    41230.0
     Reverse Arrhenius coefficients:               1.00E+11    0.0    10600.0
557. XC7H13-Z+HO2=XC7H13O-Z+OH                     9.64E+12    0.0        0.0
     Reverse Arrhenius coefficients:               5.41E+14   -0.7    15380.0
558. XC7H13-Z+CH3O2=XC7H13O-Z+CH3O                 9.64E+12    0.0        0.0
     Reverse Arrhenius coefficients:               5.28E+16   -1.3    20140.0
559. XC7H13O-Z=IC3H7CHO+C3H5-T                     7.52E+21   -2.4    30190.0
     Reverse Arrhenius coefficients:               1.00E+11    0.0    11900.0
560. YC7H15O2=YC7H15+O2                            3.41E+23   -2.4    37210.0
     Reverse Arrhenius coefficients:               3.00E+12    0.0        0.0
561. YC7H15+YC7H15O2=YC7H15O+YC7H15O               7.00E+12    0.0    -1000.0
     Reverse Arrhenius coefficients:               5.36E+16   -1.0    32910.0
562. YC7H15O2+HO2=YC7H15O2H+O2                     1.75E+10    0.0    -3275.0
     Reverse Arrhenius coefficients:               3.78E+13   -0.8    33610.0
563. YC7H15O2+H2O2=YC7H15O2H+HO2                   2.40E+12    0.0    10000.0
     Reverse Arrhenius coefficients:               2.40E+12    0.0    10000.0
564. YC7H15O2+CH3O2=YC7H15O+CH3O+O2                1.40E+16   -1.6     1860.0
     Warning...all REV parameters are zero...          0.00000E+00 0.00000E+00 0.00000E+00
               this reaction will be treated as irreversible
565. YC7H15O2+YC7H15O2=O2+YC7H15O+YC7H15O          1.40E+16   -1.6     1860.0
     Warning...all REV parameters are zero...          0.00000E+00 0.00000E+00 0.00000E+00
               this reaction will be treated as irreversible
566. YC7H15O2H=YC7H15O+OH                          1.00E+16    0.0    39000.0
     Reverse Arrhenius coefficients:               1.40E+07    1.9    -5702.0
567. YC7H15O=IC4H9+CH3COCH3                        8.19E+23   -2.9    18020.0
     Reverse Arrhenius coefficients:               1.00E+11    0.0    11900.0
568. YC7H15O2=YC7H14OOH-Y2                         1.25E+10    0.0    19100.0
     Reverse Arrhenius coefficients:               2.79E+08    0.1     7940.0
569. YC7H15O2=XC7H14+HO2                           1.01E+43   -9.4    41490.0
     Reverse Arrhenius coefficients:               3.39E+32   -7.3    16660.0
570. YC7H15O2=YC7H14+HO2                           5.04E+38   -8.1    40490.0
     Reverse Arrhenius coefficients:               7.82E+27   -5.8    18260.0
571. YC7H14OOH-Y2=OH+CH3COCH3+IC4H8                5.00E+13    0.0    25500.0
     Warning...all REV parameters are zero...          0.00000E+00 0.00000E+00 0.00000E+00
               this reaction will be treated as irreversible
572. ACC6H10+OH=ACC6H9-D+H2O                       3.12E+06    2.0     -298.0
     Reverse Arrhenius coefficients:               5.49E+08    1.4    32460.0
573. ACC6H10+HO2=ACC6H9-D+H2O2                     9.64E+03    2.6    13910.0
     Reverse Arrhenius coefficients:               1.01E+07    1.7    15210.0
574. ACC6H10+CH3O2=ACC6H9-D+CH3O2H                 9.64E+03    2.6    13910.0
     Reverse Arrhenius coefficients:               4.14E+07    1.5    14490.0
575. ACC6H9-D+HO2=IC3H5CHO+C2H3+OH                 8.91E+12    0.0        0.0
```

```
     Warning...all REV parameters are zero...          0.00000E+00 0.00000E+00 0.00000E+00
               this reaction will be treated as irreversible
576. NEOC5H11=IC4H8+CH3                               8.47E+17   -1.1    32930.0
     Reverse Arrhenius coefficients:                  1.30E+03    2.5     8520.0
577. NEOC5H11+HO2=NEOC5H11O+OH                        7.00E+12    0.0    -1000.0
     Reverse Arrhenius coefficients:                  1.45E+11    0.8    24900.0
578. NEOC5H11+CH3O2=NEOC5H11O+CH3O                    7.00E+12    0.0    -1000.0
     Reverse Arrhenius coefficients:                  9.05E+09    1.1    29140.0
579. NEOC5H11O2=NEOC5H11+O2                           9.75E+20   -2.4    34530.0
     Reverse Arrhenius coefficients:                  1.99E+17   -2.1        0.0
580. NEOC5H11+NEOC5H11O2=NEOC5H11O+NEOC5H11O          7.00E+12    0.0    -1000.0
     Reverse Arrhenius coefficients:                  4.47E+09    1.1    28610.0
581. NEOC5H11O2+HO2=NEOC5H11O2H+O2                    1.75E+10    0.0    -3275.0
     Reverse Arrhenius coefficients:                  3.84E+13   -0.8    33620.0
582. NEOC5H11O2+H2O2=NEOC5H11O2H+HO2                  2.40E+12    0.0    10000.0
     Reverse Arrhenius coefficients:                  2.40E+12    0.0    10000.0
583. NEOC5H11O2+CH3O2=NEOC5H11O+CH3O+O2               1.40E+16   -1.6     1860.0
     Warning...all REV parameters are zero...          0.00000E+00 0.00000E+00 0.00000E+00
               this reaction will be treated as irreversible
584. NEOC5H11O2+NEOC5H11O2=O2+NEOC5H11O+NEOC5H11O     1.40E+16   -1.6     1860.0
     Warning...all REV parameters are zero...          0.00000E+00 0.00000E+00 0.00000E+00
               this reaction will be treated as irreversible
585. NEOC5H11O2H=NEOC5H11O+OH                         1.50E+16    0.0    42500.0
     Reverse Arrhenius coefficients:                  2.88E+07    1.9    -3022.0
586. NEOC5H11O=CH2O+TC4H9                             2.65E+25   -3.2    23930.0
     Reverse Arrhenius coefficients:                  2.00E+11    0.0    11900.0
587. NEOC5H11O2=NEOC5H10OOH                           1.12E+11    0.0    24400.0
     Reverse Arrhenius coefficients:                  9.14E+10   -0.5     8950.0
588. NEOC5H10OOH=OH+CH2O+IC4H8                        3.01E+17   -1.2    29950.0
     Warning...all REV parameters are zero...          0.00000E+00 0.00000E+00 0.00000E+00
               this reaction will be treated as irreversible
589. NEOC5H10OOH=IC4H7OOH+CH3                         9.03E+21   -2.3    32830.0
     Reverse Arrhenius coefficients:                  1.25E+11    0.0    10100.0
590. NEOC5H10OOH-O2=NEOC5H10OOH+O2                    1.37E+25   -3.7    35700.0
     Reverse Arrhenius coefficients:                  1.99E+17   -2.1        0.0
591. NEOC5H10OOH-O2=NEOC5H9Q2-N                       2.50E+10    0.0    21400.0
     Reverse Arrhenius coefficients:                  4.44E+10   -0.5    10960.0
592. NEOC5H9Q2-N=NEOC5KET+OH                          9.00E+14    0.0     1500.0
     Reverse Arrhenius coefficients:                  1.67E+09    1.6    31880.0
593. NEOC5KET=NEOC5KETOX+OH                           1.50E+16    0.0    42000.0
     Reverse Arrhenius coefficients:                  2.01E+09    1.5    -4125.0
594. NEOC5KETOX=TC3H6CHO+CH2O                         2.48E+21   -2.5    15830.0
     Reverse Arrhenius coefficients:                  1.00E+11    0.0    11900.0
595. C4H7CHO2-2+OH=C4H7CO2-2+H2O                      3.37E+12    0.0     -616.0
     Reverse Arrhenius coefficients:                  5.59E+12    0.0    36800.0
596. C4H7CHO2-2+OH=CH3CHO+CH3CHCHO                    1.00E+11    0.0        0.0
     Reverse Arrhenius coefficients:                  8.91E+07    2.1    13480.0
597. C4H7CHO2-2+HO2=C4H7CO2-2+H2O2                    1.00E+12    0.0    11920.0
     Reverse Arrhenius coefficients:                  9.84E+12   -0.3    17880.0
598. C4H7CHO2-2+CH3O2=C4H7CO2-2+CH3O2H                2.80E+12    0.0    13600.0
     Reverse Arrhenius coefficients:                  1.13E+14   -0.5    18840.0
599. C4H7CO2-2=C4H72-2+CO                             4.68E+20   -3.4    41360.0
     Reverse Arrhenius coefficients:                  1.50E+11    0.0     4810.0
600. IC3H6CHCHO+OH=TC3H6CHO+CH2O                      1.00E+11    0.0        0.0
     Reverse Arrhenius coefficients:                  1.39E+11    0.1    16080.0
601. PC7H15=TC4H9+C3H6                                2.31E+23   -2.8    29340.0
     Reverse Arrhenius coefficients:                  1.50E+11    0.0     7200.0
602. PC7H15=OC7H14+H                                  1.28E+13   -0.1    36260.0
     Reverse Arrhenius coefficients:                  1.00E+13    0.0     2500.0
603. PC7H15+O2=OC7H14+HO2                             3.00E-29    0.0     3000.0
     Reverse Arrhenius coefficients:                  2.00E-29    0.0    17500.0
604. PC7H15+HO2=PC7H15O+OH                            7.00E+12    0.0    -1000.0
     Reverse Arrhenius coefficients:                  3.08E+17   -1.1    27860.0
605. PC7H15+CH3O2=PC7H15O+CH3O                        7.00E+12    0.0    -1000.0
     Reverse Arrhenius coefficients:                  1.93E+16   -0.8    32100.0
606. OC7H14=CC6H11-B+CH3                              3.09E+24   -2.5    74100.0
     Reverse Arrhenius coefficients:                  1.02E+14   -0.3     -131.0
607. OC7H14+OH=NEOC5H11+CH3CHO                        2.00E+10    0.0    -4000.0
     Warning...all REV parameters are zero...          0.00000E+00 0.00000E+00 0.00000E+00
               this reaction will be treated as irreversible
608. OC7H14+O=TC4H9+HCO+C2H4                          2.00E+10    0.0    -1050.0
     Warning...all REV parameters are zero...          0.00000E+00 0.00000E+00 0.00000E+00
               this reaction will be treated as irreversible
609. PC7H15O2=PC7H15+O2                               2.76E+22   -2.4    38110.0
     Reverse Arrhenius coefficients:                  1.25E+12    0.0        0.0
610. PC7H15+PC7H15O2=PC7H15O+PC7H15O                  7.00E+12    0.0    -1000.0
     Reverse Arrhenius coefficients:                  4.50E+15   -0.7    30950.0
611. PC7H15O2+HO2=PC7H15O2H+O2                        1.75E+10    0.0    -3275.0
     Reverse Arrhenius coefficients:                  4.53E+13   -0.8    33640.0
612. PC7H15O2+H2O2=PC7H15O2H+HO2                      2.40E+12    0.0    10000.0
     Reverse Arrhenius coefficients:                  2.40E+12    0.0    10000.0
613. PC7H15O2+CH3O2=PC7H15O+CH3O+O2                   1.40E+16   -1.6     1860.0
     Warning...all REV parameters are zero...          0.00000E+00 0.00000E+00 0.00000E+00
               this reaction will be treated as irreversible
614. PC7H15O2+PC7H15O2=O2+PC7H15O+PC7H15O             1.40E+16   -1.6     1860.0
     Warning...all REV parameters are zero...          0.00000E+00 0.00000E+00 0.00000E+00
               this reaction will be treated as irreversible
615. PC7H15O2H=PC7H15O+OH                             1.00E+16    0.0    39000.0
     Reverse Arrhenius coefficients:                  7.71E+06    2.1    -7162.0
616. PC7H15O=CH3CHO+NEOC5H11                          7.50E+17   -1.3    18870.0
     Reverse Arrhenius coefficients:                  5.00E+10    0.0    12900.0
617. PC7H15O2=OC7H14+HO2                              5.04E+38   -8.1    40490.0
     Reverse Arrhenius coefficients:                  3.74E+28   -5.7    17490.0
618. IC8H18=AC8H17+H                                  5.75E+17   -0.4   101200.0
     Reverse Arrhenius coefficients:                  1.00E+14    0.0        0.0
```

619.	IC8H18=BC8H17+H	3.30E+18	-0.7	98730.0
	Reverse Arrhenius coefficients:	1.00E+14	0.0	0.0
620.	IC8H18=CC8H17+H	1.15E+19	-0.9	95430.0
	Reverse Arrhenius coefficients:	1.00E+14	0.0	0.0
621.	IC8H18=DC8H17+H	1.92E+17	-0.4	100400.0
	Reverse Arrhenius coefficients:	1.00E+14	0.0	0.0
622.	IC8H18=YC7H15+CH3	1.64E+27	-2.8	83930.0
	Reverse Arrhenius coefficients:	1.63E+13	0.0	-596.0
623.	IC8H18=PC7H15+CH3	1.38E+26	-2.6	85860.0
	Reverse Arrhenius coefficients:	1.93E+14	-0.3	0.0
624.	IC8H18=TC4H9+IC4H9	7.83E+29	-3.9	84150.0
	Reverse Arrhenius coefficients:	3.59E+14	-0.8	0.0
625.	IC8H18=NEOC5H11+IC3H7	2.45E+23	-2.0	83400.0
	Reverse Arrhenius coefficients:	3.59E+14	-0.8	0.0
626.	IC8H18+H=AC8H17+H2	7.34E+05	2.8	8147.0
	Reverse Arrhenius coefficients:	5.10E+01	3.4	10480.0
627.	IC8H18+H=BC8H17+H2	5.74E+05	2.5	4124.0
	Reverse Arrhenius coefficients:	6.94E+00	3.5	8954.0
628.	IC8H18+H=CC8H17+H2	6.02E+05	2.4	2583.0
	Reverse Arrhenius coefficients:	2.10E+00	3.6	10710.0
629.	IC8H18+H=DC8H17+H2	1.88E+05	2.8	6280.0
	Reverse Arrhenius coefficients:	3.91E+01	3.4	9417.0
630.	IC8H18+O=AC8H17+OH	8.55E+03	3.0	3123.0
	Reverse Arrhenius coefficients:	3.12E-01	3.7	4048.0
631.	IC8H18+O=BC8H17+OH	4.77E+04	2.7	2106.0
	Reverse Arrhenius coefficients:	3.03E-01	3.7	5524.0
632.	IC8H18+O=CC8H17+OH	3.83E+05	2.4	1140.0
	Reverse Arrhenius coefficients:	7.00E-01	3.6	7858.0
633.	IC8H18+O=DC8H17+OH	2.85E+05	2.5	3645.0
	Reverse Arrhenius coefficients:	3.12E+01	3.1	5370.0
634.	IC8H18+OH=AC8H17+H2O	2.63E+07	1.8	1431.0
635.	IC8H18+OH=BC8H17+H2O	9.00E+05	2.0	-1133.0
	Reverse Arrhenius coefficients:	1.16E+02	2.9	18590.0
636.	IC8H18+OH=CC8H17+H2O	1.70E+06	1.9	-1450.0
	Reverse Arrhenius coefficients:	6.30E+01	3.0	21570.0
637.	IC8H18+OH=DC8H17+H2O	1.78E+07	1.8	1431.0
	Reverse Arrhenius coefficients:	3.94E+04	2.3	19460.0
638.	IC8H18+CH3=AC8H17+CH4	4.26E-14	8.1	4154.0
	Reverse Arrhenius coefficients:	2.70E-15	8.2	8031.0
639.	IC8H18+CH3=BC8H17+CH4	2.70E+04	2.3	7287.0
	Reverse Arrhenius coefficients:	2.99E+02	2.8	13660.0
640.	IC8H18+CH3=CC8H17+CH4	6.01E-10	6.4	893.0
	Reverse Arrhenius coefficients:	1.91E-12	7.1	10560.0
641.	IC8H18+CH3=DC8H17+CH4	1.47E-01	3.9	6808.0
	Reverse Arrhenius coefficients:	2.79E-02	4.1	11480.0
642.	IC8H18+HO2=AC8H17+H2O2	6.12E+01	3.6	17160.0
643.	IC8H18+HO2=BC8H17+H2O2	6.32E+01	3.4	13720.0
644.	IC8H18+HO2=CC8H17+H2O2	4.33E+02	3.0	12090.0
645.	IC8H18+HO2=DC8H17+H2O2	4.08E+01	3.6	17160.0
646.	IC8H18+CH3O=AC8H17+CH3OH	4.74E+11	0.0	7000.0
	Reverse Arrhenius coefficients:	1.20E+10	0.0	9200.0
647.	IC8H18+CH3O=BC8H17+CH3OH	1.10E+11	0.0	5000.0
	Reverse Arrhenius coefficients:	8.90E+09	0.0	7200.0
648.	IC8H18+CH3O=CC8H17+CH3OH	1.90E+10	0.0	2800.0
	Reverse Arrhenius coefficients:	1.00E+10	0.0	5200.0
649.	IC8H18+CH3O=DC8H17+CH3OH	3.20E+11	0.0	7000.0
	Reverse Arrhenius coefficients:	1.20E+10	0.0	9200.0
650.	IC8H18+O2=AC8H17+HO2	6.30E+13	0.0	50760.0
	Reverse Arrhenius coefficients:	2.30E+10	0.3	-1592.0
651.	IC8H18+O2=BC8H17+HO2	1.40E+13	0.0	48210.0
	Reverse Arrhenius coefficients:	8.89E+08	0.6	-1649.0
652.	IC8H18+O2=CC8H17+HO2	7.00E+12	0.0	46060.0
	Reverse Arrhenius coefficients:	1.28E+08	0.9	-499.0
653.	IC8H18+O2=DC8H17+HO2	4.20E+13	0.0	50760.0
	Reverse Arrhenius coefficients:	4.58E+10	0.3	-792.0
654.	IC8H18+C2H3=AC8H17+C2H4	1.50E+12	0.0	18000.0
	Reverse Arrhenius coefficients:	2.57E+12	0.0	25400.0
655.	IC8H18+C2H3=BC8H17+C2H4	4.00E+11	0.0	16800.0
	Reverse Arrhenius coefficients:	2.00E+12	0.0	24200.0
656.	IC8H18+C2H3=CC8H17+C2H4	2.00E+11	0.0	14300.0
	Reverse Arrhenius coefficients:	2.50E+12	0.0	23000.0
657.	IC8H18+C2H3=DC8H17+C2H4	1.00E+12	0.0	18000.0
	Reverse Arrhenius coefficients:	2.57E+12	0.0	25400.0
658.	XC7H14+CH3=AC8H17	1.30E+03	2.5	8520.0
	Reverse Arrhenius coefficients:	1.25E+13	0.3	28320.0
659.	IC4H8+IC4H9=AC8H17	6.09E+02	2.5	8520.0
	Reverse Arrhenius coefficients:	2.46E+14	-0.1	26780.0
660.	YC7H14+CH3=BC8H17	1.30E+03	2.5	8520.0
	Reverse Arrhenius coefficients:	4.70E+12	0.5	28210.0
661.	OC7H14+CH3=BC8H17	1.30E+03	2.5	8520.0
	Reverse Arrhenius coefficients:	3.60E+10	0.9	29410.0
662.	IC4H8+TC4H9=CC8H17	6.09E+02	2.5	6130.0
	Reverse Arrhenius coefficients:	6.24E+14	-0.1	25890.0
663.	C3H6+NEOC5H11=DC8H17	4.00E+02	2.5	8520.0
	Reverse Arrhenius coefficients:	3.73E+08	1.6	27020.0
664.	AC8H17=DC8H17	1.39E+11	0.0	15400.0
	Reverse Arrhenius coefficients:	4.16E+11	0.0	16200.0
665.	AC8H17=CC8H17	3.71E+11	0.0	20400.0
	Reverse Arrhenius coefficients:	1.86E+10	0.6	26190.0
666.	IC8H18+CH3O2=AC8H17+CH3O2H	2.08E+00	4.0	18280.0
667.	IC8H18+CH3O2=BC8H17+CH3O2H	1.02E+01	3.6	14810.0
668.	IC8H18+CH3O2=CC8H17+CH3O2H	1.37E+02	3.1	13190.0
669.	IC8H18+CH3O2=DC8H17+CH3O2H	1.39E+00	4.0	18280.0
670.	IC8H18+AC8H17O2=AC8H17+AC8H17O2H	1.81E+13	0.0	20430.0
	Reverse Arrhenius coefficients:	1.44E+10	0.0	15000.0

```
671. IC8H18+BC8H17O2=AC8H17+BC8H17O2H          1.81E+13    0.0    20430.0
     Reverse Arrhenius coefficients:           1.44E+10    0.0    15000.0
672. IC8H18+CC8H17O2=AC8H17+CC8H17O2H          1.81E+13    0.0    20430.0
     Reverse Arrhenius coefficients:           1.44E+10    0.0    15000.0
673. IC8H18+DC8H17O2=AC8H17+DC8H17O2H          1.81E+13    0.0    20430.0
     Reverse Arrhenius coefficients:           1.44E+10    0.0    15000.0
674. IC8H18+AC8H17O2=BC8H17+AC8H17O2H          4.03E+12    0.0    17700.0
     Reverse Arrhenius coefficients:           1.44E+10    0.0    15000.0
675. IC8H18+BC8H17O2=BC8H17+BC8H17O2H          4.03E+12    0.0    17700.0
     Reverse Arrhenius coefficients:           1.44E+10    0.0    15000.0
676. IC8H18+CC8H17O2=BC8H17+CC8H17O2H          4.03E+12    0.0    17700.0
     Reverse Arrhenius coefficients:           1.44E+10    0.0    15000.0
677. IC8H18+DC8H17O2=BC8H17+DC8H17O2H          4.03E+12    0.0    17700.0
     Reverse Arrhenius coefficients:           1.44E+10    0.0    15000.0
678. IC8H18+AC8H17O2=CC8H17+AC8H17O2H          2.00E+12    0.0    16000.0
     Reverse Arrhenius coefficients:           1.44E+10    0.0    15000.0
679. IC8H18+BC8H17O2=CC8H17+BC8H17O2H          2.00E+12    0.0    16000.0
     Reverse Arrhenius coefficients:           1.44E+10    0.0    15000.0
680. IC8H18+CC8H17O2=CC8H17+CC8H17O2H          2.00E+12    0.0    16000.0
     Reverse Arrhenius coefficients:           1.44E+10    0.0    15000.0
681. IC8H18+DC8H17O2=CC8H17+DC8H17O2H          2.00E+12    0.0    16000.0
     Reverse Arrhenius coefficients:           1.44E+10    0.0    15000.0
682. IC8H18+AC8H17O2=DC8H17+AC8H17O2H          1.21E+13    0.0    20430.0
     Reverse Arrhenius coefficients:           1.44E+10    0.0    15000.0
683. IC8H18+BC8H17O2=DC8H17+BC8H17O2H          1.21E+13    0.0    20430.0
     Reverse Arrhenius coefficients:           1.44E+10    0.0    15000.0
684. IC8H18+CC8H17O2=DC8H17+CC8H17O2H          1.21E+13    0.0    20430.0
     Reverse Arrhenius coefficients:           1.44E+10    0.0    15000.0
685. IC8H18+DC8H17O2=DC8H17+DC8H17O2H          1.21E+13    0.0    20430.0
     Reverse Arrhenius coefficients:           1.44E+10    0.0    15000.0
686. IC8H18+IC4H6OH=AC8H17+IC4H7OH             7.05E+02    3.3    19840.0
     Reverse Arrhenius coefficients:           2.77E-01    3.9     6526.0
687. IC8H18+IC4H6OH=BC8H17+IC4H7OH             1.57E+02    3.3    18170.0
     Reverse Arrhenius coefficients:           1.07E-02    4.3     7350.0
688. IC8H18+IC4H6OH=CC8H17+IC4H7OH             8.44E+01    3.3    17170.0
     Reverse Arrhenius coefficients:           1.66E-03    4.5     9648.0
689. IC8H18+IC4H6OH=DC8H17+IC4H7OH             4.70E+02    3.3    19840.0
     Reverse Arrhenius coefficients:           5.53E-01    3.9     7326.0
690. AC8H17O2=AC8H17+O2                        3.46E+20   -1.7    35720.0
     Reverse Arrhenius coefficients:           4.52E+12    0.0        0.0
691. BC8H17O2=BC8H17+O2                        1.05E+23   -2.3    38840.0
     Reverse Arrhenius coefficients:           7.54E+12    0.0        0.0
692. CC8H17O2=CC8H17+O2                        3.62E+24   -2.6    36010.0
     Reverse Arrhenius coefficients:           1.41E+13    0.0        0.0
693. DC8H17O2=DC8H17+O2                        3.46E+20   -1.7    34920.0
     Reverse Arrhenius coefficients:           4.52E+12    0.0        0.0
694. AC8H17+AC8H17O2=AC8H17O+AC8H17O           7.00E+12    0.0    -1000.0
     Reverse Arrhenius coefficients:           6.48E+13   -0.2    29360.0
695. AC8H17+BC8H17O2=AC8H17O+BC8H17O           7.00E+12    0.0    -1000.0
     Reverse Arrhenius coefficients:           4.99E+13   -0.1    28230.0
696. AC8H17+CC8H17O2=AC8H17O+CC8H17O           7.00E+12    0.0    -1000.0
     Reverse Arrhenius coefficients:           4.35E+13   -0.2    30170.0
697. AC8H17+DC8H17O2=AC8H17O+DC8H17O           7.00E+12    0.0    -1000.0
     Reverse Arrhenius coefficients:           3.25E+13   -0.2    29360.0
698. BC8H17+AC8H17O2=BC8H17O+AC8H17O           7.00E+12    0.0    -1000.0
     Reverse Arrhenius coefficients:           9.04E+15   -0.8    31350.0
699. BC8H17+BC8H17O2=BC8H17O+BC8H17O           7.00E+12    0.0    -1000.0
     Reverse Arrhenius coefficients:           6.96E+15   -0.8    30220.0
700. BC8H17+CC8H17O2=BC8H17O+CC8H17O           7.00E+12    0.0    -1000.0
     Reverse Arrhenius coefficients:           6.07E+15   -0.8    32160.0
701. BC8H17+DC8H17O2=BC8H17O+DC8H17O           7.00E+12    0.0    -1000.0
     Reverse Arrhenius coefficients:           4.54E+15   -0.8    31350.0
702. CC8H17+AC8H17O2=CC8H17O+AC8H17O           7.00E+12    0.0    -1000.0
     Reverse Arrhenius coefficients:           1.46E+17   -1.1    30460.0
703. CC8H17+BC8H17O2=CC8H17O+BC8H17O           7.00E+12    0.0    -1000.0
     Reverse Arrhenius coefficients:           1.12E+17   -1.0    29330.0
704. CC8H17+CC8H17O2=CC8H17O+CC8H17O           7.00E+12    0.0    -1000.0
     Reverse Arrhenius coefficients:           9.80E+16   -1.1    31270.0
705. CC8H17+DC8H17O2=CC8H17O+DC8H17O           7.00E+12    0.0    -1000.0
     Reverse Arrhenius coefficients:           7.32E+16   -1.1    30460.0
706. DC8H17+AC8H17O2=DC8H17O+AC8H17O           7.00E+12    0.0    -1000.0
     Reverse Arrhenius coefficients:           3.25E+13   -0.2    28560.0
707. DC8H17+BC8H17O2=DC8H17O+BC8H17O           7.00E+12    0.0    -1000.0
     Reverse Arrhenius coefficients:           2.50E+13   -0.1    27430.0
708. DC8H17+CC8H17O2=DC8H17O+CC8H17O           7.00E+12    0.0    -1000.0
     Reverse Arrhenius coefficients:           2.18E+13   -0.2    29370.0
709. DC8H17+DC8H17O2=DC8H17O+DC8H17O           7.00E+12    0.0    -1000.0
     Reverse Arrhenius coefficients:           1.63E+13   -0.2    28560.0
710. AC8H17+HO2=AC8H17O+OH                     7.00E+12    0.0    -1000.0
     Reverse Arrhenius coefficients:           2.18E+15   -0.5    25880.0
711. BC8H17+HO2=BC8H17O+OH                     7.00E+12    0.0    -1000.0
     Reverse Arrhenius coefficients:           3.04E+17   -1.1    27870.0
712. CC8H17+HO2=CC8H17O+OH                     7.00E+12    0.0    -1000.0
     Reverse Arrhenius coefficients:           4.91E+18   -1.4    26980.0
713. DC8H17+HO2=DC8H17O+OH                     7.00E+12    0.0    -1000.0
     Reverse Arrhenius coefficients:           1.09E+15   -0.5    25080.0
714. AC8H17+CH3O2=AC8H17O+CH3O                 7.00E+12    0.0    -1000.0
     Reverse Arrhenius coefficients:           1.36E+14   -0.2    30120.0
715. BC8H17+CH3O2=BC8H17O+CH3O                 7.00E+12    0.0    -1000.0
     Reverse Arrhenius coefficients:           1.90E+16   -0.8    32110.0
716. CC8H17+CH3O2=CC8H17O+CH3O                 7.00E+12    0.0    -1000.0
     Reverse Arrhenius coefficients:           3.07E+17   -1.1    31220.0
717. DC8H17+CH3O2=DC8H17O+CH3O                 7.00E+12    0.0    -1000.0
     Reverse Arrhenius coefficients:           6.84E+13   -0.2    29320.0
718. AC8H17O2+HO2=AC8H17O2H+O2                 1.75E+10    0.0    -3275.0
```

```
     Reverse Arrhenius coefficients:                4.07E+13   -0.8    33620.0
719. BC8H17O2+HO2=BC8H17O2H+O2                      1.75E+10    0.0    -3275.0
     Reverse Arrhenius coefficients:                3.75E+13   -0.8    33610.0
720. CC8H17O2+HO2=CC8H17O2H+O2                      1.75E+10    0.0    -3275.0
     Reverse Arrhenius coefficients:                3.75E+13   -0.8    33610.0
721. DC8H17O2+HO2=DC8H17O2H+O2                      1.75E+10    0.0    -3275.0
     Reverse Arrhenius coefficients:                4.07E+13   -0.8    33620.0
722. H2O2+AC8H17O2=HO2+AC8H17O2H                    2.40E+12    0.0    10000.0
     Reverse Arrhenius coefficients:                2.40E+12    0.0    10000.0
723. H2O2+BC8H17O2=HO2+BC8H17O2H                    2.40E+12    0.0    10000.0
     Reverse Arrhenius coefficients:                2.40E+12    0.0    10000.0
724. H2O2+CC8H17O2=HO2+CC8H17O2H                    2.40E+12    0.0    10000.0
     Reverse Arrhenius coefficients:                2.40E+12    0.0    10000.0
725. H2O2+DC8H17O2=HO2+DC8H17O2H                    2.40E+12    0.0    10000.0
     Reverse Arrhenius coefficients:                2.40E+12    0.0    10000.0
726. AC8H17O2+CH3O2=AC8H17O+CH3O+O2                 1.40E+16   -1.6     1860.0
     Warning...all REV parameters are zero...          0.00000E+00 0.00000E+00 0.00000E+00
               this reaction will be treated as irreversible
727. BC8H17O2+CH3O2=BC8H17O+CH3O+O2                 1.40E+16   -1.6     1860.0
     Warning...all REV parameters are zero...          0.00000E+00 0.00000E+00 0.00000E+00
               this reaction will be treated as irreversible
728. CC8H17O2+CH3O2=CC8H17O+CH3O+O2                 1.40E+16   -1.6     1860.0
     Warning...all REV parameters are zero...          0.00000E+00 0.00000E+00 0.00000E+00
               this reaction will be treated as irreversible
729. DC8H17O2+CH3O2=DC8H17O+CH3O+O2                 1.40E+16   -1.6     1860.0
     Warning...all REV parameters are zero...          0.00000E+00 0.00000E+00 0.00000E+00
               this reaction will be treated as irreversible
730. AC8H17O2+AC8H17O2=O2+AC8H17O+AC8H17O           1.40E+16   -1.6     1860.0
     Warning...all REV parameters are zero...          0.00000E+00 0.00000E+00 0.00000E+00
               this reaction will be treated as irreversible
731. AC8H17O2+BC8H17O2=AC8H17O+BC8H17O+O2           1.40E+16   -1.6     1860.0
     Warning...all REV parameters are zero...          0.00000E+00 0.00000E+00 0.00000E+00
               this reaction will be treated as irreversible
732. AC8H17O2+CC8H17O2=AC8H17O+CC8H17O+O2           1.40E+16   -1.6     1860.0
     Warning...all REV parameters are zero...          0.00000E+00 0.00000E+00 0.00000E+00
               this reaction will be treated as irreversible
733. AC8H17O2+DC8H17O2=AC8H17O+DC8H17O+O2           1.40E+16   -1.6     1860.0
     Warning...all REV parameters are zero...          0.00000E+00 0.00000E+00 0.00000E+00
               this reaction will be treated as irreversible
734. BC8H17O2+BC8H17O2=O2+BC8H17O+BC8H17O           1.40E+16   -1.6     1860.0
     Warning...all REV parameters are zero...          0.00000E+00 0.00000E+00 0.00000E+00
               this reaction will be treated as irreversible
735. BC8H17O2+CC8H17O2=BC8H17O+CC8H17O+O2           1.40E+16   -1.6     1860.0
     Warning...all REV parameters are zero...          0.00000E+00 0.00000E+00 0.00000E+00
               this reaction will be treated as irreversible
736. BC8H17O2+DC8H17O2=BC8H17O+DC8H17O+O2           1.40E+16   -1.6     1860.0
     Warning...all REV parameters are zero...          0.00000E+00 0.00000E+00 0.00000E+00
               this reaction will be treated as irreversible
737. CC8H17O2+CC8H17O2=O2+CC8H17O+CC8H17O           1.40E+16   -1.6     1860.0
     Warning...all REV parameters are zero...          0.00000E+00 0.00000E+00 0.00000E+00
               this reaction will be treated as irreversible
738. CC8H17O2+DC8H17O2=CC8H17O+DC8H17O+O2           1.40E+16   -1.6     1860.0
     Warning...all REV parameters are zero...          0.00000E+00 0.00000E+00 0.00000E+00
               this reaction will be treated as irreversible
739. DC8H17O2+DC8H17O2=O2+DC8H17O+DC8H17O           1.40E+16   -1.6     1860.0
     Warning...all REV parameters are zero...          0.00000E+00 0.00000E+00 0.00000E+00
               this reaction will be treated as irreversible
740. AC8H17O2H=AC8H17O+OH                           1.00E+16    0.0    39000.0
     Reverse Arrhenius coefficients:                1.75E+07    1.9    -6742.0
741. BC8H17O2H=BC8H17O+OH                           1.00E+16    0.0    39000.0
     Reverse Arrhenius coefficients:                1.46E+07    2.0    -7862.0
742. CC8H17O2H=CC8H17O+OH                           1.00E+16    0.0    39000.0
     Reverse Arrhenius coefficients:                1.27E+07    1.9    -5922.0
743. DC8H17O2H=DC8H17O+OH                           1.00E+16    0.0    39000.0
     Reverse Arrhenius coefficients:                8.77E+06    1.9    -6742.0
744. AC8H17O=YC7H15+CH2O                            5.69E+24   -3.2    19140.0
     Reverse Arrhenius coefficients:                1.00E+11    0.0    11900.0
745. BC8H17O=TC4H9+IC3H7CHO                         3.11E+26   -3.6    15980.0
     Reverse Arrhenius coefficients:                1.00E+11    0.0    11900.0
746. BC8H17O=IC3H7+TC4H9CHO                         3.33E+23   -2.9    18470.0
     Reverse Arrhenius coefficients:                6.25E+10    0.0    12900.0
747. CC8H17O=NEOC5H11+CH3COCH3                      1.21E+20   -1.7    12340.0
     Reverse Arrhenius coefficients:                1.00E+11    0.0    11900.0
748. DC8H17O=PC7H15+CH2O                            6.08E+22   -2.7    20470.0
     Reverse Arrhenius coefficients:                1.00E+11    0.0    11900.0
749. AC8H17O2=AC8H16OOH-A                           7.50E+10    0.0    24000.0
750. AC8H17O2=AC8H16OOH-B                           2.50E+10    0.0    20450.0
751. AC8H17O2=AC8H16OOH-C                           1.56E+09    0.0    16650.0
752. BC8H17O2=BC8H16OOH-A                           1.12E+11    0.0    24000.0
753. DC8H17O2=DC8H16OOH-B                           2.50E+10    0.0    20450.0
754. AC8H16OOH-A=IC8ETERAA+OH                       3.00E+11    0.0    14250.0
     Warning...all REV parameters are zero...          0.00000E+00 0.00000E+00 0.00000E+00
               this reaction will be treated as irreversible
755. AC8H16OOH-B=IC8ETERAB+OH                       3.00E+11    0.0    14250.0
     Warning...all REV parameters are zero...          0.00000E+00 0.00000E+00 0.00000E+00
               this reaction will be treated as irreversible
756. AC8H16OOH-C=IC8ETERAC+OH                       2.74E+10    0.0     7000.0
     Warning...all REV parameters are zero...          0.00000E+00 0.00000E+00 0.00000E+00
               this reaction will be treated as irreversible
757. BC8H16OOH-A=IC8ETERAB+OH                       3.00E+11    0.0    14250.0
     Warning...all REV parameters are zero...          0.00000E+00 0.00000E+00 0.00000E+00
               this reaction will be treated as irreversible
758. DC8H16OOH-B=IC8ETERBD+OH                       3.00E+11    0.0    14250.0
     Warning...all REV parameters are zero...          0.00000E+00 0.00000E+00 0.00000E+00
               this reaction will be treated as irreversible
```

```
759. AC8H16OOH-A=OH+CH2O+XC7H14                    9.09E+17   -1.3    28580.0
     Warning...all REV parameters are zero...          0.00000E+00 0.00000E+00 0.00000E+00
              this reaction will be treated as irreversible
760. AC8H16OOH-B=OH+CH2O+YC7H14                    1.25E+17   -1.1    28210.0
     Warning...all REV parameters are zero...          0.00000E+00 0.00000E+00 0.00000E+00
              this reaction will be treated as irreversible
761. BC8H16OOH-A=OH+IC3H7CHO+IC4H8                 3.12E+21   -2.4    26330.0
     Warning...all REV parameters are zero...          0.00000E+00 0.00000E+00 0.00000E+00
              this reaction will be treated as irreversible
762. DC8H16OOH-B=OH+CH2O+OC7H14                    1.12E+15   -0.5    30930.0
     Warning...all REV parameters are zero...          0.00000E+00 0.00000E+00 0.00000E+00
              this reaction will be treated as irreversible
763. AC8H16OOH-A=IC4H7OOH+TC4H9                    1.51E+24   -3.1    26840.0
     Reverse Arrhenius coefficients:               1.25E+11    0.0    12300.0
764. AC8H16OOH-AO2=AC8H16OOH-A+O2                  3.25E+20   -1.6    34920.0
     Reverse Arrhenius coefficients:               4.52E+12    0.0        0.0
765. AC8H16OOH-BO2=AC8H16OOH-B+O2                  1.36E+23   -2.4    37280.0
     Reverse Arrhenius coefficients:               7.54E+12    0.0        0.0
766. BC8H16OOH-AO2=BC8H16OOH-A+O2                  2.98E+20   -1.6    34900.0
     Reverse Arrhenius coefficients:               4.52E+12    0.0        0.0
767. DC8H16OOH-BO2=DC8H16OOH-B+O2                  1.36E+23   -2.4    38080.0
     Reverse Arrhenius coefficients:               7.54E+12    0.0        0.0
768. AC8H16OOH-AO2=IC8KETAA+OH                     2.50E+10    0.0    21000.0
769. AC8H16OOH-BO2=IC8KETAB+OH                     2.50E+10    0.0    21000.0
770. BC8H16OOH-AO2=IC8KETBA+OH                     1.25E+10    0.0    17450.0
771. DC8H16OOH-BO2=IC8KETDB+OH                     2.50E+10    0.0    21000.0
772. IC8ETERAA+OH=XC7H14+HCO+H2O                   1.25E+12    0.0        0.0
     Warning...all REV parameters are zero...          0.00000E+00 0.00000E+00 0.00000E+00
              this reaction will be treated as irreversible
773. IC8ETERAB+OH=YC7H14+HCO+H2O                   1.25E+12    0.0        0.0
     Warning...all REV parameters are zero...          0.00000E+00 0.00000E+00 0.00000E+00
              this reaction will be treated as irreversible
774. IC8ETERAC+OH=IC4H8+TC3H6CHO+H2O               1.25E+12    0.0        0.0
     Warning...all REV parameters are zero...          0.00000E+00 0.00000E+00 0.00000E+00
              this reaction will be treated as irreversible
775. IC8ETERBD+OH=OC7H14+HCO+H2O                   1.25E+12    0.0        0.0
     Warning...all REV parameters are zero...          0.00000E+00 0.00000E+00 0.00000E+00
              this reaction will be treated as irreversible
776. IC8ETERAA+OH=IC3H5CHO+IC4H9+H2O               1.25E+12    0.0        0.0
     Warning...all REV parameters are zero...          0.00000E+00 0.00000E+00 0.00000E+00
              this reaction will be treated as irreversible
777. IC8ETERAB+OH=IC4H8+IC3H7CO+H2O                1.25E+12    0.0        0.0
     Warning...all REV parameters are zero...          0.00000E+00 0.00000E+00 0.00000E+00
              this reaction will be treated as irreversible
778. IC8ETERAC+OH=CH2O+YC7H13-Y2+H2O               1.25E+12    0.0        0.0
     Warning...all REV parameters are zero...          0.00000E+00 0.00000E+00 0.00000E+00
              this reaction will be treated as irreversible
779. IC8ETERAA+HO2=XC7H14+HCO+H2O2                 2.50E+12    0.0    17700.0
     Warning...all REV parameters are zero...          0.00000E+00 0.00000E+00 0.00000E+00
              this reaction will be treated as irreversible
780. IC8ETERAB+HO2=YC7H14+HCO+H2O2                 2.50E+12    0.0    17700.0
     Warning...all REV parameters are zero...          0.00000E+00 0.00000E+00 0.00000E+00
              this reaction will be treated as irreversible
781. IC8ETERAC+HO2=IC4H8+TC3H6CHO+H2O2             2.50E+12    0.0    17700.0
     Warning...all REV parameters are zero...          0.00000E+00 0.00000E+00 0.00000E+00
              this reaction will be treated as irreversible
782. IC8ETERBD+HO2=OC7H14+HCO+H2O2                 2.50E+12    0.0    17700.0
     Warning...all REV parameters are zero...          0.00000E+00 0.00000E+00 0.00000E+00
              this reaction will be treated as irreversible
783. IC8ETERAA+HO2=IC3H5CHO+IC4H9+H2O2             2.50E+12    0.0    17700.0
     Warning...all REV parameters are zero...          0.00000E+00 0.00000E+00 0.00000E+00
              this reaction will be treated as irreversible
784. IC8ETERAB+HO2=IC4H8+IC3H7CO+H2O2              2.50E+12    0.0    17700.0
     Warning...all REV parameters are zero...          0.00000E+00 0.00000E+00 0.00000E+00
              this reaction will be treated as irreversible
785. IC8ETERAC+HO2=CH2O+YC7H13-Y2+H2O2             2.50E+12    0.0    17700.0
     Warning...all REV parameters are zero...          0.00000E+00 0.00000E+00 0.00000E+00
              this reaction will be treated as irreversible
786. IC8KETAA=CH2O+DC6H12CHO-D+OH                  1.00E+16    0.0    39000.0
     Warning...all REV parameters are zero...          0.00000E+00 0.00000E+00 0.00000E+00
              this reaction will be treated as irreversible
787. IC8KETAB=IC3H7CHO+TC3H6CHO+OH                 1.00E+16    0.0    39000.0
     Warning...all REV parameters are zero...          0.00000E+00 0.00000E+00 0.00000E+00
              this reaction will be treated as irreversible
788. IC8KETBA=CH2O+IC3H7COC3H6-T+OH                1.00E+16    0.0    39000.0
     Warning...all REV parameters are zero...          0.00000E+00 0.00000E+00 0.00000E+00
              this reaction will be treated as irreversible
789. IC8KETDB=TC4H9CHO+CH3CHCHO+OH                 1.00E+16    0.0    39000.0
     Warning...all REV parameters are zero...          0.00000E+00 0.00000E+00 0.00000E+00
              this reaction will be treated as irreversible
790. DC6H12CHO-D=IC3H5CHO+IC3H7                    7.83E+15   -0.6    31510.0
     Reverse Arrhenius coefficients:               1.00E+11    0.0     8300.0
791. IC3H7COC3H6-T=IC3H6CO+IC3H7                   1.22E+17   -0.6    42050.0
     Reverse Arrhenius coefficients:               1.00E+11    0.0    11900.0
792. IC4H6OH+H2O=IC4H7OH+OH                        5.88E+06    1.9    30240.0
     Reverse Arrhenius coefficients:               3.12E+06    2.0     -298.0
793. IC4H6OH+CH4=IC4H7OH+CH3                       3.57E+02    3.1    22870.0
     Reverse Arrhenius coefficients:               2.21E+00    3.5     5675.0
794. IC4H6OH+C3H6=IC4H7OH+C3H5-A                   2.51E+02    3.2    18640.0
     Reverse Arrhenius coefficients:               5.75E+02    3.1    18660.0
795. IC4H6OH+CH3CHO=IC4H7OH+CH3CO                  1.36E+09    1.4    17940.0
     Reverse Arrhenius coefficients:               5.30E+06    2.0    16240.0
796. C3H5-A+CH2O=C3H6+HCO                          6.30E+08    1.9    18190.0
     Reverse Arrhenius coefficients:               9.16E+06    2.2    17700.0
797. IC3H6CHCOCH3+OH=AC3H5CHCOCH3+H2O              1.53E+08    1.5     8775.0
```

```
     Reverse Arrhenius coefficients:               1.34E+10    1.0    41430.0
798. IC3H6CHCOCH3+OH=IC3H6CHCOCH2+H2O              5.10E+11    0.0     1192.0
     Reverse Arrhenius coefficients:               6.12E+07   -0.5    28070.0
799. IC3H6CHCOCH3+OH=IC3H7CHO+CH3CO                1.00E+11    0.0        0.0
     Reverse Arrhenius coefficients:               3.84E+06    1.0    15550.0
800. IC3H6CHCOCH3+HO2=AC3H5CHCOCH3+H2O2            2.74E+04    2.5    15500.0
     Reverse Arrhenius coefficients:               1.42E+07    1.7    16690.0
801. IC3H6CHCOCH3+HO2=IC3H6CHCOCH2+H2O2            2.38E+04    2.5    14690.0
     Reverse Arrhenius coefficients:               1.69E+01    1.8    10110.0
802. IC3H6CHCOCH3+CH3O2=AC3H5CHCOCH3+CH3O2H        5.00E+10    0.0    11920.0
     Reverse Arrhenius coefficients:               1.07E+14   -1.0    12390.0
803. IC3H6CHCOCH3+CH3O2=IC3H6CHCOCH2+CH3O2H        3.01E+12    0.0    17580.0
     Reverse Arrhenius coefficients:               8.81E+09   -1.0    12270.0
804. AC3H5CHCOCH3+HO2=IC3H5CHO+CH3CO+OH            1.00E+12    0.0        0.0
     Reverse Arrhenius coefficients:               1.00E+00    0.0        0.0
805. IC3H6CHCOCH2=IC4H7+CH2CO                      1.40E+14   -1.6    50750.0
     Reverse Arrhenius coefficients:               8.00E+10    0.0    11900.0

UNITS for the preceding reactions (unless otherwise noted):
      A units mole-cm-sec-K, E units cal/mole
```